

## Response to reviews

Reviewer comments are in **bold**. Author responses are in plain text. Excerpts from the manuscript are in *italics*. Modifications to the manuscript are in *blue italics*. Page and line numbers in the responses correspond to those in the ACPD paper.

### Review #1

**The presented paper by de Sá et al, 'Urban influence on the concentration and composition of submicron particulate matter in central Amazonia' gives a very clear overview of the aerosol particle composition during the wet season in the Amazon region. The authors use two different methods to analyse AMS data. PMF, which gives an overview of the particle composition and fuzzy c-means algorithm to study the anthropogenic influence on the aerosol in Amazon. I have few minor comments which are addressed in the following:**

We thank the reviewer for the input, and the revised manuscript takes into account the comments and questions, as detailed in the responses below.

**1. in the Introduction line 30, information on isoprene emissions compared to other biogenic or even anthropogenic VOCs could be added. Eg., how much isoprene is estimated to be emitted globally, how much of it is emitted by the amazon rainforest?**

We thank the reviewer for this suggestion. Information on the importance of isoprene emissions, especially in the Amazon, is added to the revised manuscript, as follows:

Line 36:

*~~For tropical forests, isoprene emissions are especially important in PM production (Martin et al., 2010a; Chen et al., 2015) Isoprene accounts for half of global BVOC mass emissions, and tropical forests are responsible for about 80% of terpenoid emissions (Guenther et al., 2012). In the Amazon, isoprene is the dominant BVOC emitted by vegetation and is estimated to contribute to about half of the organic PM concentrations under background conditions (Kuhn et al., 2010; Chen et al., 2015; Yáñez-Serrano et al., 2015) (Kuhn et al., 2010; Chen et al., 2015; Yáñez-Serrano et al., 2015).~~*

**2.a Also in the Introduction,, in line with the measurement period that you are describing here, how many days of data did you collect during the IOP1.**

The whole duration of IOP1 (Feb 1 to Mar 31, 2014) was the nominal operation time for all instruments including the AMS. The AMS data coverage is shown in Figure 1. The referred sentence in the introduction is clarified, as follows:

Line 60:

*The analysis employs data sets collected in the wet season from February 1 to March 31, 2014, corresponding to the first Intensive Operating Period (IOP1) of the GoAmazon2014/5 experiment (Martin et al., 2016).* ~~*corresponding to the wet season during the period of February 1 to March 31, 2014.*~~

**2.b How frequently was the site influenced by the Manaus pollution during the time period presented in the manuscript?**

We appreciate the suggestion, and the revised text includes this information as follows.

Line 72:

*The site was situated in a pasture of 2.5 km × 2 km surrounded by forest. Based on modeled flow trajectories of the pollution plume, the T3 site intercepted the plume about 40% of the time (Martin et al., 2017).*

**3. in Methodology you mention 'V' and 'W' mode data. Maybe this is common knowledge but in my opinion it is useful to add a short description of what that means at least in the supplementary material.**

The text is adjusted to restrict the use of these technical terms to the Supplementary Material, and an explanation of what these modes mean is included there.

Line 95:

*Organic, sulfate, ammonium, nitrate, and chloride PM mass concentrations were obtained from "V-mode" data. The choice of ions to fit was aided by "W-mode" data, which were collected for one of every five days.* ~~*quantified.*~~

Line 208:

*Positive-matrix factorization was applied to the time series of the organic component of the high-resolution "V-mode" mass spectra (Ulbrich et al., 2009).*

Supplementary material, line 3:

*Quantification of mass concentrations by the AMS was obtained from "V-mode" data, which corresponds to the shorter ion time-of-flight path and is therefore the more sensitive mode. The choice of ions to fit was aided by "W-mode" data, which corresponds to the longer ion time-of-flight path and is therefore the mode with higher mass resolution. V-mode data were collected continuously, and W-mode data were collected for one of every five days. The time series of organic mass spectra measured by the AMS in V-mode was analyzed by positive-matrix factorization (PMF) using a standard analysis toolkit (Ulbrich et al., 2009). High-resolution "V-mode" data were used.*

**4. in Auxiliary measurements and datasets, l. 124: it would be nice also for the supplementary measurements to add information for what time period that data was taken and how much of data was collected during each set of measurements.**

Following this suggestion, the text is improved as follows.

Line 104:

*In complement to the AMS data set, the analysis herein incorporated auxiliary gas and particle measurements ~~from~~ collected during IOP1 at T3 (Martin et al., 2016).*

Line 124:

*At T2, non-refractory particle composition and concentration were measured by an Aerosol Chemical Speciation Monitor (ACSM; Brito et al., in preparation.) during the wet season from March 9 to April 30, 2014 (Cirino et al., submitted). ACSM measurements were ~~also~~ made at T0a during the wet season of 2015 (~~Carbone et al., in preparation.~~), from February 1 to March 31 (Andreae et al., 2015). Further AMS datasets collected ~~by AMS~~ at T0t during the wet season of 2008 (February 6 to March 22; AMAZE-08 campaign) were used in the analysis (Chen et al., 2009; Schneider et al., 2011). ~~AMS measurements made onboard the G-1 aircraft of the ARM Aerial Facility (AAF) during IOP1 also supported the analysis herein (Shilling et al., in preparation).~~*

**5. in Results and discussion, in line 180 it is important to mention here again that the measurements at T0 sites were taken in a different year. It helps the reader.**

The reviewer raises a good point, and the text is adjusted as follows. (The reviewer mentioned line 180, but the information about T0 was at line 163, and we think this is what the reviewer meant.)

Line 163:

*The NR-PM<sub>1</sub> mass concentrations at the T0 sites upwind of Manaus, ~~although measured in different years,~~ were ~~consistently around approximately~~  $1 \mu\text{g m}^{-3}$ .*

**6. Fig.3: This Figure contains too many data points, most of the points are hidden. I suggest to split the Figure into few sub-Figures, which enclose different time periods of the day. That allows to see any temporal trend of the particle evolution and to distinguish better what is happening at the different sites.**

Based on this feedback, the figure is revised to provide a better visualization of the data points. The caption of Figure 3 is adjusted as follows:

*Gray and blue circles correspond, respectively, to measurements at T3 and T2 during IOP1, in the wet season of 2014. For visualization purposes, the two datasets are plotted separately in panels a and b.*

The intention of the authors for this figure is to provide a general comparison of the PM oxidation at both sites. For the reviewer's suggestion in relation to plume evolution, we think that a more elaborate analysis beyond the scope of the authors' intention would be necessary to take into account (i) the transport time between the sites for each individual data point, (ii) whether the plume passed over both sites, and (iii) meteorological factors. Cirino et al., submitted focused on this kind of complex plume analysis. The text is adjusted to reflect these important points.

Line 198:

*The comparison depicted in Figure 3 ~~illustrates the effects of the plume over the 4 h of transport from T2 to T3 (Cirino et al., submitted).~~ indicates the effects of the plume over the 4 h of transport from T2 to T3, which were investigated in detail by Cirino et al. (submitted).*

**7. Fig.5: This Figure is easier to read and more informative, if the variables on the x-axis are grouped according to their source (biogenic, anthropogenic, background, biomass burning) other than the instrument they were measured with.**

We appreciate this suggestion. Based on it, the authors prepared both possible figures for internal discussion. In the end, the authors believe that the original figure is better for presentation. The reason is that most of the tracers have contributions from several different and in some cases unknown sources so that a definitive classification would be uncertain, and the revised figure would be a scientific over-stretch. The exceptions, such as levoglucosan which is a specific tracer for biomass burning, are explicitly mentioned in the text.

**8. Fig. 7: the air mass back-trajectories are more valuable if they are calculated as ensembles rather than single trajectories. Ensemble gives you a group of trajectories which are all equally likely.**

We thank the reviewer for this thoughtful comment, which generated significant internal discussion among the authors. Although the idea is appreciated, the use of ensembles did not seem the most appropriate or necessary tool for the analysis of Figure 7.

The backtrajectories are employed in this study in a supportive rather than central role to the clustering analysis, i.e., trajectories are not used to generate clusters but rather to help in their interpretation. In each panel of Fig. 7, trajectories are representative of the case studies shown in Fig. 6. It is visually clear that trajectories within those time periods are already clustered. Calculating ensembles for all observation times (every 12 min) over the course of the two months of the study period would have added a very large computational time and human expense that could not be afforded. Hence,

the cost-benefit of a more complex trajectory analysis was not justified, while the single trajectories still added value to the data interpretation.

## **Review #2**

**1. [T]his manuscript provides an overview of particle mass and chemical composition, with a focus on organic species in the Amazon. The authors strive to understand the anthropogenic contribution(s) to mass and influence on speciation and approach this with 2 different statistical approaches applied to online measurements. The work is interesting but seems premature. The paper relies on and cites several manuscripts that are “in preparation” to justify some arguments and conclusions and this is problematic. For example, comparison among different data sets (and presented in Figure 1) includes data not previously published, nor fully explained here.: data from ATTO sampling location “T0a-2015” is from Carbone et al., in preparation and “T2-2014” is from IOPI Brito in preparation.**

We thank the reviewer for reading the manuscript and providing valuable feedback.

For the references “in preparation”, the following revisions are made.

- (i) Carbone et al. (in preparation) is replaced by Andreae et al. (2015), which already published the T0a-2015 data used in this study.
- (ii) Brito et al. (in preparation) is replaced by Cirino et al. (submitted). This manuscript is in the final stages of peer review, and we expect that “submitted” can be replaced with a full citation for the ACP publication of the present manuscript. Both Brito and Cirino, responsible for ACSM data collection and analysis at T2, are co-authors in the present study.

For changes made to the text to address (i) and (ii) please see reply #4 to review #1. The references in the caption of Figure 1 are also accordingly updated.

We believe that these updates satisfy the reviewer’s concern about “premature”. Importantly, the comparison of the T3 composition to other sites only appears in one section of the manuscript (lines 155-205). The main conclusions, by contrast, largely come from the combined analysis of PMF and FCM on the data collected at T3, which is completely original and presented in detail in the following sections of the manuscript (lines 206-514).

**2. Organic mass variability in relation to meteorology seems to be an important finding and necessary to the arguments in this manuscript but Cirino et al. ‘in prep’ is the provided proof and readers are not left with sufficient information to understand the reasonableness of the argument.**

This reference was adjusted as follows:

Line 174:

*This influence waxes and wanes with small northerly or southerly shifts of the trade winds as well as other changes in regional circulation tied to daily meteorology (Cirino et al., in preparation Santos et al., 2014; Martin et al., 2017).*

**3. The authors also cite de Sá et al ‘in prep’ to explain why a certain analysis is beyond the scope of this paper and not presented here and explain that the analysis is currently underway (e.g., biomass burning influence (presumably screened here?)) will be discussed in the literature later and I think that is ok.**

The current manuscript focuses on the wet season. As stated in the introduction (line 48), the influence of biomass burning is minimal during the wet season. The reference to de Sá et al. (in preparation) in the introduction (line 64) was intended to highlight that there is a separate manuscript under way for the dry season (to also be submitted to the GoAmazon2014/5 Special Issue of ACP). Although related, these studies are independent.

**4. Many journals would not even accept ‘in prep’ References at all. To use such References for conclusions seems unreasonable to me. Prior to acceptance for publication I think the ‘prior’ work must first be published or properly backed up here.**

We understand the reviewer’s concerns. Please see replies 10 and 11.

**5. specific comments: Line 19/20: The choice to cite Weber et al., 2007 and Goldstein et al., 2009 here is curious. Weber et al. state in that paper: “Although NO<sub>x</sub> may be another precursor that could be influencing this system, NO<sub>x</sub>-WSOC... was weakly correlated” The R<sup>2</sup> is <0.2 I acknowledge time scales for complex chemistry matter and correlation for instantaneous values can be low even though there is a dependence, however the work by Weber does not provide support for NO<sub>x</sub> or SO<sub>2</sub> dependence as suggested by the authors here. The work by Weber et al does demonstrate a link to CO. The Goldstein analysis for particles is limited to satellite-AOT. Seasonal and spatial patterns have found these AOT observations are not due to organic fine particle mass (Ford and Heald, ACP 2013; Nguyen et al. GRL, 2016) The authors cite Xu et al., 2015 later in the manuscript and that would be a good citation here. Because the authors are talking in the manuscript here about the Southeast US, citing recent findings from the Southeast field campaigns (e.g., SOAS as in the Xu paper) and making a link with the context of those field campaigns would improve the paper.**

We greatly appreciate that the reviewer pointed out this mismatch in citations. The text is updated as follows:

Line 15:

~~In the northeastern USA, de Gouw et al. (2005) showed that organic PM concentrations correlated well with anthropogenic tracers, yet the concentrations of anthropogenic precursors were insufficient to explain the observed PM. In the southeastern USA, observations suggested that organic PM was produced mainly from BVOCs, however modulated by anthropogenic emissions of NO<sub>x</sub> and SO<sub>2</sub> (Weber et al., 2007; Goldstein et al., 2009).~~ concentrations of organic particulate matter (PM) correlated well with anthropogenic tracers, yet the concentrations of the anthropogenic precursors were insufficient to explain the observed PM concentrations. In the southeastern USA, radioisotope analysis of organic PM determined that 70% to 80% of the carbon mass had a modern origin even as correlations were observed between SOM mass concentrations and anthropogenic VOC and CO concentrations (Weber et al., 2007). This finding and those of further field studies in the region together suggested that the organic PM was produced mainly from biogenic VOCs (BVOCs) yet modulated by anthropogenic emissions of NO<sub>x</sub> and SO<sub>2</sub> (Hu et al., 2015; Xu et al., 2015a; Xu et al., 2015b; Zhang et al., 2018).

**6. I have no idea what “V” and “W” mode mean. The authors should provide an explanation if the distinction is important as they suggest.**

Please see reply #3 to review #1.

**7. Line 165: When talking about Figure 1 the authors state ‘concentrations at the T2 site were more than three times higher on average’ All of the presented averages in Figure 1b overlap within the uncertainty. Can it be stated that there is statistical significance to the difference? Figure 2 suggests a factor of 2, not 3.**

The reviewer raises an important point that needs clarification. Firstly, the bars in Figure 1b do not represent uncertainty but rather variability in the measurements. Secondly, the variability of concentrations among sites can only be fairly compared by considering different times of day as was done in Figure 2, since the variability is largely driven by the diel trends. To clarify this point to the reader, we removed the bars in Figure 1b and emphasized in the caption of Figure 1 as well as in the text that a comparison of the variability across sites is presented in Figure 2, as follows.

Figure 1 caption:

~~Bars represent means and whiskers represent the standard deviation of measurements.~~ The variability of measurements across sites is evaluated in Figure 2.

Line 170:

*The diel trends of organic and sulfate mass concentrations as well as their variabilities across the four sites are shown in Figure 2.*

**8. Figure 2 caption: Please correct the text: “Error! Reference source not found.” The panels of Figure 2 have different y-axes and this should be mentioned explicitly.**

We thank the reviewer for catching these two points, and corrections are made in the figure caption as follows:

*“... at four different sites (cf. Fig.1 and Fig. ~~Error! Reference source not found. S1~~). The ordinate scale for the T2-2014 panel is twice that of the other panels. Mass concentrations were corrected to standard temperature and pressure (273.15 K and 105 Pa). Local time is (UTC - 4 h). Lines represent means, solid markers show medians, and boxes span interquartile ranges. ~~The ordinate scale for the T2 panel differs from the other three panels. Concentrations were adjusted to standard temperature (273.15 K) and pressure (105 Pa).~~”*

**9. Figure 4 is nice, but it’s hard to read and digest.**

We understand that the information content of Figure 4 is high. This study heavily relies on the PMF results, and Figure 4 provides an important summary of the PMF factors. The authors discussed several alternative representations for this figure and believe that the present version is the best option. Importantly, the text is optimized to accompany the figure. Lines 228 - 349 of the text are paired to the reading of Figure 4. The text explains the characteristics of the factors one by one in each paragraph and systematically refers to each of the panels in that figure.

**10. Figure 9 is excellent!**

Thank you!



## References

- Andreae, M. O., Acevedo, O. C., Araùjo, A., Artaxo, P., Barbosa, C. G. G., Barbosa, H. M. J., Brito, J., Carbone, S., Chi, X., Cintra, B. B. L., da Silva, N. F., Dias, N. L., Dias-Júnior, C. Q., Ditas, F., Ditz, R., Godoi, A. F. L., Godoi, R. H. M., Heimann, M., Hoffmann, T., Kesselmeier, J., Könemann, T., Krüger, M. L., Lavric, J. V., Manzi, A. O., Lopes, A. P., Martins, D. L., Mikhailov, E. F., Moran-Zuloaga, D., Nelson, B. W., Nölscher, A. C., Santos Nogueira, D., Piedade, M. T. F., Pöhlker, C., Pöschl, U., Quesada, C. A., Rizzo, L. V., Ro, C. U., Ruckteschler, N., Sá, L. D. A., de Oliveira Sá, M., Sales, C. B., dos Santos, R. M. N., Saturno, J., Schöngart, J., Sörgel, M., de Souza, C. M., de Souza, R. A. F., Su, H., Targhetta, N., Tóta, J., Trebs, I., Trumbore, S., van Eijck, A., Walter, D., Wang, Z., Weber, B., Williams, J., Winderlich, J., Wittmann, F., Wolff, S., and Yáñez-Serrano, A. M.: The Amazon Tall Tower Observatory (ATTO): overview of pilot measurements on ecosystem ecology, meteorology, trace gases, and aerosols, *Atmos. Chem. Phys.*, 15, 10723-10776, 2015, 10.5194/acp-15-10723-2015.
- Chen, Q., Farmer, D. K., Rizzo, L. V., Pauliquevis, T., Kuwata, M., Karl, T. G., Guenther, A., Allan, J. D., Coe, H., Andreae, M. O., Pöschl, U., Jimenez, J. L., Artaxo, P., and Martin, S. T.: Submicron particle mass concentrations and sources in the Amazonian wet season (AMAZE-08), *Atmos. Chem. Phys.*, 15, 3687-3701, 2015, 10.5194/acp-15-3687-2015.
- Cirino, G. G., Brito, J., Barbosa, H. J. M., Rizzo, L. V., Tunved, P., de Sá, S. S., Jimenez, J., Palm, B. B., Carbone, S., Lavric, J., Souza, R., Wolff, S., Walter, D., Tota, J., Oliveira, M., Martin, S. T., and Artaxo, P.: Observations of Manaus urban plume evolution and interaction with biogenic emissions in GoAmazon2014/5, *Atmos Environ*, submitted.
- de Gouw, J. A., Middlebrook, A. M., Warneke, C., Goldan, P. D., Kuster, W. C., Roberts, J. M., Fehsenfeld, F. C., Worsnop, D. R., Canagaratna, M. R., Pszenny, A. A. P., Keene, W. C., Marchewka, M., Bertman, S. B., and Bates, T. S.: Budget of organic carbon in a polluted atmosphere: Results from the New England Air Quality Study in 2002, *J. Geophys. Res. Atmos.*, 110, D16305, 2005, 10.1029/2004JD005623.
- dos Santos, M. J., Silva Dias, M. A. F., and Freitas, E. D.: Influence of local circulations on wind, moisture, and precipitation close to Manaus City, Amazon Region, Brazil, *J. Geophys. Res. Atmos.*, 119, 13,233-213,249, 2014, 10.1002/2014JD021969.
- Hu, W. W., Campuzano-Jost, P., Palm, B. B., Day, D. A., Ortega, A. M., Hayes, P. L., Krechmer, J. E., Chen, Q., Kuwata, M., Liu, Y. J., de Sá, S. S., McKinney, K., Martin, S. T., Hu, M., Budisulistiorini, S. H., Riva, M., Surratt, J. D., St. Clair, J. M., Isaacman-Van Wertz, G., Yee, L. D., Goldstein, A. H., Carbone, S., Brito, J., Artaxo, P., de Gouw, J. A., Koss, A., Wisthaler, A., Mikoviny, T., Karl, T., Kaser, L., Jud, W., Hansel, A., Docherty, K. S., Alexander, M. L., Robinson, N. H., Coe, H., Allan, J. D., Canagaratna, M. R., Paulot, F., and

- Jimenez, J. L.: Characterization of a real-time tracer for isoprene epoxydiols-derived secondary organic aerosol (IEPOX-SOA) from aerosol mass spectrometer measurements, *Atmos. Chem. Phys.*, 15, 11807-11833, 2015, 10.5194/acp-15-11807-2015.
- Kuhn, U., Ganzeveld, L., Thielmann, A., Dindorf, T., Schebeske, G., Welling, M., Sciare, J., Roberts, G., Meixner, F. X., Kesselmeier, J., Lelieveld, J., Kolle, O., Ciccioli, P., Lloyd, J., Trentmann, J., Artaxo, P., and Andreae, M. O.: Impact of Manaus City on the Amazon Green Ocean atmosphere: ozone production, precursor sensitivity and aerosol load, *Atmos. Chem. Phys.*, 10, 9251-9282, 2010, 10.5194/acp-10-9251-2010.
- Martin, S. T., Artaxo, P., Machado, L. A. T., Manzi, A. O., Souza, R. A. F., Schumacher, C., Wang, J., Andreae, M. O., Barbosa, H. M. J., Fan, J., Fisch, G., Goldstein, A. H., Guenther, A., Jimenez, J. L., Pöschl, U., Silva Dias, M. A., Smith, J. N., and Wendisch, M.: Introduction: observations and modeling of the green ocean Amazon (GoAmazon2014/5), *Atmos. Chem. Phys.*, 16, 4785-4797, 2016, 10.5194/acp-16-4785-2016.
- Martin, S. T., Artaxo, P., Machado, L., Manzi, A. O., Souza, R. A. F., Schumacher, C., Wang, J., Biscaro, T., Brito, J., Calheiros, A., Jardine, K., Medeiros, A., Portela, B., Sá, S. S. d., Adachi, K., Aiken, A. C., Albrecht, R., Alexander, L., Andreae, M. O., Barbosa, H. M. J., Buseck, P., Chand, D., Comstock, J. M., Day, D. A., Dubey, M., Fan, J., Fast, J., Fisch, G., Fortner, E., Giangrande, S., Gilles, M., Goldstein, A. H., Guenther, A., Hubbe, J., Jensen, M., Jimenez, J. L., Keutsch, F. N., Kim, S., Kuang, C., Laskin, A., McKinney, K., Mei, F., Miller, M., Nascimento, R., Pauliquevis, T., Pekour, M., Peres, J., Petäjä, T., Pöhlker, C., Pöschl, U., Rizzo, L., Schmid, B., Shilling, J. E., Dias, M. A. S., Smith, J. N., Tomlinson, J. M., Tóta, J., and Wendisch, M.: The Green Ocean Amazon Experiment (GoAmazon2014/5) observes pollution affecting gases, aerosols, clouds, and rainfall over the rain forest, *Bulletin of the American Meteorological Society*, 98, 981-997, 2017, 10.1175/bams-d-15-00221.1.
- Ulbrich, I., Canagaratna, M., Zhang, Q., Worsnop, D., and Jimenez, J.: Interpretation of organic components from positive matrix factorization of aerosol mass spectrometric data, *Atmos. Chem. Phys.*, 9, 2891-2918, 2009, 10.5194/acp-9-2891-2009.
- Xu, L., Guo, H., Boyd, C. M., Klein, M., Bougiatioti, A., Cerully, K. M., Hite, J. R., Isaacman-VanWertz, G., Kreisberg, N. M., Knote, C., Olson, K., Koss, A., Goldstein, A. H., Hering, S. V., de Gouw, J., Baumann, K., Lee, S.-H., Nenes, A., Weber, R. J., and Ng, N. L.: Effects of anthropogenic emissions on aerosol formation from isoprene and monoterpenes in the southeastern United States, *Proc. Natl. Acad. Sci. USA*, 112, 37-42, 2015a, 10.1073/pnas.1417609112.
- Xu, L., Suresh, S., Guo, H., Weber, R. J., and Ng, N. L.: Aerosol characterization over the southeastern United States using high-resolution aerosol mass spectrometry: spatial and seasonal variation of aerosol composition and sources with a focus on organic nitrates, *Atmos. Chem. Phys.*, 15, 7307-7336, 2015b, 10.5194/acp-15-7307-2015.

- Yáñez-Serrano, A. M., Nölscher, A. C., Williams, J., Wolff, S., Alves, E., Martins, G. A., Bourtsoukidis, E., Brito, J., Jardine, K., Artaxo, P., and Kesselmeier, J.: Diel and seasonal changes of biogenic volatile organic compounds within and above an Amazonian rainforest, *Atmos. Chem. Phys.*, 15, 3359-3378, 2015, [10.5194/acp-15-3359-2015](https://doi.org/10.5194/acp-15-3359-2015).
- Zhang, H., Yee, L. D., and Goldstein, A. H.: Monoterpenes are the largest source of summertime organic aerosol in the southeastern United States, 2018.

# Urban influence on the concentration and composition of submicron particulate matter in central Amazonia

Suzane S. de Sá (1), Brett B. Palm (2), Pedro Campuzano-Jost (2), Douglas A. Day (2), Weiwei Hu (2), Gabriel Isaacman-VanWertz<sup>a</sup> (3), Lindsay D. Yee (3), Joel Brito<sup>b</sup> (4), Samara Carbone<sup>c</sup> (4), Igor O. Ribeiro (5), Glauber G. Cirino<sup>d</sup> (6), Yingjun J. Liu<sup>e</sup> (1), Ryan Thalman<sup>f</sup> (7), Arthur Sedlacek (7), Aaron Funk (8), Courtney Schumacher (8), John E. Shilling (9), Johannes Schneider (10), Paulo Artaxo (4), Allen H. Goldstein (3), Rodrigo A.F. Souza (5), Jian Wang (7), Karena A. McKinney<sup>g</sup> (1), Henrique Barbosa (4), M. Lizabeth Alexander (11), Jose L. Jimenez (2), Scot T. Martin\* (1, 12)

(1) School of Engineering and Applied Sciences, Harvard University, Cambridge, Massachusetts, USA

(2) Department of Chemistry and Cooperative Institute for Research in Environmental Sciences, University of Colorado, Boulder, Colorado, USA

(3) Department of Environmental Science, Policy, and Management, University of California, Berkeley, California, USA

(4) Institute of Physics, University of São Paulo, São Paulo, Brazil

(5) School of Technology, Amazonas State University, Manaus, Amazonas, Brazil

(6) National Institute for Amazonian Research, Manaus, Amazonas, Brazil

(7) Brookhaven National Laboratory, Upton, New York, USA

(8) Department of Atmospheric Sciences, Texas A&M University, College Station, Texas, USA

(9) Atmospheric Sciences and Global Change Division, Pacific Northwest National Laboratory, Richland, WA, USA

(10) Particle Chemistry Department, Max Planck Institute for Chemistry, Mainz, Germany

(11) Environmental Molecular Sciences Laboratory, Pacific Northwest National Laboratory, Richland, Washington, USA

(12) Department of Earth and Planetary Sciences, Harvard University, Cambridge, Massachusetts, USA

<sup>a</sup> Now at Department of Civil and Environmental Engineering, Virginia Tech, Blacksburg, Virginia, USA

<sup>b</sup> Now at Laboratory for Meteorological Physics (LaMP), University Blaise Pascal, Aubière, France

<sup>c</sup> Now at Federal University of Uberlândia, Uberlândia, Minas Gerais, Brazil

<sup>d</sup> Now at Department of Meteorology, Geosciences Institute, Federal University of Pará, Belém, Brazil

<sup>e</sup> Now at University of California, Berkeley, California, USA

<sup>f</sup> Now at Department of Chemistry, Snow College, Richfield, Utah, USA

<sup>g</sup> Now at Colby College, Waterville, Maine, USA

Submitted: February 2018

*Atmospheric Chemistry and Physics*

\*To Whom Correspondence Should be Addressed

*E-mail: [scot\\_martin@harvard.edu](mailto:scot_martin@harvard.edu)*

*<https://martin.seas.harvard.edu/>*

1 **Abstract**

2           Fundamental to quantifying the influence of human activities on climate and air quality is  
3 an understanding of how anthropogenic emissions affect the concentrations and composition of  
4 airborne particulate matter (PM). The central Amazon basin, especially around the city of  
5 Manaus, Brazil, has experienced rapid changes in the past decades due to ongoing urbanization.  
6 Herein, changes in the concentration and composition of submicron PM due to pollution  
7 downwind of the Manaus metropolitan region are reported as part of the GoAmazon2014/5  
8 experiment. A high-resolution time-of-flight aerosol mass spectrometer (HR-ToF-AMS) and a  
9 suite of other gas- and particle-phase instruments were deployed at the “T3” research site, 70 km  
10 downwind of Manaus, during the wet season. At this site, organic components represented on  
11 average  $79 \pm 7\%$  of the non-refractory  $PM_{10}$  mass concentration, which was in the same range as  
12 several upwind sites. The organic  $PM_{10}$  was, however, considerably more oxidized at T3  
13 compared to upwind measurements. Positive-matrix factorization (PMF) was applied to the time  
14 series of organic mass spectra collected at the T3 site, yielding three factors representing  
15 secondary processes ( $73 \pm 15\%$  of total organic mass concentration) and three factors  
16 representing primary anthropogenic emissions ( $27 \pm 15\%$ ). Fuzzy c-means clustering (FCM) was  
17 applied to the afternoon time series of concentrations of  $NO_y$ , ozone, total particle number, black  
18 carbon, and sulfate. Four clusters were identified and characterized by distinct air mass origins  
19 and particle compositions. Two clusters, Bkgd-1 and Bkgd-2, were associated with background  
20 conditions. Bkgd-1 appeared to represent near-field atmospheric PM production and oxidation of  
21 a day or less. Bkgd-2 appeared to represent material transported and oxidized for two or more  
22 days, often with out-of-basin contributions. Two other clusters, Pol-1 and Pol-2, represented the  
23 Manaus influence, one apparently associated with the northern region of Manaus and the other

24 with the southern region of the city. A composite of the PMF and FCM analyses provided  
25 insights into the anthropogenic effects on PM concentration and composition. The increase in  
26 mass concentration of submicron PM ranged from 25% to 200% under polluted compared to  
27 background conditions, including contributions from both primary and secondary PM.  
28 Furthermore, a comparison of PMF factor loadings for different clusters suggested a shift in the  
29 pathways of PM production under polluted conditions. Nitrogen oxides may have played a  
30 critical role in these shifts. Increased concentrations of nitrogen oxides can shift pathways of PM  
31 production from HO<sub>2</sub>-dominant to NO-dominant as well as increase the concentrations of  
32 oxidants in the atmosphere. Consequently, the oxidation of biogenic and anthropogenic precursor  
33 gases as well as the oxidative processing of pre-existing atmospheric PM can be accelerated. The  
34 combined set of results demonstrates the susceptibility of atmospheric chemistry, air quality, and  
35 associated climate forcing to anthropogenic perturbations over tropical forests.

1 **1. Introduction**

2 Secondary organic material (SOM) constitutes a large fraction of the atmospheric particle  
3 burden (Hallquist et al., 2009; Jimenez et al., 2009) and therefore has important effects on the  
4 Earth’s radiation balance, atmospheric visibility, and human health. SOM is a complex mixture  
5 of compounds resulting from many chemical pathways, and the processes underlying the  
6 production of SOM remain poorly understood. Models are especially challenged to accurately  
7 represent production of SOM in regions where there is a mix of biogenic and anthropogenic  
8 emissions (de Gouw et al., 2008; Glasius and Goldstein, 2016; Shrivastava et al., 2017). Possible  
9 shifts in the contributing mechanisms of SOM production between background and polluted  
10 conditions must be understood and quantified for distinct environments on the globe to test and  
11 enable accurate modeling predictions.

12 Several field observations, mainly in mid-latitudes of the Northern Hemisphere, and  
13 modeling efforts have suggested that the production of SOM from biogenic precursor  
14 compounds becomes more efficient in polluted air (Weber et al., 2007; Goldstein et al., 2009;  
15 Hoyle et al., 2011; Huang et al., 2014; Zhang et al., 2018). ~~Weber et al., 2007; Goldstein et al.,~~  
16 ~~2009; Hoyle et al., 2011; Huang et al., 2014; Zhang et al., 2018).~~ In the northeastern USA, de  
17 Gouw et al. (2005) showed that organic PM concentrations correlated well with anthropogenic  
18 tracers, yet the concentrations of anthropogenic precursors were insufficient to explain the  
19 observed PM. In the southeastern USA, observations suggested that organic PM was produced  
20 mainly from BVOCs, however modulated by anthropogenic emissions of NO<sub>x</sub> and SO<sub>2</sub> (Weber  
21 et al., 2007; Goldstein et al., 2009). concentrations of organic particulate matter (PM) correlated  
22 well with anthropogenic tracers, yet the concentrations of the anthropogenic precursors were  
23 insufficient to explain the observed PM concentrations. In the southeastern USA, radioisotope

24 [analysis of organic PM determined that 70% to 80% of the carbon mass had a modern origin](#)  
25 [even as correlations were observed between SOM mass concentrations and anthropogenic VOC](#)  
26 [and CO concentrations \(Weber et al., 2007\). This finding and those of further field studies in the](#)  
27 [region together suggested that the organic PM was produced mainly from biogenic VOCs](#)  
28 [\(BVOCs\) yet modulated by anthropogenic emissions of NO<sub>x</sub> and SO<sub>2</sub> \(Hu et al., 2015; Xu et al.,](#)  
29 [2015a; Xu et al., 2015b; Zhang et al., 2018\).](#) In the western USA, ground and aircraft  
30 measurements observed the highest organic PM increases when air masses having high [BVOC](#)  
31 ~~concentrations of biogenic VOCs (BVOCs)~~ intercepted anthropogenic emissions (Setyan et al.,  
32 2012; Shilling et al., 2013). A metastudy for several locations in the USA concluded that [air](#)  
33 [downwind of urban areas](#) had increased organic PM concentrations due to the photochemical  
34 production of SOM (De Gouw and Jimenez, 2009). Models have estimated that [50%](#) to 70% of  
35 the biogenic SOM mass concentration in several locations is modulated by anthropogenic  
36 emissions (Carlton et al., 2010; Heald et al., 2011; Spracklen et al., 2011). In addition, global-  
37 scale modeling studies have estimated an increase of 20% to 60% in the global annual mean  
38 SOM concentration relative to the pre-industrial period (Tsigaridis et al., 2006; Hoyle et al.,  
39 2009).

40 Many possible mechanisms may contribute to the effects of anthropogenic emissions on  
41 increased SOM production, including changes in gas-particle partitioning, new particle  
42 production and growth, and particle acidity. Changes in the concentrations of nitrogen oxides,  
43 however, should be regarded as a critical factor (Hoyle et al., 2011 and references therein).  
44 Different NO<sub>x</sub> regimes favor distinct gas-phase oxidation pathways, leading to different  
45 oxidation products and particle yields, as evidenced in isoprene photo-oxidation (Kroll et al.,  
46 2005, 2006; Hallquist et al., 2009; Worton et al., 2013; Liu et al., 2016b; Liu et al., 2016a). ~~For~~



47 [tropical forests, isoprene emissions are especially important in PM production \(Martin et al.,](#)  
48 [2010a; Chen et al., 2015\)](#)[Isoprene accounts for half of global BVOC mass emissions, and tropical](#)  
49 [forests are responsible for about 80% of terpenoid emissions \(Guenther et al., 2012\). In the](#)  
50 [Amazon, isoprene is the dominant BVOC emitted by vegetation and is estimated to contribute to](#)  
51 [about half of the organic PM concentrations under background conditions \(Kuhn et al., 2010;](#)  
52 [Chen et al., 2015; Yáñez-Serrano et al., 2015\)](#). Under HO<sub>2</sub>-dominant conditions (i.e., low NO<sub>x</sub>),  
53 isoprene epoxydiols (IEPOX) are produced in the gas phase and, through heterogenous reactions  
54 involving sulfate, PM is produced (Paulot et al., 2009; Surratt et al., 2010). Depending on the  
55 relative importance of increased concentrations of sulfate and NO<sub>x</sub> associated with pollution in a  
56 given region, an enhancement or suppression of IEPOX-derived PM production relative to  
57 background conditions may occur (Xu et al., 2015a; de Sá et al., 2017).

58 ~~Amazonia, the largest tropical forest in the world and a large global source of SOM, is~~  
59 ~~comparatively understudied relative to northern mid-latitude regions, especially with respect to~~  
60 ~~the influence of pollution on the SOM lifecycle (Martin et al., 2010a). Manaus, a city of over two~~  
61 ~~million people in the central Amazon, continuously releases an urban plume into an otherwise~~  
62 ~~mostly unperturbed region (Kuhn et al., 2010; Martin et al., 2017). The region downwind of~~  
63 ~~Manaus, especially in the wet season in the absence of regional fires (Artaxo et al., 2013), offers~~  
64 ~~a natural laboratory for the investigation of biogenic-anthropogenic interactions and the resulting~~  
65 ~~consequences for the amount and composition of PM in the region.~~ As part of GoAmazon2014/5,  
66 de Sá et al. (2017) demonstrated that PM derived from IEPOX generally decreased under  
67 polluted compared to background conditions downwind of Manaus. Nitrogen oxides in the  
68 pollution plume suppressed the production of isoprene hydroxyhydroperoxides (Liu et al.,  
69 2016b), leading to a decrease in the production of gas phase IEPOX and consequently of IEPOX-

70 derived PM (de Sá et al., 2017). ~~HEPOX-derived PM was the exclusive focus of de Sá et al.~~  
71 ~~(2017).~~

72 Amazonia, the largest tropical forest in the world and a large global source of SOM, is  
73 comparatively understudied relative to northern mid-latitude regions, especially with respect to  
74 the influence of pollution on the SOM lifecycle (Martin et al., 2010a). Manaus, a city of over two  
75 million people in the central Amazon, continuously releases an urban plume into an otherwise  
76 mostly unperturbed region (Kuhn et al., 2010; Martin et al., 2017). The region downwind of  
77 Manaus, especially in the wet season in the absence of regional fires (Artaxo et al., 2013), offers  
78 a natural laboratory for the investigation of biogenic-anthropogenic interactions and the resulting  
79 consequences for the amount and composition of PM in the region..

80 The present study investigates the influences of urban pollution on the concentration and  
81 composition of fine particles in central Amazonia, focusing on organic PM and its several  
82 component classes. The analysis employs data sets collected ~~during~~ in the wet season from  
83 February 1 to March 31, 2014, corresponding to the first Intensive Operating Period (IOP1) of  
84 the GoAmazon2014/5 experiment (Martin et al., 2016), ~~corresponding to the wet season during~~  
85 ~~the period of February 1 to March 31, 2014.~~ A separate publication is planned for IOP2,  
86 corresponding to the dry season period of August 15 to October 15, when biomass burning  
87 emissions were prevalent (de Sá et al., in preparation). Herein, positive-matrix factorization  
88 (PMF) of organic mass spectra measured by aerosol mass spectrometry (AMS) in conjunction  
89 with a clustering analysis of pollution indicators by Fuzzy c-means are employed to investigate  
90 the changes in particle concentration and composition associated with the influence of urban  
91 pollution downwind of Manaus.

## 92 **2. Methodology**

### 93 **2.1 Site description**

94 The primary site of this study, named “T3” (3.2133 °S, 60.5987 °W), was located 70 km  
95 to the west of Manaus, Brazil, in central Amazonia (Martin et al., 2016). The site was situated in  
96 a pasture of 2.5 km × 2 km surrounded by forest. [Based on modeled flow trajectories of the](#)  
97 [pollution plume, the T3 site intercepted the plume about 40% of the time \(Martin et al., 2017\).](#)  
98 Auxiliary sites “T0a” and “T0t”, served as references for background conditions in relation to T3  
99 (Figure S1). Site T0a (2.1466 °S, 59.0050 °W) refers to the Amazonian Tall Tower Observatory  
100 (ATTO; Andreae et al., 2015), located 150 km to the northeast of Manaus. Site T0t (2.5946°S,  
101 60.2093°W) was situated 60 km to the north-northwest of Manaus in the Cuieiras Biological  
102 Reserve (“ZF2”) and refers to tower “TT34”, established in 2008 for the AMAZE-08 experiment  
103 (Martin et al., 2010b). The T0 sites were typically upwind of Manaus, with only occasional  
104 transport of pollution to these sites (Andreae et al., 2015; Chen et al., 2015). Auxiliary site “T2”  
105 served as a reference for polluted conditions. This site was located just across the Rio Negro  
106 (3.1392°S, 60.1315°W), 8 km from the southwestern edge of Manaus and typically downwind of  
107 urban emissions during the daytime.

### 108 **2.2 Aerosol Mass Spectrometry**

109 Characterization of the atmospheric PM was obtained using a High-Resolution Time-of-  
110 Flight Aerosol Mass Spectrometer (hereafter AMS; Aerodyne, Inc., Billerica, Massachusetts,  
111 USA; DeCarlo et al., 2006; Canagaratna et al., 2007). Detailed aspects of the AMS operation in  
112 GoAmazon2014/5 were presented in de Sá et al. (2017). In brief, the instrument was housed  
113 within a temperature-controlled research container, and the inlet to the instrument sampled from  
114 5 m above ground level. Ambient measurements for this study were obtained every other 4 min.

115 The other 4 min were used for analysis of output from an oxidation flow reactor as presented in  
116 Palm et al. (2018).

117 Data analysis was performed using *SQUIRREL* (1.56D) and *PIKA* (1.14G) of the AMS  
118 software suite (Sueper and collaborators; DeCarlo et al., 2006). Organic, sulfate, ammonium,  
119 nitrate, and chloride PM mass concentrations were ~~obtained from “V-mode” data. The choice of~~  
120 ~~ions to fit was aided by “W-mode” data, which were collected for one of every five~~  
121 ~~days-quantified.~~ “Sulfate” and “nitrate” concentrations reported by the AMS may include  
122 contributions from both organic and inorganic species (Farmer et al., 2010; Liao et al., 2015).  
123 Organic and inorganic nitrate concentrations were estimated based on the ratio of  $\text{NO}_2^+$  to  $\text{NO}^+$   
124 signal intensity, as described in Section S2 (Fry et al., 2009; Farmer et al., 2010; Fry et al.,  
125 2013). The organic elemental ratios, O:C and H:C, were calculated following the methods of  
126 Canagaratna et al. (2015).

### 127 **2.3 Auxiliary measurements and datasets**

128 In complement to the AMS data set, the analysis herein incorporated auxiliary gas and  
129 particle measurements ~~from~~ collected during IOP1 at T3 (Martin et al., 2016). Mass  
130 concentrations of molecular and tracer organic species in the gas and particle phases were  
131 measured by a Semi-Volatile Thermal Desorption Aerosol Gas Chromatograph (SV-TAG) at a  
132 time resolution of one hour (Isaacman-VanWertz et al., 2016). Concentrations of volatile organic  
133 compounds (VOCs) were measured by a Proton-Transfer-Reaction Time-of-Flight Mass  
134 Spectrometer (PTR-ToF-MS; Liu et al., 2016b). In the Mobile Aerosol Observing System  
135 (MAOS) of the ARM Climate Research Facility (ACRF; Martin et al., 2016), measurements of  
136  $\text{NO}_y$  were made using a chemiluminescence-based instrument (Air Quality Design). The raw  
137  $\text{NO}_y$  measurements (10-s resolution) were averaged across 30-min intervals to dampen the

138 influence of brief local events. In addition, ozone concentrations were measured by an ultraviolet  
139 photometric analyzer (Thermo Fisher, model 49i, Ozone Analyzer). Particle number  
140 concentrations were measured by a Condensation Particle Counter (TSI, model 3772). Black  
141 carbon (BC) concentrations were measured both by a 7-wavelength aethalometer (Magee  
142 Scientific, model AE-31) and a Single Particle Soot Photometer (SP2; Droplet Measurement  
143 Techniques). The two datasets differed by a factor of up to three in absolute mass concentrations,  
144 as observed in other studies (Subramanian et al., 2007; Cappa et al., 2008; Lack et al., 2008), but  
145 they agreed well in the temporal trend. The analysis herein for BC is thus restricted to the  
146 temporal trends. Wind direction, solar irradiance, and precipitation rate were measured by the  
147 ARM Mobile Facility (AMF-1), which was also part of the ACRF.

148 Additional measurements from T0a, T0t, and T2 were also used in the analysis. At T2,  
149 non-refractory particle composition and concentration were measured by an Aerosol Chemical  
150 Speciation Monitor (ACSM; ~~Brito et al., in preparation~~.) during the wet season from March 9 to  
151 April 30, 2014 (Cirino et al., submitted). ACSM measurements were ~~also~~ made at T0a during the  
152 wet season of 2015 ~~(Carbone et al., in preparation)~~, from February 1 to March 31 (Andreae et  
153 al., 2015). Further AMS datasets collected ~~by AMS~~ at T0t during the wet season of 2008  
154 (February 6 to March 22; AMAZE-08 campaign) were used in the analysis (Chen et al.,  
155 2009; Schneider et al., 2011). ~~AMS measurements made onboard the G-1 aircraft of the ARM~~  
156 ~~Aerial Facility (AAF) during IOP1 also supported the analysis herein (Shilling et al., in~~  
157 ~~preparation)~~.

## 158 **2.4 Air mass backtrajectories and precipitation rates**

159 Simulations of two-day backward air mass trajectories, starting at 100 m above T3, were  
160 made using HYSPLIT4 (Draxler and Hess, 1998). Input meteorological data were obtained

161 from the Global Data Assimilation System (GDAS), provided by the NOAA Air Resources  
162 Laboratory (ARL), on a regular grid of  $0.5^\circ \times 0.5^\circ$ , 18 pressure levels, and 3-h intervals.  
163 Trajectory steps were calculated for every 12 min.

164 Information on precipitation along the trajectories was obtained from the S-band radar of  
165 the System for Amazon Protection (SIPAM) in Manaus (Machado et al., 2014). The radar had a  
166 beam width of  $1.8^\circ$ , and it scanned 17 elevation angles every 12 min. Data were recorded to a  
167 range of 240 km at 500-m gate spacing. The reflectivity fields were quality controlled to remove  
168 non-meteorological echo and calibrated against the satellite precipitation radar of the Tropical  
169 Rainfall Measuring Mission and Global Precipitation Measurement (TRMM-GPM; Kummerow  
170 et al., 1998; Hou et al., 2014). Ground clutter was used to analyze the stability of the calibration.  
171 The data were gridded at  $2 \text{ km} \times 2 \text{ km}$  in the horizontal and 0.5 km in the vertical using the  
172 NCAR *Radx* software. The reflectivity at 2.5 km in altitude was converted to rain rates based on  
173 the data sets of a Joss-Waldvogel disdrometer (Joss and Waldvogel, 1967), located at T3, 70 km  
174 downwind of the radar.

### 175 **3. Results and discussion**

#### 176 **3.1 Fine-mode PM composition**

177 The time series of mass concentrations of  $\text{PM}_{10}$  species at T3 during the wet season of  
178 2014 are plotted in Figure 1a. Organic material dominated the composition, contributing  $79 \pm 7\%$   
179 (average  $\pm$  one standard deviation), followed by sulfate ( $13 \pm 5\%$ ). The standard deviation  
180 quantifies the variability across the time series. Average non-refractory (NR)  $\text{PM}_{10}$  mass  
181 concentrations and compositions at T3 as well as at three other sites in the region are represented  
182 in Figure 1b. The two T0 sites corresponded to predominantly background conditions. By  
183 contrast, the T2 site represented conditions just downwind of Manaus, and depending on wind

184 direction experienced fresh Manaus pollution or background air. The comparison in Figure 1b  
185 demonstrates that the organic component consistently constituted 70% to 80% of NR-PM<sub>1</sub> across  
186 sites in this region in the wet season, for both background and polluted conditions, in line with  
187 previous observations (Chen et al., 2009; Martin et al., 2010a).

188 Even as the relative composition was similar across all sites, there were differences in the  
189 absolute mass concentrations (Figure 1b, top panel). The NR-PM<sub>1</sub> mass concentrations at the T0  
190 sites upwind of Manaus, although measured in different years, were approximately consistently  
191 around 1 µg m<sup>-3</sup>. The concentrations at the T2 site just downwind of Manaus were more than  
192 three times higher on average (3.3 µg m<sup>-3</sup>). Average concentrations at the T3 site (1.7 µg m<sup>-3</sup>),  
193 several hours downwind of Manaus, were lower compared to those at T2. This relative  
194 progression from T0, to T2, and then to T3 can be understood as a first-order quantification of  
195 the overall effect of Manaus emissions in increasing the airborne PM burden in the downwind  
196 region.

197 The diel trends of organic and sulfate mass concentrations as well as their variabilities  
198 across the four sites are shown in Figure 2. Lines represent means, solid markers show medians,  
199 and boxes span interquartile ranges. Organic mass concentrations and associated variability were  
200 higher at the T3 site compared to the T0 sites, markedly so in the afternoon hours. The greater  
201 variability at T3 is in line with a time-varying influence of Manaus emissions. This influence  
202 waxes and wanes with small northerly or southerly shifts of the trade winds as well as other  
203 changes in regional circulation tied to daily meteorology (Cirino et al., submitted); (dos Santos et  
204 al., 2014; Martin et al., 2017). The higher afternoon mass concentrations at T3 can be attributed  
205 to a combination of (i) an oxidant-rich, sunlight-fed plume that increases the production rate of  
206 secondary PM and (ii) faster near-surface winds during the day that transport PM from Manaus

207 to T3 with less loss by deposition and dispersion compared to more-stagnant air at night. Among  
208 all sites, the T2 observations had both the highest average organic mass concentrations and the  
209 largest variability. These characteristics of the T2 dataset can be explained by a combination of  
210 (i) the proximity of the site to Manaus, (ii) the rapid and 180° changes in wind direction caused  
211 by the intersection of the trade winds with a local river breeze (dos Santos et al., 2014), and (iii)  
212 possible contributions of emissions from brick kilns, located mostly southwest of the site,  
213 especially during night time (Martin et al., 2016; Cirino et al., submitted).

214 The diel trends of the sulfate mass concentrations were in large part similar to those of  
215 the organic mass concentrations. One distinction in the case of sulfate, however, is that the  
216 variability at the T0 sites is similar to that at the T3 site. The explanation is that the background  
217 sources of sulfate, including not only in-basin emissions but also out-of-basin long-range  
218 transport, are variable and significant enough to make the variability at the background sites  
219 similar to that at the T3 site (de Sá et al., 2017).

220 Overall, the organic PM<sub>1</sub> at T3 was highly oxidized, as indicated by the position of gray  
221 markers in the plot of Figure 3. By contrast, the blue markers represent the dataset collected at  
222 T2 during the same period. The datasets encompass all times of days and all conditions at both  
223 sites. Datasets from background sites collected in different years are shown in Figure S2. Points  
224 to the upper left represent more oxidized material, and points to the lower right represent less  
225 oxidized material (Ng et al., 2011a). The comparison depicted in Figure 3 ~~illustrates the effects~~  
226 ~~of the plume over the 4 h of transport from T2 to T3~~ (Cirino et al., submitted). indicates the  
227 effects of the plume over the 4 h of transport from T2 to T3, which were investigated in detail by  
228 Cirino et al. (submitted). The plot suggests that the enhanced oxidative cycle associated with  
229 higher OH and O<sub>3</sub> concentrations in the pollution plume might cause (i) the production of highly



230 oxidized SOM, from both biogenic and anthropogenic precursors including aromatic compounds  
231 (Chhabra et al., 2011; Lambe et al., 2011), and (ii) the accelerated oxidative processing of pre-  
232 existing organic PM by OH and O<sub>3</sub> (Martin et al., 2017). The implication is that the emissions  
233 from Manaus can significantly affect the mechanisms that produce or modify fine-mode PM over  
234 the tropical forest.

### 235 **3.2 Characterization of organic PM by positive-matrix factorization**

236 Positive-matrix factorization was applied to the time series of the organic component of  
237 the high-resolution “V-mode” mass spectra (Ulbrich et al., 2009c). Diagnostics of the PMF  
238 analysis are presented in the Supplement (Section S1; Figures S3 and S4). Herein, “factor  
239 profile” and “factor loading” refer to the mathematical products of the multivariate statistical  
240 analysis, whereas “mass spectrum” and “mass concentration” refer to direct measurements.

241 A six-factor solution was obtained based both on the numerical diagnostics of the PMF  
242 algorithm and the judged scientific meaningfulness of the resolved factors (Section S1). The  
243 factor profiles, diel trends of the factor loadings, and the time series of the factor loadings and  
244 other related measurements are plotted in Figures 4a, 4b, and 4c, respectively. The inset of  
245 Figure 4a shows the mean fractional loading contribution of each factor during the analysis  
246 period. The correlations of factor loadings with co-located measurements of gas- and particle-  
247 phase species are shown in Figure 5.

248 The scientific interpretation of each factor was based on a combination of (i) the  
249 characteristics of the factor profile (i.e., “mass spectrum”), as referenced to a worldwide database  
250 of AMS spectra and PMF analyses (Ulbrich et al., 2009c; Ulbrich et al., 2009a, 2009b), and (ii)  
251 the temporal correlations between the factor loading and other co-located measurements. Three  
252 factors interpreted as primary emissions of organic PM were resolved: an anthropogenic-

253 dominated factor (hereafter, “ADOA”), a biomass burning factor (“BBOA”), and a fossil-fuel  
254 hydrocarbon-like factor (“HOA”). Three factors interpreted as secondary production and  
255 processing were resolved: a more-oxidized oxygenated factor (“MO-OOA”), a less-oxidized  
256 oxygenated factor (“LO-OOA”), and an isoprene epoxydiols-derived factor (“IEPOX-SOA”).

257         The HOA factor profile had characteristic ions of  $C_4H_7^+$  and  $C_4H_9^+$  at nominal values of  
258  $m/z$  55 and 57, respectively (Figure 4a). It had an oxygen-to-carbon (O:C) ratio of  $0.18 \pm 0.02$ ,  
259 the lowest among the six factors (Table 1). In line with the AMS PMF literature, the HOA factor  
260 represents a class of primary hydrocarbon-like organic compounds that are typically associated  
261 with traffic emissions (Zhang et al., 2005). In the present study, the HOA factor loadings  
262 accounted for 6% of the organic mass concentrations on average (Figure 4a, inset). As a point of  
263 comparison, the average in the southeastern USA typically varies from 9% to 15% (Xu et al.,  
264 2015b). The lower relative contribution of 6% in this study might in part be due to a larger  
265 relative role of secondary production in the environment of a tropical forest. In addition, the  
266 distance from Manaus to the T3 site might allow time for substantial vertical mixing, dilution,  
267 and subsequent evaporation of primary emissions into entrained background air (Robinson et al.,  
268 2007; Liu et al., accepted; Shilling et al., in preparation). Finally, the possible differences in  
269 emission profiles associated with different types of regional economic development between the  
270 Brazilian Amazon and [the southeastern](#) USA (e.g., fleet density, fuel matrix, industry, and so  
271 forth) should also be considered. The HOA factor loading decreased during the day, which can  
272 be explained by the growth of the planetary boundary layer (PBL) and the subsequent dilution of  
273 the concentrations of primary emissions (Figure 4b). The time series of HOA factor loading did  
274 not correlate well ( $R < 0.5$ ) with any of the co-located measurements at T3 (Figure 5). It is  
275 plotted alongside the time series of  $NO_y$  concentration in Figure 4c.

276 The BBOA factor profile was characterized by distinct peaks of  $C_2H_4O_2^+$  ( $m/z$  60) and  
277  $C_3H_5O_2^+$  ( $m/z$  73), as shown in Figure 4a. These peaks can be attributed to levoglucosan and  
278 other anhydrous sugars that result from biomass pyrolysis (Schneider et al., 2006; Cubison et al.,  
279 2011). Correlations of the factor loadings with the mass concentrations of levoglucosan and  
280 vanillin ( $R > 0.8$ ) measured by SV-TAG corroborate the association with biomass burning  
281 (Figure 4c). The BBOA factor of this study had an O:C ratio of  $0.61 \pm 0.08$  (Table 1), which is  
282 consistent with large contributions from levoglucosan (O:C of 0.83) and similar sugars. The  
283 factor loading on average accounted for 9% of the organic  $PM_1$  mass concentration (Figure 4a,  
284 inset). This result is consistent with the low incidence of fires in the Amazon during the wet  
285 season (Martin et al., 2016). The BBOA factor loading typically decreased during the day  
286 (Figure 4b), which is suggestive of the dilution of local sources during the development of the  
287 PBL rather than long-range transport. Emissions from local fires around T3, including trash and  
288 tree burning, as well as from wood-fueled brick kilns along the road from Manaus to T3 might  
289 have contributed to this factor.

290 The ADOA factor profile, distinguished prominently by the  $C_7H_7^+$  ion at  $m/z$  91, also had  
291 characteristic ions of  $C_4H_7^+$  at  $m/z$  55 and  $C_3H_5^+$  at  $m/z$  41 (Figure 4a). A peak at  $m/z$  91 can arise  
292 from many sources, including biogenic and anthropogenic emissions (Ng et al., 2011b). In itself,  
293  $m/z$  91 therefore does not serve as a tracer for a specific source or process without consideration  
294 of the atmospheric context. Factors having a characteristic  $m/z$  91 peak (usually labeled “91 fac”)  
295 typically have been associated with biogenic emissions (Robinson et al., 2011; Budisulistiorini et  
296 al., 2015; Chen et al., 2015; Riva et al., 2016). The ADOA factor profile of this study, however,  
297 more strongly resembles the mass spectra previously reported for PM emissions from cooking  
298 activities (Lanz et al., 2007; Mohr et al., 2012) than those from “91 fac” (Section S1; Figure S5).

299 The ratio of  $m/z$  55 to  $m/z$  57 of the ADOA factor was 4.1. This ratio lies in the range of 2 to 10  
300 reported for several factors representing primary cooking emissions and is well above the range  
301 of 0.8 to 1.4 reported for factors associated with traffic emissions, i.e., HOA (Mohr et al., 2012  
302 and references therein; Hu et al., 2016). Even though the ADOA factor profile has a large  
303 contribution from non-oxygenated ions, similar to [the HOA factor](#) and consistent with a  
304 dominance by primary emissions, it also contains considerable signal from oxygenated ions,  
305 resulting in a relatively higher O:C of  $0.40 \pm 0.05$  (Table 1). The factor loading on average  
306 accounted for 13% of the organic  $PM_{10}$  mass concentration (Figure 4a, inset). The factor loading  
307 decreased as the PBL developed during the day, consistent with dominant non-photochemical,  
308 primary sources (Figure 4b). Furthermore, there were increases, albeit small, in factor loading at  
309 12:00 and 18:00 (local time), suggestive of breakfast-time and lunch-time cooking activities in  
310 Manaus based on a transport time of 4 to 6 h between the city and the T3 site (Martin et al.,  
311 2016; Cirino et al., submitted). Manaus typically has four rush-hour periods each day from 6:30  
312 to 8:00, 12:00 to 13:30, 16:30 to 18:30, and 21:00 to 22:00. Traffic peaking at these hours may  
313 therefore also have contributed to the ADOA factor. Correlations between factor loading and  
314 external measurements exceeded  $R = 0.5$  for many anthropogenic markers, including  
315 concentrations of aromatics (e.g., benzene, toluene, and  $C_8$  and  $C_9$  species), carbon monoxide,  
316 particle count, and  $NO_y$  (Figure 4c, Figure 5). Contributions from secondary processes cannot be  
317 ruled out, and it is possible that PM production from anthropogenic VOCs might have also been  
318 captured in this factor. Overall, the ADOA factor was interpreted in the present study as an  
319 indicator of anthropogenic influence associated with several sources in Manaus, most  
320 importantly cooking and possibly traffic emissions.

321 The IEPOX-SOA factor profile had marker ions of  $C_4H_5^+$  ( $m/z$  53) and  $C_5H_6O^+$  ( $m/z$  82)  
322 (Figure 4a; Lin et al., 2012; Hu et al., 2015; de Sá et al., 2017). It had an O:C ratio of  $0.9 \pm 0.10$   
323 (Table 1). The factor loading on average accounted for 17% of the organic  $PM_1$  mass  
324 concentration (Figure 4a, inset). There were high correlations ( $R > 0.8$ ) between factor loadings  
325 and concentrations of  $C_5$ -alkenetriols and 2-methyltetrols, which are markers of IEPOX-derived  
326 PM, produced by the photo-oxidation of isoprene under  $HO_2$ -dominant conditions (Surratt et al.,  
327 2010; Lin et al., 2012; Figure 4c). The increase in factor loading during daytime was consistent  
328 with a photochemical source (Figure 4b). There were also correlations between factor loadings  
329 and concentrations of sulfate and some acids, such as tricarballic acid (TCA; Figure 5), in  
330 agreement with the association of IEPOX-derived PM and sulfate/acidity observed in other  
331 studies (Budisulistiorini et al., 2013; Nguyen et al., 2014; Kuwata et al., 2015). Overall, this  
332 factor was therefore interpreted as representative of PM produced from isoprene photo-oxidation  
333 under  $HO_2$ -dominant conditions. The effects of urban pollution on the loadings of this factor  
334 were the focus of a previous publication (de Sá et al., 2017).

335 The two remaining factors, LO-OOA and MO-OOA, were also associated with secondary  
336 atmospheric processes. The LO-OOA and MO-OOA factors had O:C ratios of  $0.72 \pm 0.10$  and  
337  $1.09 \pm 0.17$ , respectively. The LO-OOA factor was characterized by the greatest ratio of signal  
338 intensity of the  $C_2H_3O^+$  ion ( $m/z$  43) to that of the  $CO_2^+$  ion ( $m/z$  44) (Figure 4a) compared to all  
339 other factors. This factor is usually attributed to lower-generation, less-oxidized, higher-volatility  
340 secondary organic PM (Jimenez et al., 2009). By comparison, the MO-OOA factor profile had  
341 the strongest  $CO_2^+$  ( $m/z$  44) peak among all factors (Figure 4a). This factor is usually attributed  
342 to higher-generation, more-oxidized, less-volatile secondary organic PM or extensively oxidized

343 primary PM of any type that has resided in the atmosphere for several days or more (Jimenez et  
344 al., 2009).

345 The LO-OOA factor loading on average accounted for 25% of the organic PM<sub>1</sub> mass  
346 concentration (Figure 4a, inset). The factor loading correlated better with the estimated  
347 concentrations of inorganic nitrate than with organic or total nitrate (Figure 5; Section S2 and  
348 Figure S6), which is consistent with the interpretation of the higher volatility associated with this  
349 factor (Jimenez et al., 2009; Zhang et al., 2011). The factor loading also correlated ( $R > 0.7$ ) with  
350 the concentrations of 2-methylglyceric acid and methyl-butyl-tricarboxylic acid (MBTCA),  
351 which are products of isoprene and monoterpene oxidation, respectively, under NO-dominant  
352 conditions (Figure 4c; Figure 5). The factor loading increased starting at 9:00 (local time) and  
353 peaked in the afternoon hours (Figure 4b). This diel trend, tied to the sunlight cycle, tracked the  
354 typical daily emission patterns of isoprene and monoterpenes from the surrounding forest  
355 (Yáñez-Serrano et al., 2015). The absence of a sharp decline at sunset and the higher variability  
356 at nighttime may also indicate a contribution by terpene ozonolysis. For these several reasons,  
357 the LO-OOA factor was interpreted herein as secondary organic PM produced mostly within  
358 several hours of observations by many possible pathways, including (i) the photo-oxidation of  
359 isoprene along non-IEPOX pathways, (ii) the photo-oxidation of terpenes and other biogenic  
360 VOCs along both HO<sub>2</sub>- and NO-dominant reaction pathways, (iii) the ozonolysis of terpenes, and  
361 (iv) the possible production of SOM from anthropogenic emissions from Manaus.

362 The MO-OOA factor loading on average accounted for 30% of the organic PM<sub>1</sub> mass  
363 concentration (Figure 4a, inset). The factor loading correlated ( $R > 0.7$ ) with the mass  
364 concentrations of several particle-phase carboxylic acids as well as the concentrations of sulfate,  
365 ammonium, and ozone (Figure 5). The time series of malic acid and ozone concentrations are

366 shown alongside the MO-OOA factor loadings in Figure 4c. Malic acid is a highly oxidized  
367 compound (O:C of 1.25), which may have many different sources (Röhrl and Lammel, 2002; van  
368 Pinxteren et al., 2014). The MO-OOA factor loading increased starting at 8:00 (local time;  
369 sunrise was at 6:00) and peaked between 10:00 and 16:00, with a large variability in the factor  
370 loadings in the afternoon hours among different days (Figure 4b). The afternoon increase and  
371 day-to-day variability were consistent with strong but variable photochemical processing leading  
372 to further oxidation of organic PM during the day, depending on daily weather. The high O:C of  
373  $1.09 \pm 0.17$  could also be indicative of production of PM from aromatic compounds emitted from  
374 Manaus (Chhabra et al., 2011; Lambe et al., 2011). Overall, this factor was interpreted to  
375 represent highly oxidized PM from multiple processes. Species initially associated with HOA,  
376 BBOA, ADOA, IEPOX-SOA, and LO-OOA factors may converge after sufficient atmospheric  
377 oxidation to become represented by the MO-OOA factor (Jimenez et al., 2009; Palm et al.,  
378 2018).

### 379 **3.3 Shifts in PM with anthropogenic influences**

#### 380 **3.3.1 Cluster Analysis**

381 To further investigate changes in the concentration and composition of PM associated  
382 with anthropogenic influences, a Fuzzy c-means (FCM) algorithm was applied to the time series  
383 of concentrations of particle number,  $\text{NO}_y$ , ozone, black carbon, and sulfate measurements at the  
384 T3 site (Bezdek et al., 1984). The analysis was fully independent of the PMF results. For each  
385 point in time, these concentrations represented the spatial coordinates of the data point. As  
386 discussed below, four clusters were identified. Based on measures of spatial similarity, the  
387 clustering algorithm attributed to each data point a degree of membership relative to each of the  
388 four clusters (Section S3; Figure S7 and Figure S8).

389           The scope of the clustering analysis was restricted to afternoon time points for which ten-  
390 hour air mass backtrajectories did not intersect significant precipitation and for which solar  
391 irradiance at T3 averaged over the previous 4 h was higher than  $200 \text{ W m}^{-2}$  (Section S3). This  
392 scope aimed at capturing fair-weather conditions and thereby minimizing the role of otherwise  
393 confounding processes, such as boundary layer dynamics and wet deposition. The elimination of  
394 trajectories having precipitation, however, should not be regarded as fully accurate given the  
395 uncertainties in the HYSPLIT trajectories. The scoped dataset spanned 24 afternoons.

396           Four clusters were identified based on minimization of the FCM objective function as  
397 well as a subjective assessment of meaningful interpretation of the set of clusters (Section S3).  
398 The FCM algorithm returned a matrix containing the degrees of membership (ranging from 0 to  
399 1) to each of the four clusters (columns) for each point in time (rows). For any given time point  
400 (i.e., row), the sum of its degrees of membership to clusters (i.e., sum across columns) was  
401 always unity, by definition. A collection of examples, representing 37% of the analyzed data  
402 points by FCM, is shown in Figure 6a. For times predominantly associated with only one cluster  
403 (e.g., Feb 9 and Feb 10), the corresponding air mass backtrajectories are plotted in Figure 7. The  
404 FCM algorithm also returned the coordinates of cluster centroids, which are listed in Table 2.

405           Two clusters of data were interpreted as “background” and labeled “Bkgd-1” and “Bkgd-  
406 2”. They were characterized by  $\text{NO}_y < 1 \text{ ppb}$ , ozone  $< 20 \text{ ppb}$ , and particle number  $< 1200 \text{ cm}^{-3}$   
407 (Table 2; Figure 6). The two clusters differed especially in that Bkgd-2 had significantly larger  
408 concentrations of sulfate and black carbon. A comparison of the datasets of Feb 13  
409 (predominantly Bkgd-1) and Feb 16 (predominantly Bkgd-2) in Figure 6 highlights these  
410 differences. Concentrations of sulfate and black carbon were  $0.15$  and  $0.10 \mu\text{g m}^{-3}$ , respectively,  
411 on Feb 13, compared to  $0.40$  and  $0.15 \mu\text{g m}^{-3}$  on Feb 16. The backtrajectories associated with



412 Bkgd-1 had both northeasterly and southeasterly components. The wind fields, out of line with  
413 the trade winds, may suggest passage through recent weather systems and may imply wet  
414 deposition, which in turn might explain lower gas and particle concentrations (Table 2). These  
415 recent weather systems might not have been excluded from the scoped dataset because of  
416 inaccuracies in the intersections of the backtrajectories with precipitation data, as discussed  
417 above, or because they were more distant than captured by the 10-h backtrajectories. Consistent  
418 with this hypothesis, the centroid value calculated for the 4-h averaged solar irradiance at T3  
419 (Section 3.3.2) was lower for Bkgd-1 ( $400 \text{ W m}^{-2}$ ) compared to the other clusters ( $600 \text{ W m}^{-2}$ ),  
420 suggesting an association of Bkgd-1 with overcast conditions. By comparison, the  
421 backtrajectories associated with Bkgd-2 were predominantly from the northeast, coming from the  
422 direction of the T0t and T0a sites (Figure 7), in line with the dominant trade winds of the wet  
423 season. The air masses of Bkgd-2 may have experienced less wet deposition and may represent  
424 more extensive atmospheric oxidation than those of Bkgd-1. They may also have carried PM  
425 contributions from out-of-basin sources, which would be consistent with the higher sulfate and  
426 black carbon concentrations of Bkgd-2 compared to Bkgd-1 (Chen et al., 2009; Pöhlker et al.,  
427 2017).

428 Two other clusters were interpreted as “polluted” and labeled “Pol-1” and “Pol-2”. They  
429 were characterized by concentrations of  $\text{NO}_y > 1 \text{ ppb}$ , ozone  $> 20 \text{ ppb}$ , and particle number  $>$   
430  $1200 \text{ cm}^{-3}$  (Table 2; Figure 6). The dataset of the afternoon of Mar 9 illustrates a shift in  
431 dominance from Pol-2 to Pol-1 (Figure 6). Although Pol-1 and Pol-2 both have high  
432 concentrations of sulfate and other pollutants, they differ in the extent of those high  
433 concentrations. The explanation may be that these clusters represent different source regions.  
434 Pol-1 may be associated with emissions from the northern region of Manaus, and Pol-2 may be

435 associated with emissions from the southern region of Manaus. Industry, power production, and  
436 oil refineries are concentrated in the southeastern region of Manaus (Figure S9; Medeiros et al.,  
437 2017). Population density and commercial activity is concentrated in the southwestern portion of  
438 the city where downtown is located (Figure S10). Aircraft observations show that concentrations  
439 of sulfate as well as other pollutants are higher in the urban outflow from the southern compared  
440 to the northern region of Manaus (Figure S10). Directional plots of SO<sub>2</sub> and particle number  
441 concentrations observed at the T2 site further demonstrate the heterogeneity in Manaus  
442 emissions (Figure S10). This hypothesis of a geographical difference in source regions  
443 qualitatively aligns with the differences in backtrajectories characteristic of times dominated by  
444 Pol-1 and Pol-2 (Figure 7). This interpretation does imply, however, that the backtrajectories  
445 may have a 20° inaccuracy. Such inaccuracy is reasonable for the application of HYSPLIT  
446 modeling in this region given (i) the absence of surface weather stations and (ii) the relatively  
447 large scale of input wind fields (i.e., 50 km) compared to the scale of modeling (i.e., 70 km from  
448 T3 to Manaus and a city cross section of 20 km).

### 449 **3.3.2 Comparison of PM among clusters**

450 The characteristic PM composition associated with each cluster was determined by  
451 calculating the centroid coordinates of the clusters for the AMS species and PMF factors  
452 (Section S3). The centroid coordinate of a cluster for a given variable is defined as a weighted  
453 mean of that variable across all points in time, where the weight is the degree of membership of  
454 each data point to that cluster. A comparison of PM<sub>1</sub> concentrations and compositions for the  
455 four clusters is shown in Figure 8. Values are listed in Table 2.

456 The NR-PM<sub>1</sub> mass concentrations increased by 25% to 200% in clusters Pol-1 and Pol-2  
457 compared to clusters Bkgd-1 and Bkgd-2 (Figure 8a). Increases in sulfate and associated

458 ammonium concentrations had a smaller yet non-negligible role in the increased PM<sub>1</sub> mass  
459 concentrations. Sources of sulfate other than Manaus sustain relatively high concentrations in the  
460 Amazon basin, as represented by the Bkgd-2 cluster (Chen et al., 2009; de Sá et al., 2017).  
461 Compared to these regional background concentrations (i.e., Bkgd-2 cluster), the increases in  
462 sulfate concentrations were significant only for air masses associated with the heavily  
463 industrialized and densely populated southern region of Manaus (i.e., Pol-2 cluster).

464         With respect to the composition of the organic PM, Figure 8b shows that the Bkgd-1  
465 cluster had large contribution from the LO-OOA factor. By comparison, the Bkgd-2 cluster had  
466 larger contributions from the MO-OOA and IEPOX-SOA factors. A comparison of 13 Feb and  
467 16 Feb of 2014 (Figure 6d) illustrates these findings. The low mass concentrations and the  
468 dominant contribution by the LO-OOA factor suggest that the Bkgd-1 cluster may represent  
469 conditions under which secondary organic PM was produced within recent hours through photo-  
470 oxidation of VOCs emitted by the forest and subsequent condensation of secondary organic  
471 material. The low sulfate concentrations for Bkgd-1 may rationalize the absence of a significant  
472 contribution by the IEPOX-SOA factor. Isoprene photo-oxidation may have contributed to PM  
473 production by pathways other than IEPOX uptake (Krechmer et al., 2015; Riva et al., 2016). By  
474 comparison, for Bkgd-2, the higher mass concentrations and the greater contributions by IEPOX-  
475 SOA and MO-OOA factors suggest that this cluster may represent conditions under which  
476 secondary organic PM was a combination of material produced both on that day as well as on  
477 previous days. During transport, the organic PM may have undergone extensive atmospheric  
478 oxidation by a combination of surface and condensed-phase chemistry, including cloud water  
479 processes (Carlton et al., 2006; Ervens et al., 2011; Hoyle et al., 2011; Perraud et al., 2012).

480 Concentrations and composition of the Bkgd-2 cluster may therefore represent an extensive  
481 geographical footprint.

482 The organic PM concentration and composition associated with the Pol-1 and Pol-2  
483 clusters were distinct from those of the Bkgd-1 and Bkgd-2 clusters (Figure 8). The mass  
484 concentrations of organic PM were greater by 25% to 150% for Pol-1 and Pol-2. According to  
485 the PMF factors (Figure 8b), the larger part of this increase in organic PM between the  
486 background and polluted clusters was tied to the production of secondary organic PM, although  
487 primary emissions also contributed significantly. By comparison, for both Bkgd-1 and Bkgd-2  
488 clusters, contributions by primary emissions were negligible, as indicated by the low summed  
489 contribution of factors of primary origin (i.e., ADOA, BBOA, and HOA) to the organic PM<sub>1</sub> (<  
490 10%). For Pol-1 and Pol-2, the ADOA factor loading on average accounted for 10% of the  
491 organic mass concentration at T3, serving as a strong marker of Manaus pollution. A comparison  
492 of [February 9 Feb](#) and [March 9 Mar](#) with [February 13 Feb](#) and [16 Feb](#) illustrates these findings  
493 (Figure 6d).

494 In regard to secondary organic PM, the IEPOX-SOA factor loading decreased by almost  
495 50% under polluted compared to background conditions. de Sá et al. (2017) attributed this  
496 decrease to the suppression of IEPOX production by elevated NO concentrations. This  
497 suppression typically outweighed possible enhancements in IEPOX uptake and subsequent PM  
498 production because of elevated sulfate concentrations. By contrast, the LO-OOA and MO-OOA  
499 factor loadings increased by 50% to 100% under polluted conditions. These increases exceeded  
500 the decrease in IEPOX-SOA factor loadings, resulting in a net increase of around 100% in mass  
501 concentration of secondary organic PM (Figure 8).

502           The shifts in the processes governing the production of secondary organic PM because of  
503 increased  $\text{NO}_x$ , OH, and  $\text{O}_3$  concentrations characteristic of the pollution plume were complex  
504 and non-linear (Figure 9a). Overall, the oxidation pathways were driven faster. The relatively  
505 high  $f_{\text{CO}_2^+}$  values and O:C ratios of all factors (Table 1), including those associated with primary  
506 emissions, compared to typical values at other locations worldwide (Canagaratna et al., 2015),  
507 corroborate this interpretation. Ozone concentrations in the plume increase by 200% to 300%,  
508 and hydroxyl radical concentrations increased by 250% or more (Liu et al., accepted). As  $\text{HO}_2$ -  
509 dominant pathways were inhibited, NO-dominant pathways became active. Increased oxidant  
510 concentrations may also have promoted additional multigenerational chemistry of semi- or  
511 intermediate-volatility species (Robinson et al., 2007). Oxidation of VOCs by aqueous-phase  
512 reactions, including in-cloud processing, and oxidation of biomass burning emissions may also  
513 have played roles to varying degrees on different days (Carlton et al., 2006; Ervens et al., 2011;  
514 Hoyle et al., 2011; Perraud et al., 2012). In addition, when primary and secondary PM mass  
515 concentrations increased, further uptake of oxidized semi-volatile molecules could have been  
516 thermodynamically favored according to partitioning theory, representing a positive feedback on  
517 the increase of mass concentrations (Pankow, 1994; Odum et al., 1996; Carlton et al., 2010).

518           The increase in the LO-OOA and MO-OOA factor loadings associated with Pol-1 and  
519 Pol-2 indicates that the net effect of this accelerated and modified chemistry was the quick  
520 production and further oxidation of secondary organic PM. Precursors may have included both  
521 the wide range of biogenic VOCs as well as contributions from anthropogenic precursors, such  
522 as gas-phase species from vehicle emissions or evaporated primary material (Nordin et al., 2013;  
523 Presto et al., 2014). The LO-OOA factor loading was important for the polluted conditions of  
524 Pol-1 and Pol-2 as well as for the clean conditions of Bkgd-1. This result is not necessarily

525 because of an in-common molecular composition but rather because of an in-common process,  
526 i.e., fresh production of secondary organic PM (Figure 9b). Likewise, the MO-OOA factor  
527 loading was important for Pol-1, Pol-2, and Bkgd-2 because this factor represented an in-  
528 common process, i.e., extensive oxidation (Figure 9b). In the case of the MO-OOA factor, there  
529 is also an overall in-common composition characterized by highly oxidized species even as  
530 precursor species and subsequent oxidation pathways differed (Jimenez et al., 2009).

531         The complexity of the real atmospheric processes, as illustrated in Figure 9, is to some  
532 extent captured by the instrumental and analytical tools herein employed. Positive-matrix  
533 factorization identified several broad classes of organic PM. Some PMF factors had sufficiently  
534 unique signatures that they could be associated to one specific source and/or process (e.g., HOA  
535 and IEPOX-SOA). Other factors, in contrast, represented a wide range of sources that shared in-  
536 common processes (e.g., LO-OOA and MO-OOA). The clustering analysis contextualized the  
537 PMF results and demonstrated that the effects of the urban pollution were neither limited to nor  
538 captured by a single PMF factor. Instead, the urban plume influenced several PMF factors in  
539 different ways and to different extents. The implication is that changes in the AMS spectral  
540 signature of the organic PM caused by polluted conditions may not be sufficiently unique to  
541 allow for its complete separation by PMF analysis alone, especially in respect to the production  
542 of secondary organic PM. In this context, the Fuzzy c-means analysis served herein as a useful  
543 tool to incorporate auxiliary datasets and thereby to further understand anthropogenic influences  
544 on PM production and characteristics.

#### 545 **4. Summary and conclusions**

546         Changes in the concentrations and the composition of fine-mode PM due to the influence  
547 of anthropogenic emissions were investigated for the Amazonian wet season. Organic material

548 dominated the submicron composition, consistently representing between 70% and 80% of the  
549 PM<sub>1</sub> mean mass concentration across measurement sites upwind and downwind of Manaus and  
550 across different levels of pollution. Absolute mass concentrations, however, varied significantly  
551 among sites. Average concentrations downwind of Manaus were 100% to 200% higher than  
552 those upwind. Furthest downwind at T3, the organic component was more oxidized compared to  
553 that at the T2 site.

554 Positive-matrix factorization and Fuzzy c-means clustering were applied to the datasets to  
555 obtain a composite analysis of the shifts in PM<sub>1</sub> concentrations and composition under polluted  
556 conditions. Based on the FCM clustering, every point in time at T3 was interpreted as being  
557 affected by a combination of four influences, as represented by four clusters. Two background  
558 (Bkgd-1 and Bkgd-2) and two polluted (Pol-1 and Pol-2) clusters were identified. Particle mass  
559 concentrations were double for polluted compared to background conditions. Contributions from  
560 secondary processes dominated (> 80%) for both background and polluted conditions.

561 In terms of primary emissions, absolute contributions increased by a factor of five or  
562 more under polluted conditions, corresponding to an increase from < 10% to 15% of total PM<sub>1</sub>.  
563 The ADOA factor loading increased over five-fold for the polluted compared to the background  
564 clusters, and this factor thus served as a strong tracer of Manaus pollution. BBOA and HOA  
565 factor loadings, associated with biomass burning and fossil fuels, respectively, increased by two-  
566 fold with pollution. The ADOA factor loading represented 61% to 76% of the total primary  
567 factor loadings for the Pol-1 and Pol-2 clusters.

568 As for the secondary processes, the analysis further finds that the pollution plume acted  
569 both to shift pathways of secondary organic PM production and to accelerate the atmospheric  
570 oxidation of pre-existing organic PM. The oxidation of biogenic PM precursors shifted from

571 HO<sub>2</sub>- to NO-dominant pathways, and the oxidation of anthropogenic precursors possibly  
572 contributed to increased PM concentrations. The IEPOX-SOA factor loadings were highest for  
573 the Bkgd-2 cluster, associated with long-range transport under background conditions, and  
574 decreased by almost 50% for the polluted clusters, in line with a shift of isoprene oxidation from  
575 HO<sub>2</sub>- to NO-dominant pathways. Concomitantly, the LO-OOA factor loading increased by more  
576 than 50% for these clusters, suggesting rapid in-plume production of secondary organic PM  
577 through several pathways. The LO-OOA factor was also important for the Bkgd-1 cluster,  
578 associated with fresh background conditions, which is suggestive of recent biogenic organic PM  
579 production. The MO-OOA factor had large relative contributions in the Bkgd-2, Pol-1, and Pol-2  
580 clusters, suggestive of significant oxidative processing associated with these clusters. Increases  
581 of up to 300% in the MO-OOA factor loadings for Pol-1 and Pol-2 relative to background  
582 conditions of Bkgd-1 showed the effects of an accelerated oxidation cycle, leading to highly  
583 oxidized PM downwind of Manaus. Based on this and related studies (Liu et al., 2016b; de Sá et  
584 al., 2017; Martin et al., 2017), the critical lever seems to be increased concentrations of nitrogen  
585 oxides in the pollution plume for both directly shifting and indirectly accelerating mechanisms of  
586 secondary organic PM production in central Amazonia during the wet season.

587         The altered composition under anthropogenic influences also affects the physical  
588 properties of the PM<sub>1</sub>. Bateman et al. (2017), using the results of the PMF analysis presented  
589 herein, reported a shift from predominantly liquid PM under background conditions to a  
590 considerable presence of non-liquid PM above 50% RH under polluted conditions. Non-liquid  
591 PM can have different reactive chemistry from liquid PM (Li et al., 2015; Liu et al., 2018). A  
592 linear relationship between the increase in particle rebound fraction and the sum of ADOA,  
593 BBOA, and HOA factor loadings had an  $R^2$  of 0.7. The highest individual correlation was with



594 the ADOA factor loading (Bateman, personal communication). In addition, Thalman et al.  
595 (2017), also using the PMF results reported herein, concluded that the larger relative contribution  
596 of secondary organic material during the daytime compared to the nighttime was the primary  
597 driver of the diel trend of higher particle hygroscopicity during the day compared to the night, as  
598 tied to cloud condensation nuclei (CCN) properties.

599         This study communicates a snapshot of the changes that occur in the atmospheric  
600 composition over a tropical forest because of regional urbanization. In the context of a forest in  
601 transition (Davidson et al., 2012), the findings herein provide a quantitative assessment of the  
602 effects of urban pollution on the forested surroundings of Manaus. The studied region and the  
603 observed changes in atmospheric composition represent a microcosm that might become more  
604 widespread through Amazonia as urbanization trends continue in the future. Further  
605 investigations of the specific chemical pathways and physical mechanisms that enhance PM  
606 production in the urban plume are warranted to understand what other pollutants are critical for  
607 control in the context of ongoing and future air quality regulation in the study region as well as  
608 for other tropical forested environments worldwide.

**Acknowledgments.** Institutional support was provided by the Central Office of the Large Scale Biosphere Atmosphere Experiment in Amazonia (LBA), the National Institute of Amazonian Research (INPA), and Amazonas State University (UEA). We acknowledge support from the Atmospheric Radiation Measurement (ARM) Climate Research Facility, a user facility of the United States Department of Energy (DOE, DE-SC0006680), Office of Science, sponsored by the Office of Biological and Environmental Research, and support from the Atmospheric System Research (ASR, DE-SC0011115, DE-SC0011105) program of that office. Additional funding was provided by the Amazonas State Research Foundation (FAPEAM 062.00568/2014 and 134/2016), the São Paulo State Research Foundation (FAPESP 2013/05014-0), the USA National Science Foundation (1106400 and 1332998), and the Brazilian Scientific Mobility Program (CsF/CAPES). S. S. de Sá acknowledges support by the Faculty for the Future Fellowship of the Schlumberger Foundation. BBP is grateful for a US EPA STAR Graduate Fellowship (FP-91761701-0). The authors thank Paulo Castillo for his assistance in quality-checking the black carbon data from MAOS. Data access from the Sistema de Proteção da Amazônia (SIPAM) is gratefully acknowledged. The research was conducted under scientific license 001030/2012-4 of the Brazilian National Council for Scientific and Technological Development (CNPq).

## References

- Andreae, M. O., Acevedo, O. C., Araùjo, A., Artaxo, P., Barbosa, C. G. G., Barbosa, H. M. J., Brito, J., Carbone, S., Chi, X., Cintra, B. B. L., da Silva, N. F., Dias, N. L., Dias-Júnior, C. Q., Ditas, F., Ditz, R., Godoi, A. F. L., Godoi, R. H. M., Heimann, M., Hoffmann, T., Kesselmeier, J., Könemann, T., Krüger, M. L., Lavric, J. V., Manzi, A. O., Lopes, A. P., Martins, D. L., Mikhailov, E. F., Moran-Zuloaga, D., Nelson, B. W., Nölscher, A. C., Santos Nogueira, D., Piedade, M. T. F., Pöhlker, C., Pöschl, U., Quesada, C. A., Rizzo, L. V., Ro, C. U., Ruckteschler, N., Sá, L. D. A., de Oliveira Sá, M., Sales, C. B., dos Santos, R. M. N., Saturno, J., Schöngart, J., Sörgel, M., de Souza, C. M., de Souza, R. A. F., Su, H., Targhetta, N., Tóta, J., Trebs, I., Trumbore, S., van Eijck, A., Walter, D., Wang, Z., Weber, B., Williams, J., Winderlich, J., Wittmann, F., Wolff, S., and Yáñez-Serrano, A. M.: The Amazon Tall Tower Observatory (ATTO): overview of pilot measurements on ecosystem ecology, meteorology, trace gases, and aerosols, *Atmos. Chem. Phys.*, 15, 10723-10776, 2015, 10.5194/acp-15-10723-2015.
- Artaxo, P., Rizzo, L. V., Brito, J. F., Barbosa, H. M. J., Arana, A., Sena, E. T., Cirino, G. G., Bastos, W., Martin, S. T., and Andreae, M. O.: Atmospheric aerosols in Amazonia and land use change: from natural biogenic to biomass burning conditions, *Faraday Disc.*, 165, 203-235, 2013, 10.1039/C3FD00052D.
- Bateman, A. P., Gong, Z., Harder, T. H., de Sá, S. S., Wang, B., Castillo, P., China, S., Liu, Y., O'Brien, R. E., Palm, B. B., Shiu, H. W., Cirino, G. G., Thalman, R., Adachi, K., Alexander, M. L., Artaxo, P., Bertram, A. K., Buseck, P. R., Gilles, M. K., Jimenez, J. L., Laskin, A., Manzi, A. O., Sedlacek, A., Souza, R. A. F., Wang, J., Zaveri, R., and Martin, S. T.: Anthropogenic influences on the physical state of submicron particulate matter over a tropical forest, *Atmos. Chem. Phys.*, 17, 1759-1773, 2017, 10.5194/acp-17-1759-2017.
- Bezdek, J. C., Ehrlich, R., and Full, W.: FCM: The fuzzy c-means clustering algorithm, *Computers & Geosciences*, 10, 191-203, 1984.
- Brito, J., Carbone, S., de Sá, S. S., Martin, S. T., and Artaxo, P., in preparation.
- Budisulistiorini, S. H., Canagaratna, M. R., Croteau, P. L., Marth, W. J., Baumann, K., Edgerton, E. S., Shaw, S. L., Knipping, E. M., Worsnop, D. R., Jayne, J. T., Gold, A., and Surratt, J. D.: Real-time continuous characterization of secondary organic aerosol derived from isoprene epoxydiols in downtown Atlanta, Georgia, using the Aerodyne Aerosol Chemical Speciation Monitor, *Environ. Sci. Technol.*, 47, 5686-5694, 2013, 10.1021/es400023n.
- Budisulistiorini, S. H., Li, X., Bairai, S. T., Renfro, J., Liu, Y., Liu, Y. J., McKinney, K. A., Martin, S. T., McNeill, V. F., Pye, H. O. T., Nenes, A., Neff, M. E., Stone, E. A., Mueller, S., Knote, C., Shaw, S. L., Zhang, Z., Gold, A., and Surratt, J. D.: Examining the effects of anthropogenic emissions on isoprene-derived secondary organic aerosol formation during the 2013 Southern Oxidant and Aerosol Study (SOAS) at the Look Rock, Tennessee ground site, *Atmos. Chem. Phys.*, 15, 8871-8888, 2015, 10.5194/acp-15-8871-2015.

- Canagaratna, M. R., Jayne, J. T., Jimenez, J. L., Allan, J. D., Alfarra, M. R., Zhang, Q., Onasch, T. B., Drewnick, F., Coe, H., Middlebrook, A., Delia, A., Williams, L. R., Trimborn, A. M., Northway, M. J., DeCarlo, P. F., Kolb, C. E., Davidovits, P., and Worsnop, D. R.: Chemical and microphysical characterization of ambient aerosols with the aerodyne aerosol mass spectrometer, *Mass Spectrom. Rev.*, 26, 185-222, 2007, 10.1002/mas.20115.
- Canagaratna, M. R., Jimenez, J. L., Kroll, J. H., Chen, Q., Kessler, S. H., Massoli, P., Hildebrandt Ruiz, L., Fortner, E., Williams, L. R., Wilson, K. R., Surratt, J. D., Donahue, N. M., Jayne, J. T., and Worsnop, D. R.: Elemental ratio measurements of organic compounds using aerosol mass spectrometry: characterization, improved calibration, and implications, *Atmos. Chem. Phys.*, 15, 253-272, 2015, 10.5194/acp-15-253-2015.
- Cappa, C. D., Lack, D. A., Burkholder, J. B., and Ravishankara, A. R.: Bias in filter-based aerosol light absorption measurements due to organic aerosol loading: evidence from laboratory Measurements, *Aerosol Sci Technol*, 42, 1022-1032, 2008, 10.1080/02786820802389285.
- Carbone, S., Brito, J., De Sá, S. S., Martin, S. T., and Artaxo, P., in preparation.
- Carlton, A. G., Turpin, B. J., Lim, H.-J., Altieri, K. E., and Seitzinger, S.: Link between isoprene and secondary organic aerosol (SOA): Pyruvic acid oxidation yields low volatility organic acids in clouds, *Geophys. Res. Lett.*, 33, L06822, 2006, 10.1029/2005GL025374.
- Carlton, A. G., Pinder, R. W., Bhave, P. V., and Pouliot, G. A.: To What Extent Can Biogenic SOA be Controlled?, *Environ. Sci. Technol.*, 44, 3376-3380, 2010, 10.1021/es903506b.
- Chen, Q., Farmer, D. K., Schneider, J., Zorn, S. R., Heald, C. L., Karl, T. G., Guenther, A., Allan, J. D., Robinson, N., Coe, H., Kimmel, J. R., Pauliquevis, T., Borrmann, S., Pöschl, U., Andreae, M. O., Artaxo, P., Jimenez, J. L., and Martin, S. T.: Mass spectral characterization of submicron biogenic organic particles in the Amazon Basin, *Geophys. Res. Lett.*, 36, L20806, 2009, 10.1029/2009GL039880.
- Chen, Q., Farmer, D. K., Rizzo, L. V., Pauliquevis, T., Kuwata, M., Karl, T. G., Guenther, A., Allan, J. D., Coe, H., Andreae, M. O., Pöschl, U., Jimenez, J. L., Artaxo, P., and Martin, S. T.: Submicron particle mass concentrations and sources in the Amazonian wet season (AMAZE-08), *Atmos. Chem. Phys.*, 15, 3687-3701, 2015, 10.5194/acp-15-3687-2015.
- Chhabra, P., Ng, N., Canagaratna, M., Corrigan, A., Russell, L., Worsnop, D., Flagan, R., and Seinfeld, J.: Elemental composition and oxidation of chamber organic aerosol, *Atmos. Chem. Phys.*, 11, 8827-8845, 2011.
- Cirino, G. G., Brito, J., Barbosa, H. J. M., Rizzo, L. V., Tunved, P., de Sá, S. S., Jimenez, J., Palm, B. B., Carbone, S., Lavric, J., Souza, R., Wolff, S., Walter, D., Tota, J., Oliveira, M., Martin, S. T., and Artaxo, P.: Observations of Manaus urban plume evolution and interaction with biogenic emissions in GoAmazon2014/5, *Atmos Environ*, submitted.
- Cubison, M. J., Ortega, A. M., Hayes, P. L., Farmer, D. K., Day, D., Lechner, M. J., Brune, W. H., Apel, E., Diskin, G. S., Fisher, J. A., Fuelberg, H. E., Hecobian, A., Knapp, D. J., Mikoviny, T., Riemer, D., Sachse, G. W., Sessions, W., Weber, R. J., Weinheimer, A. J., Wisthaler, A., and Jimenez, J. L.: Effects of aging on organic aerosol from open biomass burning smoke in aircraft and laboratory studies, *Atmos. Chem. Phys.*, 11, 12049-12064, 2011, 10.5194/acp-11-12049-2011.
- Davidson, E. A., de Araújo, A. C., Artaxo, P., Balch, J. K., Brown, I. F., Bustamante, M. M., Coe, M. T., DeFries, R. S., Keller, M., and Longo, M.: The Amazon basin in transition, *Nature*, 481, 321-328, 2012.

- De Gouw, J. and Jimenez, J. L.: Organic Aerosols in the Earth's Atmosphere, *Environ. Sci. Technol.*, 43, 7614-7618, 2009, 10.1021/es9006004.
- de Gouw, J. A., Middlebrook, A. M., Warneke, C., Goldan, P. D., Kuster, W. C., Roberts, J. M., Fehsenfeld, F. C., Worsnop, D. R., Canagaratna, M. R., Pszenny, A. A. P., Keene, W. C., Marchewka, M., Bertman, S. B., and Bates, T. S.: Budget of organic carbon in a polluted atmosphere: Results from the New England Air Quality Study in 2002, *J. Geophys. Res. Atmos.*, 110, D16305, 2005, 10.1029/2004JD005623.
- de Gouw, J. A., Brock, C. A., Atlas, E. L., Bates, T. S., Fehsenfeld, F. C., Goldan, P. D., Holloway, J. S., Kuster, W. C., Lerner, B. M., Matthew, B. M., Middlebrook, A. M., Onasch, T. B., Peltier, R. E., Quinn, P. K., Senff, C. J., Stohl, A., Sullivan, A. P., Trainer, M., Warneke, C., Weber, R. J., and Williams, E. J.: Sources of particulate matter in the northeastern United States in summer: 1. Direct emissions and secondary formation of organic matter in urban plumes, *J. Geophys. Res. Atmos.*, 113, D08301, 2008, 10.1029/2007JD009243.
- de Sá, S. S., Palm, B. B., Campuzano-Jost, P., Day, D. A., Newburn, M. K., Hu, W., Isaacman-VanWertz, G., Yee, L. D., Thalman, R., Brito, J., Carbone, S., Artaxo, P., Goldstein, A. H., Manzi, A. O., Souza, R. A. F., Mei, F., Shilling, J. E., Springston, S. R., Wang, J., Surratt, J. D., Alexander, M. L., Jimenez, J. L., and Martin, S. T.: Influence of urban pollution on the production of organic particulate matter from isoprene epoxydiols in central Amazonia, *Atmos. Chem. Phys.*, 17, 6611-6629, 2017, 10.5194/acp-17-6611-2017.
- de Sá, S. S., Wernis, R., Palm, B. B., Yee, L. D., Isaacman-vanWertz, G., and Martin, S. T., in preparation.
- DeCarlo, P. F., Kimmel, J. R., Trimborn, A., Northway, M. J., Jayne, J. T., Aiken, A. C., Gonin, M., Fuhrer, K., Horvath, T., Docherty, K. S., Worsnop, D. R., and Jimenez, J. L.: Field-deployable, high-resolution, time-of-flight aerosol mass spectrometer, *Anal. Chem.*, 78, 8281-8289, 2006, 10.1021/ac061249n.
- dos Santos, M. J., Silva Dias, M. A. F., and Freitas, E. D.: Influence of local circulations on wind, moisture, and precipitation close to Manaus City, Amazon Region, Brazil, *J. Geophys. Res. Atmos.*, 119, 213,233-213,249, 2014, 10.1002/2014JD021969.
- Draxler, R. and Hess, G.: An overview of the HYSPLIT\_4 modeling system for trajectories, dispersion, and deposition, *Aust. Met. Mag.*, 47, 295-308, 1998.
- Ervens, B., Turpin, B., and Weber, R.: Secondary organic aerosol formation in cloud droplets and aqueous particles (aqSOA): a review of laboratory, field and model studies, *Atmos. Chem. Phys.*, 11, 11069-11102, 2011, 10.5194/acp-11-11069-2011.
- Farmer, D. K., Matsunaga, A., Docherty, K. S., Surratt, J. D., Seinfeld, J. H., Ziemann, P. J., and Jimenez, J. L.: Response of an aerosol mass spectrometer to organonitrates and organosulfates and implications for atmospheric chemistry, *Proc. Natl. Acad. Sci. USA*, 107, 6670-6675, 2010, 10.1073/pnas.0912340107.
- Fry, J. L., Kiendler-Scharr, A., Rollins, A. W., Wooldridge, P. J., Brown, S. S., Fuchs, H., Dubé, W., Mensah, A., dal Maso, M., Tillmann, R., Dorn, H. P., Brauers, T., and Cohen, R. C.: Organic nitrate and secondary organic aerosol yield from NO<sub>3</sub> oxidation of β-pinene evaluated using a gas-phase kinetics/aerosol partitioning model, *Atmos. Chem. Phys.*, 9, 1431-1449, 2009, 10.5194/acp-9-1431-2009.
- Fry, J. L., Draper, D. C., Zarzana, K. J., Campuzano-Jost, P., Day, D. A., Jimenez, J. L., Brown, S. S., Cohen, R. C., Kaser, L., Hansel, A., Cappellin, L., Karl, T., Hodzic Roux, A.,

- Turnipseed, A., Cantrell, C., Lefer, B. L., and Grossberg, N.: Observations of gas- and aerosol-phase organic nitrates at BEACHON-RoMBAS 2011, *Atmos. Chem. Phys.*, 13, 8585-8605, 2013, 10.5194/acp-13-8585-2013.
- Glasius, M. and Goldstein, A. H.: Recent discoveries and future challenges in atmospheric organic chemistry, *Environ. Sci. Technol.*, 50, 2754-2764, 2016, 10.1021/acs.est.5b05105.
- Goldstein, A. H., Koven, C. D., Heald, C. L., and Fung, I. Y.: Biogenic carbon and anthropogenic pollutants combine to form a cooling haze over the southeastern United States, *Proc. Natl Acad. Sci. USA*, 106, 8835-8840, 2009, 10.1073/pnas.0904128106.
- Guenther, A., Jiang, X., Heald, C., Sakulyanontvittaya, T., Duhl, T., Emmons, L., and Wang, X.: The Model of Emissions of Gases and Aerosols from Nature version 2.1 (MEGAN2. 1): an extended and updated framework for modeling biogenic emissions, *Geosci. Model Dev.*, 5, 1471-1492, 2012, 10.5194/gmd-5-1471-2012.
- Hallquist, M., Wenger, J. C., Baltensperger, U., Rudich, Y., Simpson, D., Claeys, M., Dommen, J., Donahue, N. M., George, C., Goldstein, A. H., Hamilton, J. F., Herrmann, H., Hoffmann, T., Iinuma, Y., Jang, M., Jenkin, M. E., Jimenez, J. L., Kiendler-Scharr, A., Maenhaut, W., McFiggans, G., Mentel, T. F., Monod, A., Prévôt, A. S. H., Seinfeld, J. H., Surratt, J. D., Szmigielski, R., and Wildt, J.: The formation, properties and impact of secondary organic aerosol: current and emerging issues, *Atmos. Chem. Phys.*, 9, 5155-5236, 2009, 10.5194/acp-9-5155-2009.
- Heald, C. L., Coe, H., Jimenez, J. L., Weber, R. J., Bahreini, R., Middlebrook, A. M., Russell, L. M., Jolleys, M., Fu, T. M., Allan, J. D., Bower, K. N., Capes, G., Crosier, J., Morgan, W. T., Robinson, N. H., Williams, P. I., Cubison, M. J., DeCarlo, P. F., and Dunlea, E. J.: Exploring the vertical profile of atmospheric organic aerosol: comparing 17 aircraft field campaigns with a global model, *Atmos. Chem. Phys.*, 11, 12673-12696, 2011, 10.5194/acp-11-12673-2011.
- Hou, A. Y., Kakar, R. K., Neeck, S., Azarbarzin, A. A., Kummerow, C. D., Kojima, M., Oki, R., Nakamura, K., and Iguchi, T.: The Global Precipitation Measurement mission, *Bull. Am. Meteorol. Soc.*, 95, 701-722, 2014, 10.1175/bams-d-13-00164.1.
- Hoyle, C. R., Myhre, G., Berntsen, T. K., and Isaksen, I. S. A.: Anthropogenic influence on SOA and the resulting radiative forcing, *Atmos. Chem. Phys.*, 9, 2715-2728, 2009, 10.5194/acp-9-2715-2009.
- Hoyle, C. R., Boy, M., Donahue, N. M., Fry, J. L., Glasius, M., Guenther, A., Hallar, A. G., Huff Hartz, K., Petters, M. D., Petäjä, T., Rosenoern, T., and Sullivan, A. P.: A review of the anthropogenic influence on biogenic secondary organic aerosol, *Atmos. Chem. Phys.*, 11, 321-343, 2011, 10.5194/acp-11-321-2011.
- Hu, W., Hu, M., Hu, W., Jimenez, J. L., Yuan, B., Chen, W., Wang, M., Wu, Y., Chen, C., Wang, Z., Peng, J., Zeng, L., and Shao, M.: Chemical composition, sources, and aging process of submicron aerosols in Beijing: Contrast between summer and winter, *J. Geophys. Res. Atmos.*, 121, 1955-1977, 2016, 10.1002/2015JD024020.
- Hu, W. W., Campuzano-Jost, P., Palm, B. B., Day, D. A., Ortega, A. M., Hayes, P. L., Krechmer, J. E., Chen, Q., Kuwata, M., Liu, Y. J., de Sá, S. S., McKinney, K., Martin, S. T., Hu, M., Budisulistiorini, S. H., Riva, M., Surratt, J. D., St. Clair, J. M., Isaacman-Van Wertz, G., Yee, L. D., Goldstein, A. H., Carbone, S., Brito, J., Artaxo, P., de Gouw, J. A., Koss, A., Wisthaler, A., Mikoviny, T., Karl, T., Kaser, L., Jud, W., Hansel, A., Docherty, K. S., Alexander, M. L., Robinson, N. H., Coe, H., Allan, J. D., Canagaratna, M. R.,

- Paulot, F., and Jimenez, J. L.: Characterization of a real-time tracer for isoprene epoxydiols-derived secondary organic aerosol (IEPOX-SOA) from aerosol mass spectrometer measurements, *Atmos. Chem. Phys.*, 15, 11807-11833, 2015, 10.5194/acp-15-11807-2015.
- Huang, R.-J., Zhang, Y., Bozzetti, C., Ho, K.-F., Cao, J.-J., Han, Y., Daellenbach, K. R., Slowik, J. G., Platt, S. M., Canonaco, F., Zotter, P., Wolf, R., Pieber, S. M., Bruns, E. A., Crippa, M., Ciarelli, G., Piazzalunga, A., Schwikowski, M., Abbaszade, G., Schnelle-Kreis, J., Zimmermann, R., An, Z., Szidat, S., Baltensperger, U., Haddad, I. E., and Prevot, A. S. H.: High secondary aerosol contribution to particulate pollution during haze events in China, *Nature*, 514, 218-222, 2014, 10.1038/nature13774.
- Isaacman-VanWertz, G., Yee, L. D., Kreisberg, N. M., Wernis, R., Moss, J. A., Hering, S. V., de Sá, S. S., Martin, S. T., Alexander, M. L., Palm, B. B., Hu, W., Campuzano-Jost, P., Day, D. A., Jimenez, J. L., Riva, M., Surratt, J. D., Viegas, J., Manzi, A., Edgerton, E., Baumann, K., Souza, R., Artaxo, P., and Goldstein, A. H.: Ambient Gas-Particle Partitioning of Tracers for Biogenic Oxidation, *Environ. Sci. Technol.*, 9952-9962, 2016, 10.1021/acs.est.6b01674.
- Jimenez, J. L., Canagaratna, M. R., Donahue, N. M., Prevot, A. S. H., Zhang, Q., Kroll, J. H., DeCarlo, P. F., Allan, J. D., Coe, H., Ng, N. L., Aiken, A. C., Docherty, K. S., Ulbrich, I. M., Grieshop, A. P., Robinson, A. L., Duplissy, J., Smith, J. D., Wilson, K. R., Lanz, V. A., Hueglin, C., Sun, Y. L., Tian, J., Laaksonen, A., Raatikainen, T., Rautiainen, J., Vaattovaara, P., Ehn, M., Kulmala, M., Tomlinson, J. M., Collins, D. R., Cubison, M. J., Dunlea, J., Huffman, J. A., Onasch, T. B., Alfarra, M. R., Williams, P. I., Bower, K., Kondo, Y., Schneider, J., Drewnick, F., Borrmann, S., Weimer, S., Demerjian, K., Salcedo, D., Cottrell, L., Griffin, R., Takami, A., Miyoshi, T., Hatakeyama, S., Shimojo, A., Sun, J. Y., Zhang, Y. M., Dzepina, K., Kimmel, J. R., Sueper, D., Jayne, J. T., Herndon, S. C., Trimborn, A. M., Williams, L. R., Wood, E. C., Middlebrook, A. M., Kolb, C. E., Baltensperger, U., and Worsnop, D. R.: Evolution of organic aerosols in the atmosphere, *Science*, 326, 1525-1529, 2009, 10.1126/science.1180353.
- Joss, J. and Waldvogel, A.: Ein Spektrograph für Niederschlagstropfen mit automatischer Auswertung, *Pure and Applied Geophysics*, 68, 240-246, 1967, 10.1007/BF00874898.
- Krechmer, J. E., Coggon, M. M., Massoli, P., Nguyen, T. B., Crounse, J. D., Hu, W., Day, D. A., Tyndall, G. S., Henze, D. K., Rivera-Rios, J. C., Nowak, J. B., Kimmel, J. R., Mauldin, R. L., Stark, H., Jayne, J. T., Sipilä, M., Junninen, H., Clair, J. M. S., Zhang, X., Feiner, P. A., Zhang, L., Miller, D. O., Brune, W. H., Keutsch, F. N., Wennberg, P. O., Seinfeld, J. H., Worsnop, D. R., Jimenez, J. L., and Canagaratna, M. R.: Formation of low volatility organic compounds and secondary organic aerosol from isoprene hydroxyhydroperoxide low-NO oxidation, *Environ. Sci. Technol.*, 49, 10330-10339, 2015, 10.1021/acs.est.5b02031.
- Kroll, J. H., Ng, N. L., Murphy, S. M., Flagan, R. C., and Seinfeld, J. H.: Secondary organic aerosol formation from isoprene photooxidation under high-NO<sub>x</sub> conditions, *Geophys. Res. Lett.*, 32, 2005, 10.1029/2005GL023637.
- Kroll, J. H., Ng, N. L., Murphy, S. M., Flagan, R. C., and Seinfeld, J. H.: Secondary organic aerosol formation from isoprene photooxidation, *Environ. Sci. Technol.*, 40, 1869-1877, 2006, 10.1021/es0524301.
- Kuhn, U., Ganzeveld, L., Thielmann, A., Dindorf, T., Schebeske, G., Welling, M., Sciare, J., Roberts, G., Meixner, F. X., Kesselmeier, J., Lelieveld, J., Kolle, O., Ciccioli, P., Lloyd,

- J., Trentmann, J., Artaxo, P., and Andreae, M. O.: Impact of Manaus City on the Amazon Green Ocean atmosphere: ozone production, precursor sensitivity and aerosol load, *Atmos. Chem. Phys.*, 10, 9251-9282, 2010, 10.5194/acp-10-9251-2010.
- Kummerow, C., Barnes, W., Kozu, T., Shiue, J., and Simpson, J.: The Tropical Rainfall Measuring Mission (TRMM) sensor package, *J. Atmos. Ocea. Technol.*, 15, 809-817, 1998, 10.1175/1520-0426(1998)015<0809:ttrmmt>2.0.co;2.
- Kuwata, M., Liu, Y., McKinney, K., and Martin, S. T.: Physical state and acidity of inorganic sulfate can regulate the production of secondary organic material from isoprene photooxidation products, *Phys. Chem. Chem. Phys.*, 17, 5670-5678, 2015, 10.1039/C4CP04942J.
- Lack, D. A., Cappa, C. D., Covert, D. S., Baynard, T., Massoli, P., Sierau, B., Bates, T. S., Quinn, P. K., Lovejoy, E. R., and Ravishankara, A. R.: Bias in filter-based aerosol light absorption measurements due to organic aerosol loading: evidence from ambient measurements, *Aerosol Sci Technol*, 42, 1033-1041, 2008, 10.1080/02786820802389277.
- Lambe, A. T., Onasch, T. B., Massoli, P., Croasdale, D. R., Wright, J. P., Ahern, A. T., Williams, L. R., Worsnop, D. R., Brune, W. H., and Davidovits, P.: Laboratory studies of the chemical composition and cloud condensation nuclei (CCN) activity of secondary organic aerosol (SOA) and oxidized primary organic aerosol (OPOA), *Atmos. Chem. Phys.*, 11, 8913-8928, 2011, 10.5194/acp-11-8913-2011.
- Lanz, V. A., Alfara, M. R., Baltensperger, U., Buchmann, B., Hueglin, C., and Prévôt, A. S. H.: Source apportionment of submicron organic aerosols at an urban site by factor analytical modelling of aerosol mass spectra, *Atmos. Chem. Phys.*, 7, 1503-1522, 2007, 10.5194/acp-7-1503-2007.
- Li, Y. J., Liu, P., Gong, Z., Wang, Y., Bateman, A. P., Bergoend, C., Bertram, A. K., and Martin, S. T.: Chemical reactivity and liquid/nonliquid states of secondary organic material, *Environ. Sci. Technol.*, 49, 13264-13274, 2015, 10.1021/acs.est.5b03392.
- Liao, J., Froyd, K. D., Murphy, D. M., Keutsch, F. N., Yu, G., Wennberg, P. O., St. Clair, J. M., Crounse, J. D., Wisthaler, A., Mikoviny, T., Jimenez, J. L., Campuzano-Jost, P., Day, D. A., Hu, W., Ryerson, T. B., Pollack, I. B., Peischl, J., Anderson, B. E., Ziemba, L. D., Blake, D. R., Meinardi, S., and Diskin, G.: Airborne measurements of organosulfates over the continental US, *J. Geophys. Res. Atmos.*, 120, 2990-3005, 2015, 10.1002/2014JD022378.
- Lin, Y.-H., Zhang, Z., Docherty, K. S., Zhang, H., Budisulistiorini, S. H., Rubitschun, C. L., Shaw, S. L., Knipping, E. M., Edgerton, E. S., Kleindienst, T. E., Gold, A., and Surratt, J. D.: Isoprene epoxydiols as precursors to secondary organic aerosol formation: acid-catalyzed reactive uptake studies with authentic compounds, *Environ. Sci. Technol.*, 46, 250-258, 2012, 10.1021/es202554c.
- Liu, J., D'Ambro, E. L., Lee, B. H., Lopez-Hilfiker, F. D., Zaveri, R. A., Rivera-Rios, J. C., Keutsch, F. N., Iyer, S., Kurten, T., Zhang, Z., Gold, A., Surratt, J. D., Shilling, J. E., and Thornton, J. A.: Efficient isoprene secondary organic aerosol formation from a non-IEPOX pathway, *Environ. Sci. Technol.*, 2016a, 10.1021/acs.est.6b01872.
- Liu, P., Li, Y. J., Wang, Y., Bateman, A. P., Zhang, Y., Gong, Z., Bertram, A. K., and Martin, S. T.: Highly viscous states affect the browning of atmospheric organic particulate matter, *ACS Cent Sci*, 2018, 10.1021/acscentsci.7b00452.



- Liu, Y., Brito, J., Dorris, M. R., Rivera-Rios, J. C., Seco, R., Bates, K. H., Artaxo, P., Duvoisin, S., Keutsch, F. N., Kim, S., Goldstein, A. H., Guenther, A. B., Manzi, A. O., Souza, R. A. F., Springston, S. R., Watson, T. B., McKinney, K. A., and Martin, S. T.: Isoprene photochemistry over the Amazon rain forest, *Proc. Natl. Acad. Sci. USA*, 113, 6125-6130, 2016b, 10.1073/pnas.1524136113.
- Liu, Y., Seco, R., Kim, S., Guenther, A. B., Goldstein, A. H., Keutsch, F. N., Springston, S. R., Watson, T. B., Artaxo, P., Souza, R. A. F., McKinney, K. A., and Martin, S. T.: Isoprene photo-oxidation products quantify the effect of pollution on hydroxyl radicals over Amazonia, *Science Advances*, accepted.
- Machado, L. A. T., Dias, M. A. F. S., Morales, C., Fisch, G., Vila, D., Albrecht, R., Goodman, S. J., Calheiros, A. J. P., Biscaro, T., Kummerow, C., Cohen, J., Fitzjarrald, D., Nascimento, E. L., Sakamoto, M. S., Cunningham, C., Chaboureau, J.-P., Petersen, W. A., Adams, D. K., Baldini, L., Angelis, C. F., Sapucci, L. F., Salio, P., Barbosa, H. M. J., Landulfo, E., Souza, R. A. F., Blakeslee, R. J., Bailey, J., Freitas, S., Lima, W. F. A., and Tokay, A.: The Chuva Project: how does convection vary across Brazil?, *Bull. Am. Meteorol. Soc.*, 95, 1365-1380, 2014, 10.1175/bams-d-13-00084.1.
- Martin, S. T., Andreae, M. O., Artaxo, P., Baumgardner, D., Chen, Q., Goldstein, A. H., Guenther, A., Heald, C. L., Mayol-Bracero, O. L., McMurry, P. H., Pauliquevis, T., Pöschl, U., Prather, K. A., Roberts, G. C., Saleska, S. R., Silva Dias, M. A., Spracklen, D. V., Swietlicki, E., and Trebs, I.: Sources and properties of Amazonian aerosol particles, *Rev. Geophys.*, 48, RG2012, 2010a, 10.1029/2008RG000280.
- Martin, S. T., Andreae, M. O., Althausen, D., Artaxo, P., Baars, H., Borrmann, S., Chen, Q., Farmer, D. K., Guenther, A., Gunthe, S. S., Jimenez, J. L., Karl, T., Longo, K., Manzi, A., Müller, T., Pauliquevis, T., Petters, M. D., Prenni, A. J., Pöschl, U., Rizzo, L. V., Schneider, J., Smith, J. N., Swietlicki, E., Tota, J., Wang, J., Wiedensohler, A., and Zorn, S. R.: An overview of the Amazonian aerosol characterization experiment 2008 (AMAZE-08), *Atmos. Chem. Phys.*, 10, 11415-11438, 2010b, 10.5194/acp-10-11415-2010.
- Martin, S. T., Artaxo, P., Machado, L. A. T., Manzi, A. O., Souza, R. A. F., Schumacher, C., Wang, J., Andreae, M. O., Barbosa, H. M. J., Fan, J., Fisch, G., Goldstein, A. H., Guenther, A., Jimenez, J. L., Pöschl, U., Silva Dias, M. A., Smith, J. N., and Wendisch, M.: Introduction: observations and modeling of the green ocean Amazon (GoAmazon2014/5), *Atmos. Chem. Phys.*, 16, 4785-4797, 2016, 10.5194/acp-16-4785-2016.
- Martin, S. T., Artaxo, P., Machado, L., Manzi, A. O., Souza, R. A. F., Schumacher, C., Wang, J., Biscaro, T., Brito, J., Calheiros, A., Jardine, K., Medeiros, A., Portela, B., Sá, S. S. d., Adachi, K., Aiken, A. C., Albrecht, R., Alexander, L., Andreae, M. O., Barbosa, H. M. J., Buseck, P., Chand, D., Comstock, J. M., Day, D. A., Dubey, M., Fan, J., Fast, J., Fisch, G., Fortner, E., Giangrande, S., Gilles, M., Goldstein, A. H., Guenther, A., Hubbe, J., Jensen, M., Jimenez, J. L., Keutsch, F. N., Kim, S., Kuang, C., Laskin, A., McKinney, K., Mei, F., Miller, M., Nascimento, R., Pauliquevis, T., Pekour, M., Peres, J., Petäjä, T., Pöhlker, C., Pöschl, U., Rizzo, L., Schmid, B., Shilling, J. E., Dias, M. A. S., Smith, J. N., Tomlinson, J. M., Tóta, J., and Wendisch, M.: The Green Ocean Amazon Experiment (GoAmazon2014/5) observes pollution affecting gases, aerosols, clouds, and rainfall over the rain forest, *Bulletin of the American Meteorological Society*, 98, 981-997, 2017, 10.1175/bams-d-15-00221.1.

- Medeiros, A. S. S., Calderaro, G., Guimarães, P. C., Magalhaes, M. R., Morais, M. V. B., Rafee, S. A. A., Ribeiro, I. O., Andreoli, R. V., Martins, J. A., Martins, L. D., Martin, S. T., and Souza, R. A. F.: Power plant fuel switching and air quality in a tropical, forested environment, *Atmos. Chem. Phys.*, 17, 8987-8998, 2017, 10.5194/acp-17-8987-2017.
- Mohr, C., DeCarlo, P. F., Heringa, M. F., Chirico, R., Slowik, J. G., Richter, R., Reche, C., Alastuey, A., Querol, X., Seco, R., Peñuelas, J., Jiménez, J. L., Crippa, M., Zimmermann, R., Baltensperger, U., and Prévôt, A. S. H.: Identification and quantification of organic aerosol from cooking and other sources in Barcelona using aerosol mass spectrometer data, *Atmos. Chem. Phys.*, 12, 1649-1665, 2012, 10.5194/acp-12-1649-2012.
- Ng, N., Canagaratna, M., Jimenez, J., Chhabra, P., Seinfeld, J., and Worsnop, D.: Changes in organic aerosol composition with aging inferred from aerosol mass spectra, *Atmos. Chem. Phys.*, 11, 6465-6474, 2011a, 10.5194/acp-11-6465-2011.
- Ng, N. L., Canagaratna, M. R., Jimenez, J. L., Zhang, Q., Ulbrich, I. M., and Worsnop, D. R.: Real-time methods for estimating organic component mass concentrations from aerosol mass spectrometer data, *Environ. Sci. Technol.*, 45, 910-916, 2011b, 10.1021/es102951k.
- Nguyen, T. B., Coggon, M. M., Bates, K. H., Zhang, X., Schwantes, R. H., Schilling, K. A., Loza, C. L., Flagan, R. C., Wennberg, P. O., and Seinfeld, J. H.: Organic aerosol formation from the reactive uptake of isoprene epoxydiols (IEPOX) onto non-acidified inorganic seeds, *Atmos. Chem. Phys.*, 14, 3497-3510, 2014, 10.5194/acp-14-3497-2014.
- Nordin, E. Z., Eriksson, A. C., Roldin, P., Nilsson, P. T., Carlsson, J. E., Kajos, M. K., Hellén, H., Wittbom, C., Rissler, J., Löndahl, J., Swietlicki, E., Svenningsson, B., Bohgard, M., Kulmala, M., Hallquist, M., and Pagels, J. H.: Secondary organic aerosol formation from idling gasoline passenger vehicle emissions investigated in a smog chamber, *Atmos. Chem. Phys.*, 13, 6101-6116, 2013, 10.5194/acp-13-6101-2013.
- Odum, J. R., Hoffmann, T., Bowman, F., Collins, D., Flagan, R. C., and Seinfeld, J. H.: Gas/particle partitioning and secondary organic aerosol yields, *Environ. Sci. Technol.*, 30, 2580-2585, 1996, 10.1021/es950943+.
- Palm, B. B., de Sá, S. S., Day, D. A., Campuzano-Jost, P., Hu, W., Seco, R., Sjostedt, S. J., Park, J. H., Guenther, A. B., Kim, S., Brito, J., Wurm, F., Artaxo, P., Thalman, R., Wang, J., Yee, L. D., Wernis, R., Isaacman-VanWertz, G., Goldstein, A. H., Liu, Y., Springston, S. R., Souza, R., Newburn, M. K., Alexander, M. L., Martin, S. T., and Jimenez, J. L.: Secondary organic aerosol formation from ambient air in an oxidation flow reactor in central Amazonia, *Atmos. Chem. Phys.*, 18, 467-493, 2018, 10.5194/acp-18-467-2018.
- Pankow, J. F.: An absorption model of gas/particle partitioning of organic compounds in the atmosphere, *Atmos. Environ.*, 28, 185-188, 1994, 10.1016/1352-2310(94)90093-0.
- Paulot, F., Crouse, J. D., Kjaergaard, H. G., Kürten, A., Clair, J. M. S., Seinfeld, J. H., and Wennberg, P. O.: Unexpected epoxide formation in the gas-phase photooxidation of isoprene, *Science*, 325, 730-733, 2009, 10.1126/science.1172910.
- Perraud, V., Bruns, E. A., Ezell, M. J., Johnson, S. N., Yu, Y., Alexander, M. L., Zelenyuk, A., Imre, D., Chang, W. L., Dabdub, D., Pankow, J. F., and Finlayson-Pitts, B. J.: Nonequilibrium atmospheric secondary organic aerosol formation and growth, *Proc. Natl Acad. Sci. USA*, 109, 2836-2841, 2012, 10.1073/pnas.1119909109.
- Pöhlker, M. L., Ditas, F., Saturno, J., Klimach, T., Hrabě de Angelis, I., Araújo, A., Brito, J., Carbone, S., Cheng, Y., Chi, X., Ditz, R., Gunthe, S. S., Kandler, K., Kesselmeier, J., Könemann, T., Lavrič, J. V., Martin, S. T., Mikhailov, E., Moran-Zuloaga, D., Rizzo, L. V., Rose, D., Su, H., Thalman, R., Walter, D., Wang, J., Wolff, S., Barbosa, H. M. J.,

- Artaxo, P., Andreae, M. O., Pöschl, U., and Pöhlker, C.: Long-term observations of cloud condensation nuclei in the Amazon rain forest – Part 2: Variability and characteristic differences under near-pristine, biomass burning, and long-range transport conditions, *Atmos. Chem. Phys. Discuss.*, 2017, 1-51, 2017, 10.5194/acp-2017-847.
- Presto, A. A., Gordon, T. D., and Robinson, A. L.: Primary to secondary organic aerosol: evolution of organic emissions from mobile combustion sources, *Atmos. Chem. Phys.*, 14, 5015-5036, 2014, 10.5194/acp-14-5015-2014.
- Riva, M., Budisulistiorini, S. H., Chen, Y., Zhang, Z., D'Ambro, E. L., Zhang, X., Gold, A., Turpin, B. J., Thornton, J. A., Canagaratna, M. R., and Surratt, J. D.: Chemical characterization of secondary organic aerosol from oxidation of isoprene hydroxyhydroperoxides, *Environ. Sci. Technol.*, 2016, 10.1021/acs.est.6b02511.
- Robinson, A. L., Donahue, N. M., Shrivastava, M. K., Weitkamp, E. A., Sage, A. M., Grieshop, A. P., Lane, T. E., Pierce, J. R., and Pandis, S. N.: Rethinking organic aerosols: semivolatile emissions and photochemical aging, *Science*, 315, 1259-1262, 2007, 10.1126/science.1133061.
- Robinson, N. H., Hamilton, J. F., Allan, J. D., Langford, B., Oram, D. E., Chen, Q., Docherty, K., Farmer, D. K., Jimenez, J. L., Ward, M. W., Hewitt, C. N., Barley, M. H., Jenkin, M. E., Rickard, A. R., Martin, S. T., McFiggans, G., and Coe, H.: Evidence for a significant proportion of Secondary Organic Aerosol from isoprene above a maritime tropical forest, *Atmos. Chem. Phys.*, 11, 1039-1050, 2011, 10.5194/acp-11-1039-2011.
- Röhl, A. and Lammel, G.: Determination of malic acid and other C4 dicarboxylic acids in atmospheric aerosol samples, *Chemosphere*, 46, 1195-1199, 2002, doi.org/10.1016/S0045-6535(01)00243-0.
- Schneider, J., Weimer, S., Drewnick, F., Borrmann, S., Helas, G., Gwaze, P., Schmid, O., Andreae, M. O., and Kirchner, U.: Mass spectrometric analysis and aerodynamic properties of various types of combustion-related aerosol particles, *Int. J. Mass Spectrom.*, 258, 37-49, 2006, 10.1016/j.ijms.2006.07.008.
- Schneider, J., Freutel, F., Zorn, S., Chen, Q., Farmer, D., Jimenez, J., Martin, S., Artaxo, P., Wiedensohler, A., and Borrmann, S.: Mass-spectrometric identification of primary biological particle markers and application to pristine submicron aerosol measurements in Amazonia, *Atmos Chem Phys*, 11, 11415-11429, 2011, doi.org/10.5194/acp-11-11415-2011.
- Setyan, A., Zhang, Q., Merkel, M., Knighton, W. B., Sun, Y., Song, C., Shilling, J. E., Onasch, T. B., Herndon, S. C., Worsnop, D. R., Fast, J. D., Zaveri, R. A., Berg, L. K., Wiedensohler, A., Flowers, B. A., Dubey, M. K., and Subramanian, R.: Characterization of submicron particles influenced by mixed biogenic and anthropogenic emissions using high-resolution aerosol mass spectrometry: results from CARES, *Atmos. Chem. Phys.*, 12, 8131-8156, 2012, 10.5194/acp-12-8131-2012.
- Shilling, J. E., Zaveri, R. A., Fast, J. D., Kleinman, L., Alexander, M. L., Canagaratna, M. R., Fortner, E., Hubbe, J. M., Jayne, J. T., Sedlacek, A., Setyan, A., Springston, S., Worsnop, D. R., and Zhang, Q.: Enhanced SOA formation from mixed anthropogenic and biogenic emissions during the CARES campaign, *Atmos. Chem. Phys.*, 13, 2091-2113, 2013, 10.5194/acp-13-2091-2013.
- Shilling, J. E., Fortner, E., Pekour, M. S., Artaxo, P., Hubbe, J. M., Longo, K. M., Machado, L. A. T., Martin, S. T., Mei, F., Springston, S. R., Tomlinson, J., and Wang, J.: Particle-

- phase chemical composition measurements onboard the G-1 research aircraft during the GoAmazon2014/5 campaign in preparation.
- Shrivastava, M., Cappa, C. D., Fan, J., Goldstein, A. H., Guenther, A. B., Jimenez, J. L., Kuang, C., Laskin, A., Martin, S. T., Ng, N. L., Petaja, T., Pierce, J. R., Rasch, P. J., Roldin, P., Seinfeld, J. H., Shilling, J., Smith, J. N., Thornton, J. A., Volkamer, R., Wang, J., Worsnop, D. R., Zaveri, R. A., Zelenyuk, A., and Zhang, Q.: Recent advances in understanding secondary organic aerosol: Implications for global climate forcing, *Rev. Geophys.*, 55, 509-559, 2017, 10.1002/2016RG000540.
- Spracklen, D. V., Jimenez, J. L., Carslaw, K. S., Worsnop, D. R., Evans, M. J., Mann, G. W., Zhang, Q., Canagaratna, M. R., Allan, J., Coe, H., McFiggans, G., Rap, A., and Forster, P.: Aerosol mass spectrometer constraint on the global secondary organic aerosol budget, *Atmos. Chem. Phys.*, 11, 12109-12136, 2011, 10.5194/acp-11-12109-2011.
- Subramanian, R., Roden, C. A., Boparai, P., and Bond, T. C.: Yellow beads and missing particles: trouble ahead for filter-based absorption measurements, *Aerosol Sci Technol*, 41, 630-637, 2007, 10.1080/02786820701344589.
- Sueper, D. and collaborators: ToF-AMS Data Analysis Software Webpage, [http://cires1.colorado.edu/jimenez-group/wiki/index.php/ToF-AMS\\_Analysis\\_Software](http://cires1.colorado.edu/jimenez-group/wiki/index.php/ToF-AMS_Analysis_Software), last access: August 2017.
- Surratt, J. D., Chan, A. W., Eddingsaas, N. C., Chan, M., Loza, C. L., Kwan, A. J., Hersey, S. P., Flagan, R. C., Wennberg, P. O., and Seinfeld, J. H.: Reactive intermediates revealed in secondary organic aerosol formation from isoprene, *Proc. Natl. Acad. Sci. USA*, 107, 6640-6645, 2010, 10.1073/pnas.0911114107.
- Thalman, R., de Sá, S. S., Palm, B. B., Barbosa, H. M. J., Pöhlker, M. L., Alexander, M. L., Brito, J., Carbone, S., Castillo, P., Day, D. A., Kuang, C., Manzi, A., Ng, N. L., Sedlacek, A. J., Souza, R., Springston, S., Watson, T., Pöhlker, C., Pöschl, U., Andreae, M. O., Artaxo, P., Jimenez, J. L., Martin, S. T., and Wang, J.: CCN activity and organic hygroscopicity of aerosols downwind of an urban region in central Amazonia: seasonal and diel variations and impact of anthropogenic emissions, *Atmos. Chem. Phys.*, 17, 11779-11801, 2017, 10.5194/acp-17-11779-2017.
- Tsigaridis, K., Krol, M., Dentener, F. J., Balkanski, Y., Lathière, J., Metzger, S., Hauglustaine, D. A., and Kanakidou, M.: Change in global aerosol composition since preindustrial times, *Atmos. Chem. Phys.*, 6, 5143-5162, 2006, 10.5194/acp-6-5143-2006.
- Ulbrich, I., Handschy, A., Lechner, M. J., and Jimenez, J.: AMS Spectral Database, 2009a, <http://cires.colorado.edu/jimenez-group/AMSsd/>, last access: August 2017.
- Ulbrich, I., Handschy, A., Lechner, M. J., and Jimenez, J.: High-Resolution AMS Spectral Database, 2009b, <http://cires.colorado.edu/jimenez-group/HRAMSsd/>, last access: August 2017.
- Ulbrich, I., Canagaratna, M., Zhang, Q., Worsnop, D., and Jimenez, J.: Interpretation of organic components from positive matrix factorization of aerosol mass spectrometric data, *Atmos. Chem. Phys.*, 9, 2891-2918, 2009c, 10.5194/acp-9-2891-2009.
- van Pinxteren, D., Neusüß, C., and Herrmann, H.: On the abundance and source contributions of dicarboxylic acids in size-resolved aerosol particles at continental sites in central Europe, *Atmos. Chem. Phys.*, 14, 3913-3928, 2014.
- Weber, R. J., Sullivan, A. P., Peltier, R. E., Russell, A., Yan, B., Zheng, M., de Gouw, J., Warneke, C., Brock, C., Holloway, J. S., Atlas, E. L., and Edgerton, E.: A study of

- secondary organic aerosol formation in the anthropogenic-influenced southeastern United States, *J. Geophys. Res. Atmos.*, 112, D13302, 2007, 10.1029/2007JD008408.
- Worton, D. R., Surratt, J. D., LaFranchi, B. W., Chan, A. W. H., Zhao, Y., Weber, R. J., Park, J.-H., Gilman, J. B., de Gouw, J., Park, C., Schade, G., Beaver, M., Clair, J. M. S., Crounse, J., Wennberg, P., Wolfe, G. M., Harrold, S., Thornton, J. A., Farmer, D. K., Docherty, K. S., Cubison, M. J., Jimenez, J.-L., Frossard, A. A., Russell, L. M., Kristensen, K., Glasius, M., Mao, J., Ren, X., Brune, W., Browne, E. C., Pusede, S. E., Cohen, R. C., Seinfeld, J. H., and Goldstein, A. H.: Observational insights into aerosol formation from isoprene, *Environ. Sci. Technol.*, 47, 11403-11413, 2013, 10.1021/es4011064.
- Xu, L., Guo, H., Boyd, C. M., Klein, M., Bougiatioti, A., Cerully, K. M., Hite, J. R., Isaacman-VanWertz, G., Kreisberg, N. M., Knote, C., Olson, K., Koss, A., Goldstein, A. H., Hering, S. V., de Gouw, J., Baumann, K., Lee, S.-H., Nenes, A., Weber, R. J., and Ng, N. L.: Effects of anthropogenic emissions on aerosol formation from isoprene and monoterpenes in the southeastern United States, *Proc. Natl. Acad. Sci. USA*, 112, 37-42, 2015a, 10.1073/pnas.1417609112.
- Xu, L., Suresh, S., Guo, H., Weber, R. J., and Ng, N. L.: Aerosol characterization over the southeastern United States using high-resolution aerosol mass spectrometry: spatial and seasonal variation of aerosol composition and sources with a focus on organic nitrates, *Atmos. Chem. Phys.*, 15, 7307-7336, 2015b, 10.5194/acp-15-7307-2015.
- Yáñez-Serrano, A. M., Nölscher, A. C., Williams, J., Wolff, S., Alves, E., Martins, G. A., Bourtsoukidis, E., Brito, J., Jardine, K., Artaxo, P., and Kesselmeier, J.: Diel and seasonal changes of biogenic volatile organic compounds within and above an Amazonian rainforest, *Atmos. Chem. Phys.*, 15, 3359-3378, 2015, 10.5194/acp-15-3359-2015.
- Zhang, H., Yee, L. D., and Goldstein, A. H.: Monoterpenes are the largest source of summertime organic aerosol in the southeastern United States, 2018.
- Zhang, Q., Alfarra, M. R., Worsnop, D. R., Allan, J. D., Coe, H., Canagaratna, M. R., and Jimenez, J. L.: Deconvolution and quantification of hydrocarbon-like and oxygenated organic aerosols based on aerosol mass spectrometry, *Environ. Sci. Technol.*, 39, 4938-4952, 2005, 10.1021/es048568l.
- Zhang, Q., Jimenez, J. L., Canagaratna, M. R., Ulbrich, I. M., Ng, N. L., Worsnop, D. R., and Sun, Y.: Understanding atmospheric organic aerosols via factor analysis of aerosol mass spectrometry: a review, *Anal. Bioanal. Chem.*, 401, 3045-3067, 2011, 10.1007/s00216-011-5355-y.

## List of Figures

**Figure 1.** (a) Mass concentrations of PM<sub>1</sub> species at T3 during the wet season of 2014 (IOP1).

Non-refractory (NR) PM<sub>1</sub> species of organic, sulfate, ammonium, nitrate, and chloride were measured by the AMS. Mass concentrations of black carbon were obtained by scaling aethalometer measurements by a factor of 2 based on the range of 1 to 3 for the comparison of SP2 to aethalometer measurements. The temporal trend of the two instruments agreed well. (b) Comparison of the summed mass concentrations of non-refractory PM<sub>1</sub> species (top) and the mass fractions of these species (bottom) at T3 and three other regional sites. T0a-2015 refers to measurements in the wet season of 2015 at the ATTO location ([Carbone et al., in preparation](#))-(Andreae et al., 2015). T0t-2008 refers to the AMAZE-08 experiment, which took place in the wet season of 2008 at the TT34 location (Chen et al., 2015). T2-2014 refers to measurements made during IOP1 at a site 8 km downwind of Manaus, just across the Black River (“Rio Negro”) ([Brito et al., in preparation](#))-(Cirino et al., submitted). Measurements at T0a in 2015 and at T2 in 2014 were made by an ACSM, and measurements at T0t in 2008 and at T3 in 2014 were made by an AMS. Concentrations were adjusted to standard temperature (273.15 K) and pressure (10<sup>5</sup> Pa). ~~Bars represent means and whiskers represent the standard deviation of measurements.~~ The variability of measurements across sites is evaluated in Figure 2.

**Figure 2.** Diel patterns of the mass concentrations of organic (top, green) and sulfate (bottom, red) species during the wet season at four different sites (cf. Fig. 1 and Fig. ~~Error! Reference source not found.~~S1). The ordinate scale for the T2-2014 panel is twice that of the other panels. Mass concentrations were corrected to standard temperature

and pressure (273.15 K and  $10^5$  Pa). Local time is (UTC - 4 h). Lines represent means, solid markers show medians, and boxes span interquartile ranges. ~~The ordinate scale for the T2 panel differs from the other three panels. Concentrations were adjusted to standard temperature (273.15 K) and pressure ( $10^5$  Pa).~~

**Figure 3.** Scatter plot of the AMS signal fraction at  $m/z$  44 ( $f_{44}$ ) against that at  $m/z$  43 ( $f_{43}$ ). Gray and blue circles correspond, respectively, to measurements at T3 and T2 during IOP1, in the wet season of 2014. For visualization purposes, the two datasets are plotted separately in panels a and b. Solid squares represent median values, and whiskers represent 10 and 90 percentiles. Dashed lines delineate the region where worldwide measurements of ambient organic  $PM_{10}$  commonly lie (Ng et al., 2011a).

**Figure 4.** Results of the PMF analysis on the time series of AMS organic mass spectra collected at T3. (a) Mass spectral profile of each factor represented at unit mass resolution. The inset shows the mean fractional loading of each factor. (b) Diel trends for the loadings of each PMF factor. Local time is (UTC - 4 h). Lines represent means, solid markers show medians, and boxes span interquartile ranges. (c) Time series of the factor loadings (left axis) and other related measurements at T3 (right axis). Methyl-butyl-tricarboxylic acid is abbreviated as MBTCA.

**Figure 5.** Column plot of Pearson  $R$  correlations between the loading of each PMF factor and values of selected measurements at T3. Abbreviations include tricarballic acid (TCA), methyl-butyl-tricarboxylic acid (MBTCA), methyl vinyl ketone (MVK), methacrolein (MACR), and isoprene hydroxyhydroperoxides (ISOPOOH). SV-TAG measurements refer to particle-phase concentrations. Isomers could not be

distinguished by PTR-ToF-MS measurements; C<sub>8</sub> and C<sub>9</sub> aromatics include the xylene and trimethylbenzene isomers, respectively.

**Figure 6.** Results of the cluster analysis by Fuzzy c-means (FCM) for afternoon periods (12:00 to 16:00 h) are presented by several case studies. (a) Degree of membership in each of the four clusters. The sum of degrees of membership across all clusters is unity. Background conditions are abbreviated as “Bkgd”, and polluted conditions are abbreviated as “Pol”. (b) Pollution indicators: concentrations of NO<sub>y</sub>, O<sub>3</sub>, black carbon (BC), and particle number count are plotted. (c) PM<sub>1</sub> mass concentrations for organic, sulfate, nitrate, and ammonium species. (d) Fractional contribution of each factor to total organic PM<sub>1</sub>.

**Figure 7.** Air mass backtrajectories associated with the four clusters of the FCM analysis for the case studies of Figure 6. Trajectories were calculated using HYSPLIT 4 in steps of 12 min for ten hours (Draxler and Hess, 1998). Image data: Google earth.

**Figure 8.** Characteristic PM composition of the FCM clusters as represented by coordinates of cluster centroids. (a) Mass concentrations of AMS species characteristic of each cluster. (b) PMF factor loadings characteristic of each cluster. Calculations are presented in more detail in the Supplementary Material (Section S3). Values plotted are shown in Table 2.

**Figure 9.** Schematic representation of (a) atmospheric processes, illustrated in a simplified manner, associated with the production of organic PM<sub>1</sub> and (b) observables of these processes as captured by the datasets and analytical approach employed in this study. In panel (a), the left side depicts the emissions of biogenic volatile organic compounds (VOCs), their atmospheric oxidation, and the production of biogenic secondary



organic PM<sub>1</sub>. The right side depicts anthropogenic emissions of gas species and particulate matter that can alter natural atmospheric concentrations and processes. There are primary organic PM<sub>1</sub> emissions from traffic, cooking, and industrial activities. Anthropogenic VOCs can be precursors for the production of secondary organic PM<sub>1</sub> and can affect the production of ozone and hydroxyl radical. NO<sub>x</sub> emissions directly and indirectly alter the natural pathways of PM<sub>1</sub> production in the atmosphere. NO<sub>x</sub> and SO<sub>x</sub> can also directly contribute to the formation of secondary inorganic PM<sub>1</sub> (not shown), which can in turn play a role in changing pathways of secondary organic PM<sub>1</sub> production. In panel (b), different PMF factors represent distinct sources and/or processes. The IEPOX-SOA factor is at the intersection of the two, as it represents both a source (i.e., isoprene emissions from the forest) and a process (i.e., photo-oxidation under HO<sub>2</sub> dominant conditions, influenced by sulfate concentrations). The dashed black line represents the natural and anthropogenic oxidative processes that transform the chemical signature of the HOA, ADOA, BBOA, IEPOX-SOA, and LO-OOA factors after sufficient atmospheric residence time into the MO-OOA factor. The clusters represent different conditions at the receptor site (i.e., T3) and therefore incorporate the meteorological and geographical histories of the air masses that reach the site and affect the observed concentrations. The different PMF factors are associated to the different clusters (solid lines) to various extents (not detailed here for simplification purposes; cf. Figure 8).

**Table 1.** Characteristics of the PMF factors derived from the AMS datasets. Listed are signal fractions  $f_{\text{CO}_2^+}$  at nominal  $m/z$  44 and oxygen-to-carbon (O:C) and hydrogen-to-carbon (H:C) ratios. Values and associated uncertainties were calculated by running PMF in “bootstrap mode” (Ulbrich et al., 2009c). Elemental ratios were calibrated by the “improved-ambient” method, which has an estimated uncertainty of 12% for O:C and 4% for H:C (Canagaratna et al., 2015).

PMF factor	$f_{\text{CO}_2^+}$	O:C	H:C
MO-OOA	$0.25 \pm 0.01$	$1.09 \pm 0.17$	$1.27 \pm 0.12$
LO-OOA	$0.14 \pm 0.02$	$0.72 \pm 0.10$	$1.49 \pm 0.07$
IEPOX-SOA	$0.17 \pm 0.01$	$0.93 \pm 0.10$	$1.39 \pm 0.07$
ADOA	$0.11 \pm 0.01$	$0.40 \pm 0.05$	$1.63 \pm 0.02$
BBOA	$0.123 \pm 0.004$	$0.61 \pm 0.08$	$1.57 \pm 0.04$
HOA	$0.048 \pm 0.006$	$0.18 \pm 0.02$	$1.94 \pm 0.02$

**Table 2.** Coordinates of cluster centroids for input variables, AMS species concentrations, and PMF factor loadings. Table entries for AMS species and PMF factors are plotted in Figure 8. The AMS species concentrations (except for sulfate) and PMF factor loadings were not used as input variables in the FCM clustering analysis.

Species	Cluster Centroid			
	Bkgd-1	Bkgd-2	Pol-1	Pol-2
<b>Input variables</b>				
Particle number (cm <sup>-3</sup> )	714	1117	2636	6697
NO <sub>y</sub> (ppb)	0.64	0.95	1.2	2.2
O <sub>3</sub> (ppb)	14	17	26	36
Black carbon (μg m <sup>-3</sup> )	0.05	0.16	0.21	0.18
Sulfate (μg m <sup>-3</sup> )	0.15	0.36	0.44	0.57
<b>AMS species concentrations (μg m<sup>-3</sup>)</b>				
Organic	0.96	2.0	2.5	2.6
Ammonium	0.05	0.12	0.15	0.21
Nitrate	0.03	0.07	0.10	0.12
Chloride	0.007	0.011	0.009	0.007
<b>PMF factor loadings (μg m<sup>-3</sup>)</b>				
MO-OOA	0.29	0.83	1.13	1.13
LO-OOA	0.38	0.41	0.62	0.77
IEPOX-SOA	0.18	0.49	0.43	0.29
ADOA	0.044	0.086	0.19	0.32
BBOA	0.028	0.054	0.081	0.063
HOA	0.017	0.027	0.039	0.040

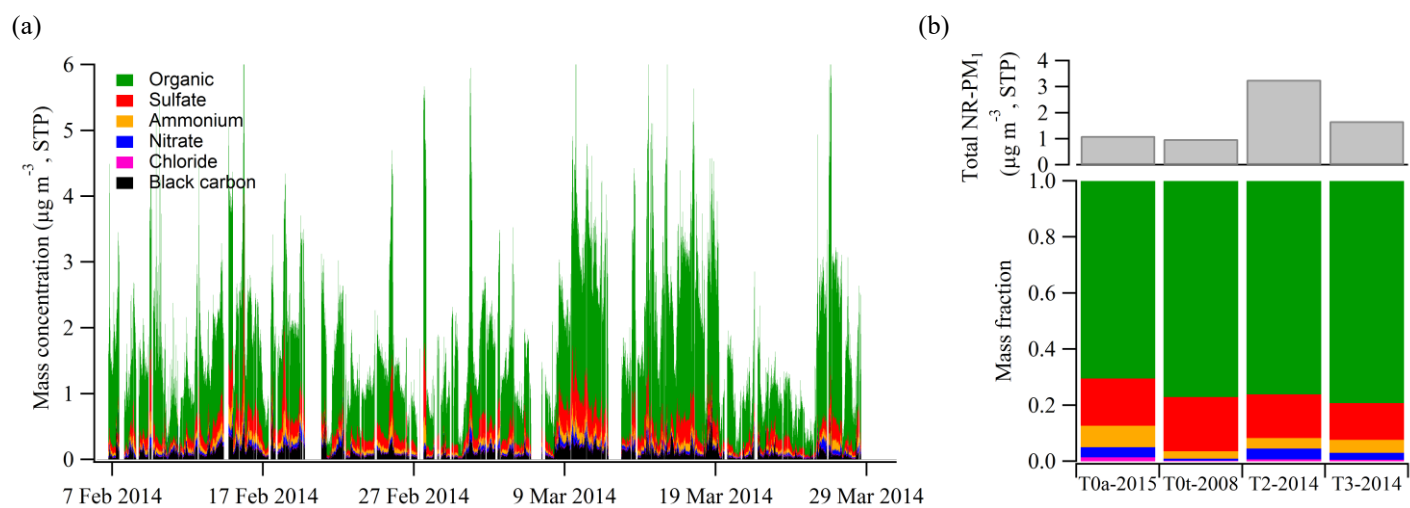


Figure 1

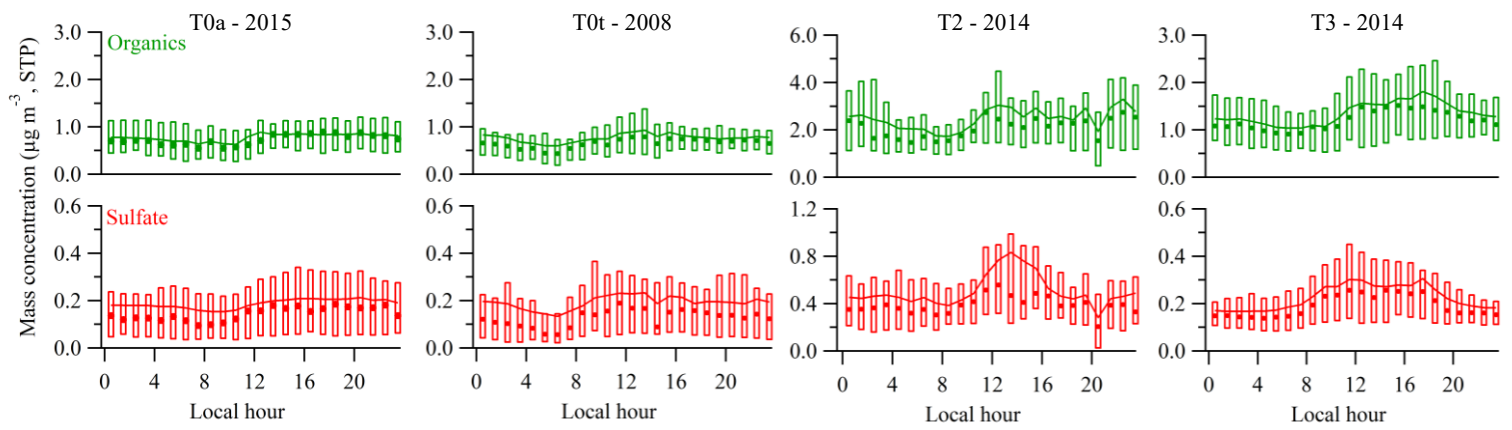


Figure 2

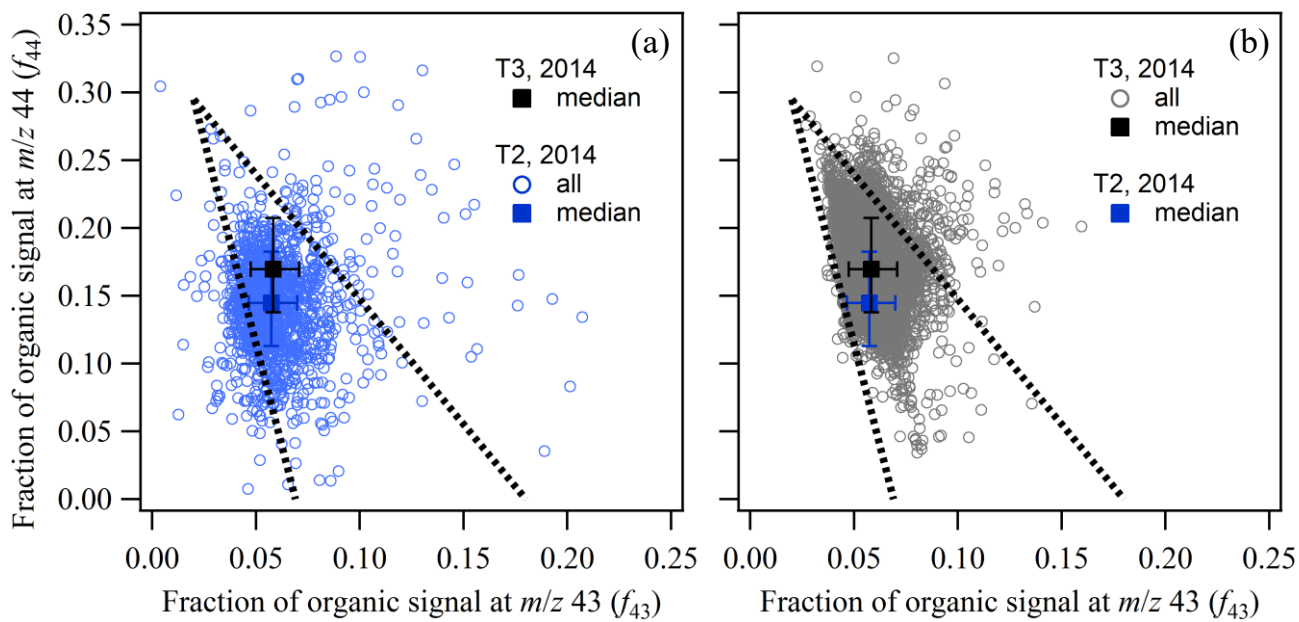


Figure 3

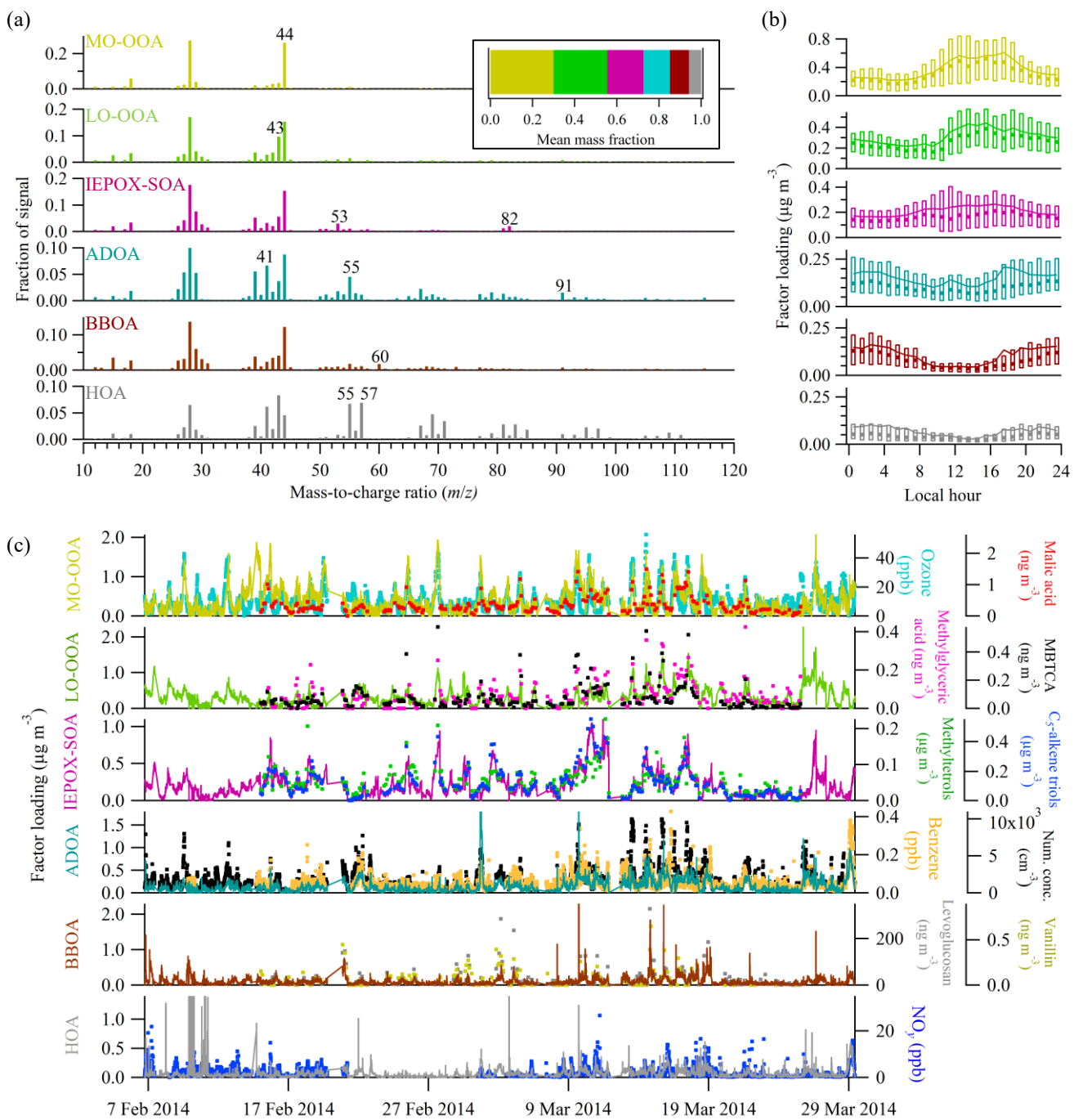


Figure 4

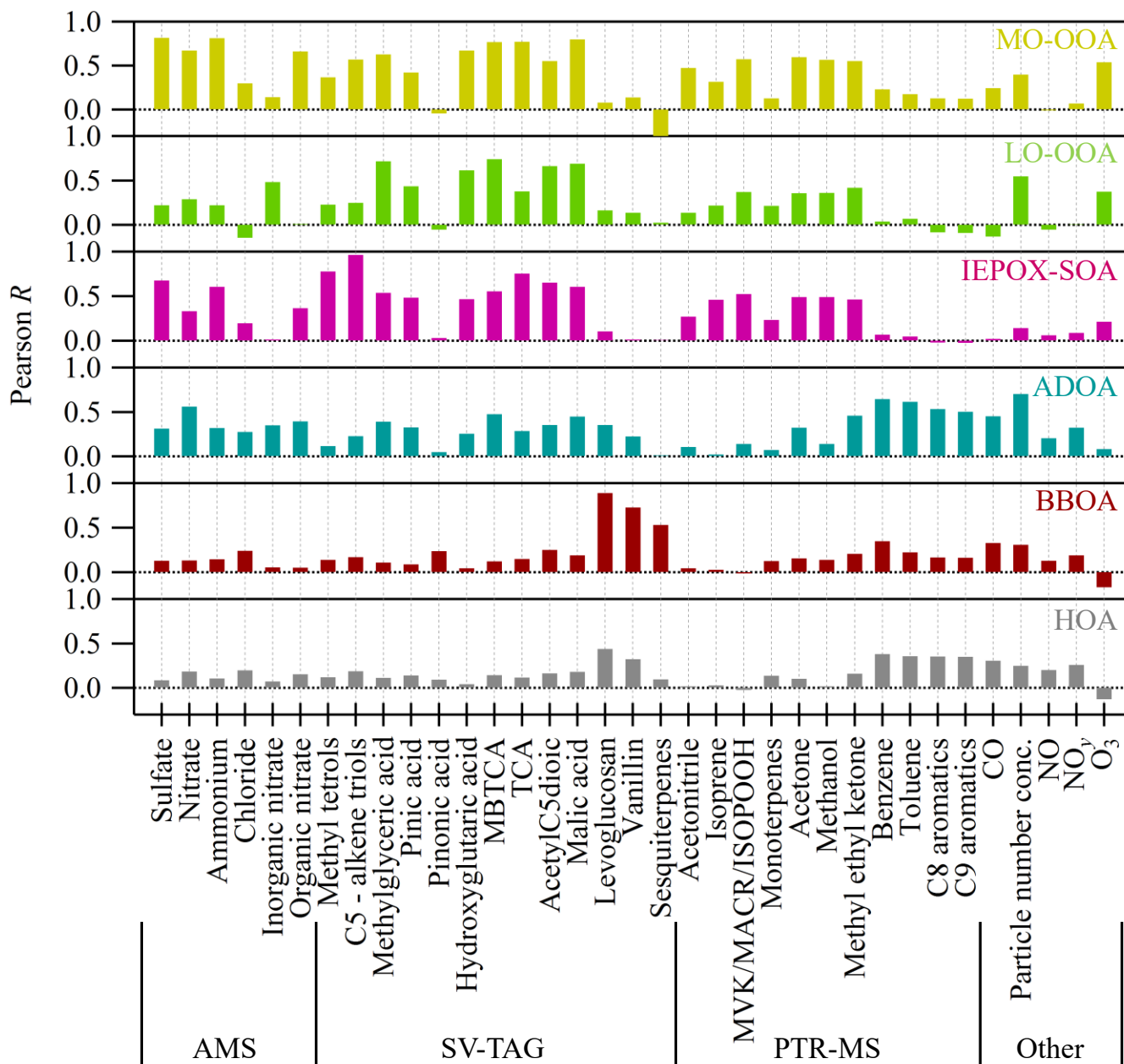


Figure 5



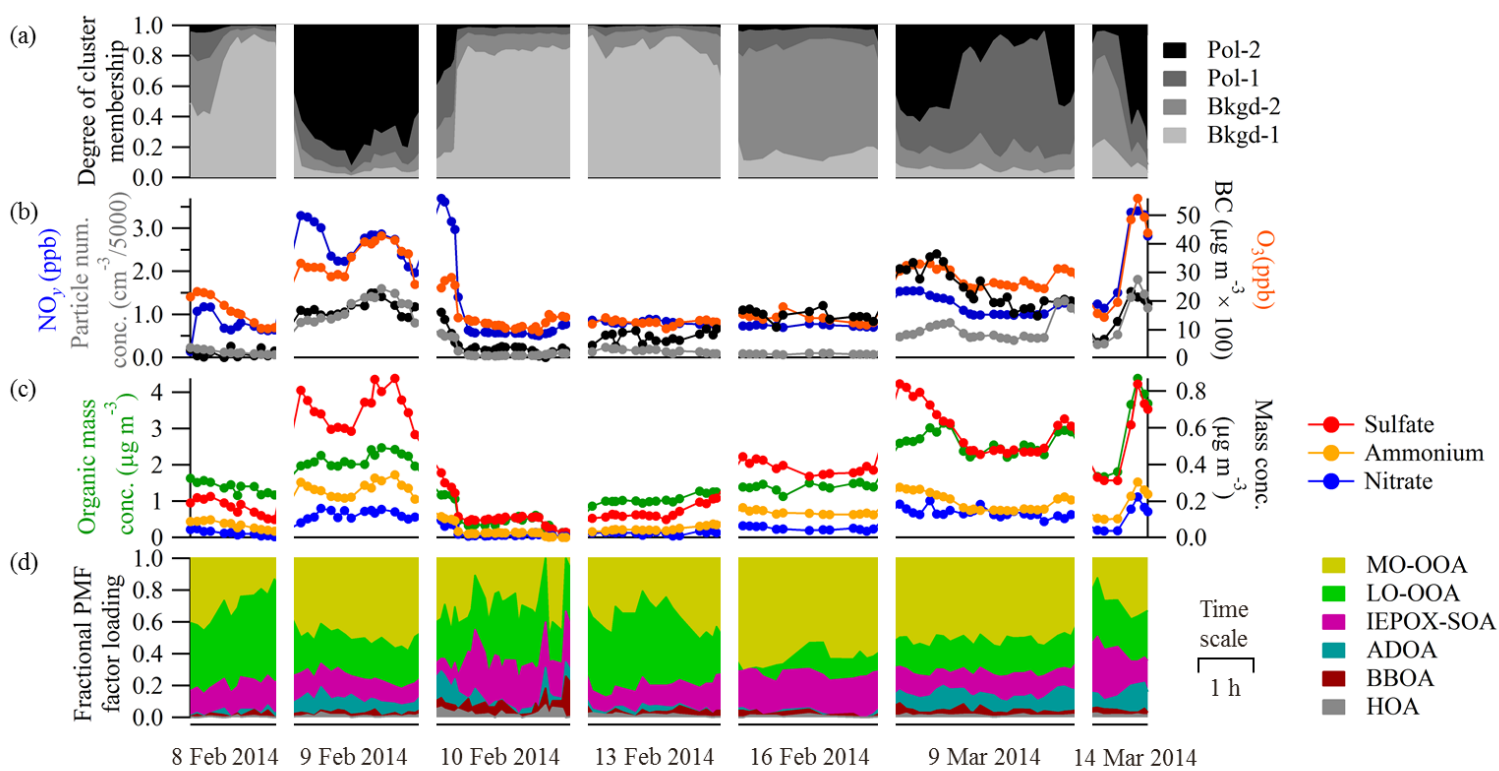


Figure 6

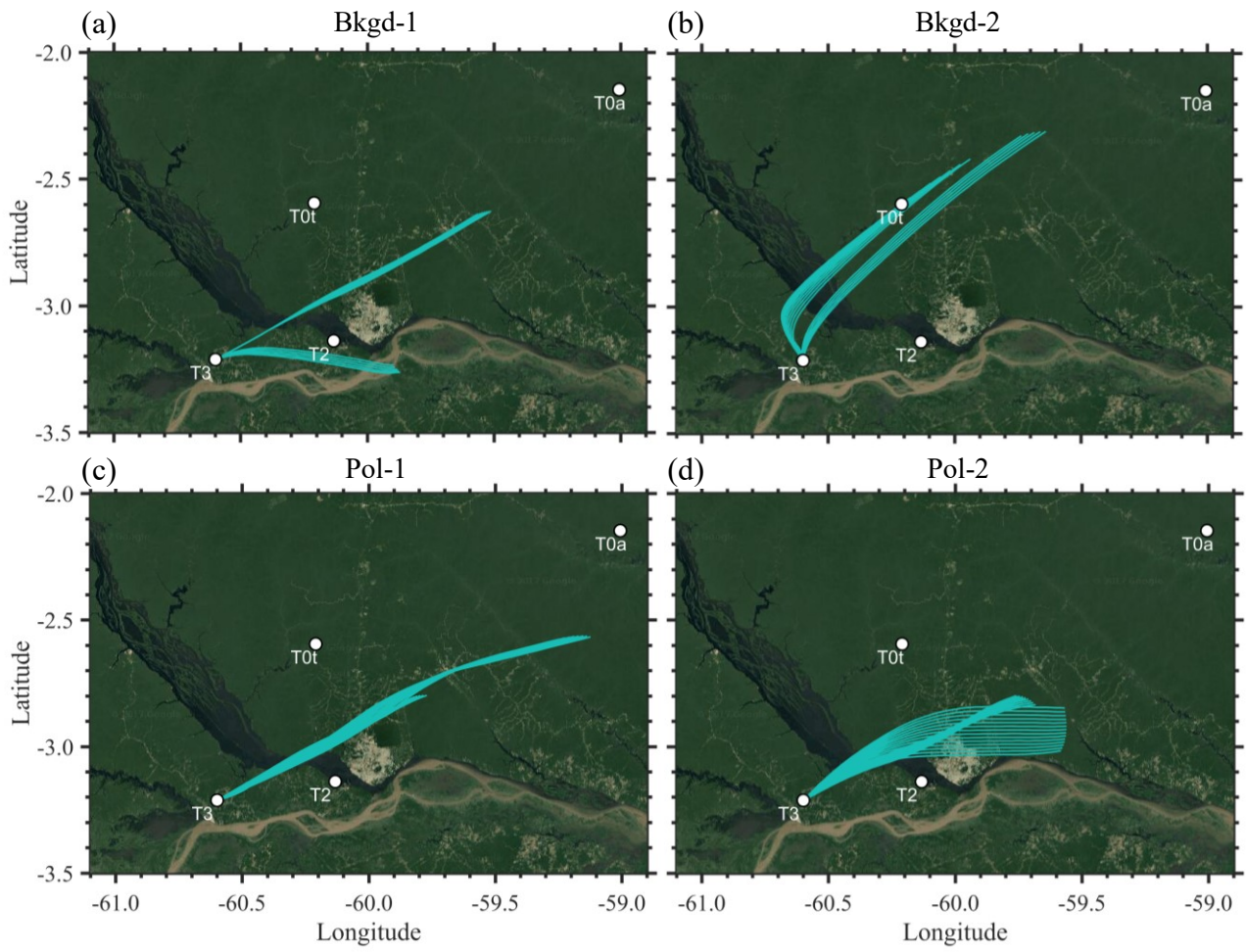


Figure 7

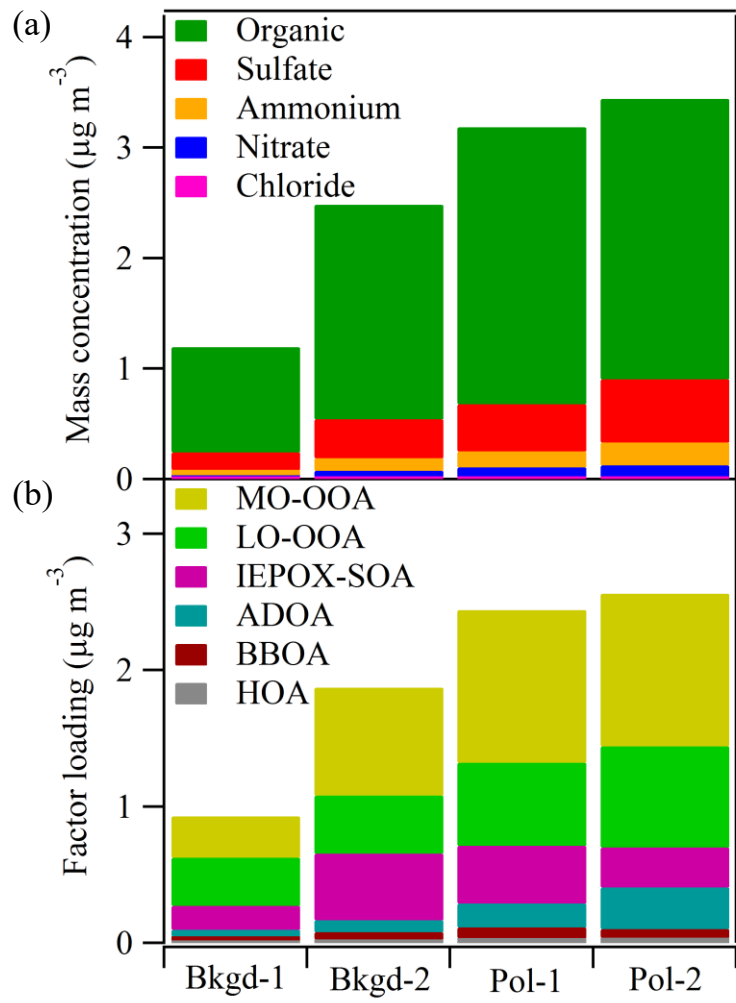


Figure 8

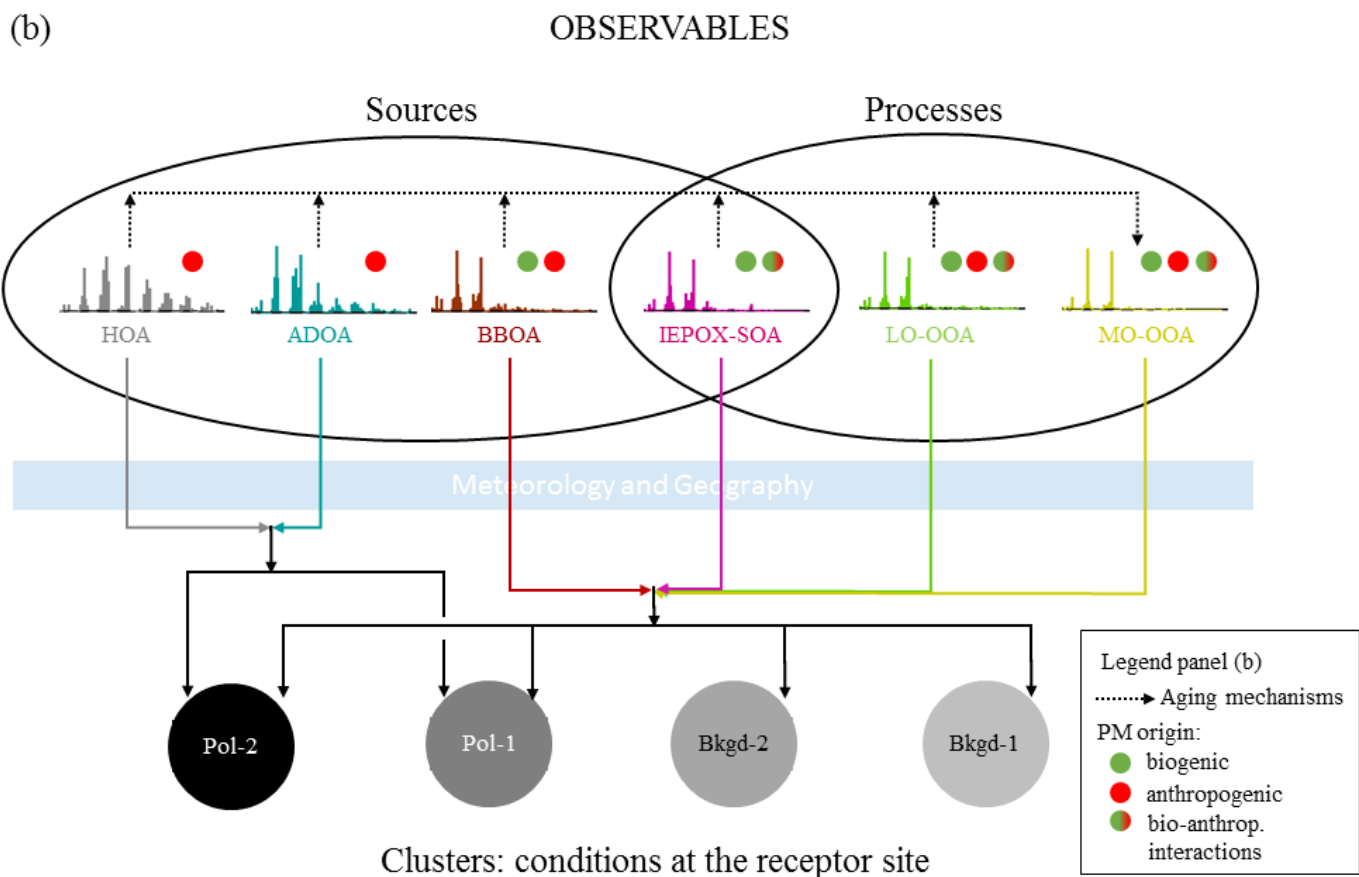
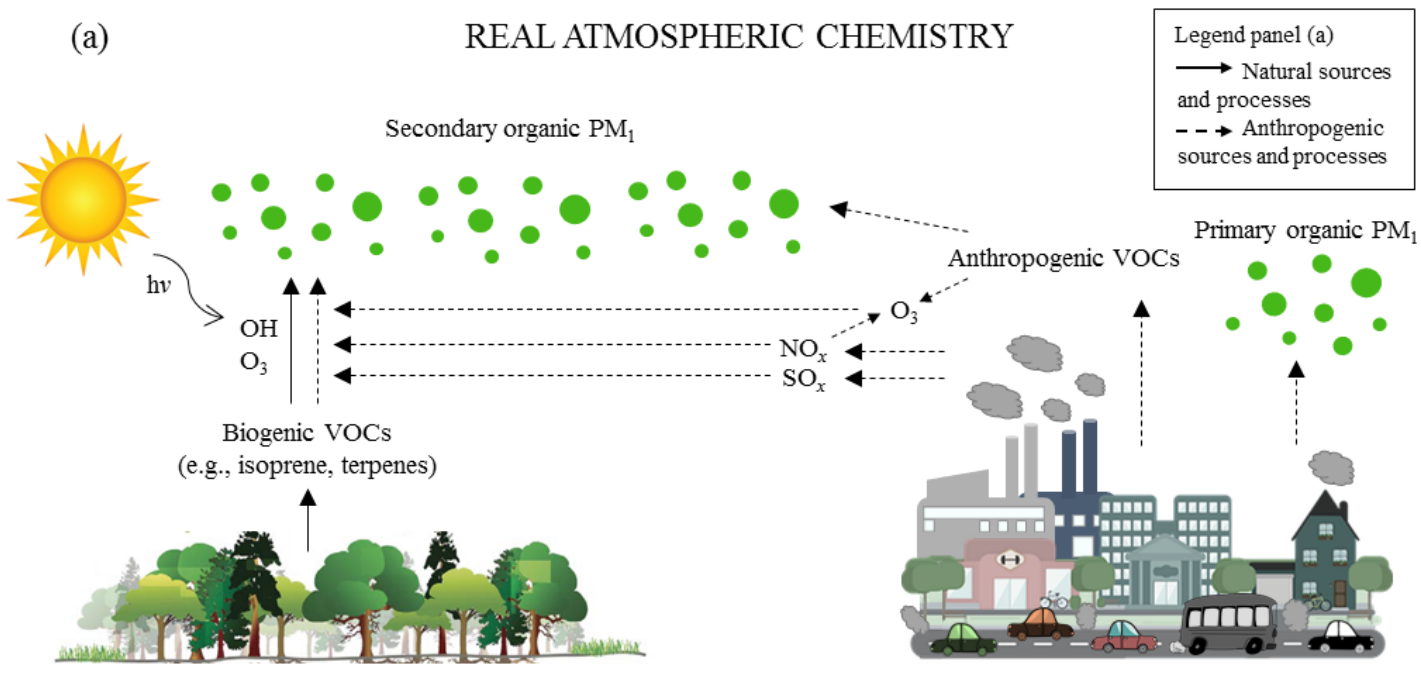


Figure 9

**Supplementary Material for**  
**Urban influence on the concentration and composition of submicron**  
**particulate matter in central Amazonia**

Suzane S. de Sá (1), Brett B. Palm (2), Pedro Campuzano-Jost (2), Douglas A. Day (2), Weiwei Hu (2), Gabriel Isaacman-VanWertz<sup>a</sup> (3), Lindsay D. Yee (3), Joel Brito<sup>b</sup> (4), Samara Carbone<sup>c</sup> (4), Igor O. Ribeiro (5), Glauber G. Cirino<sup>d</sup> (6), Yingjun J. Liu<sup>e</sup> (1), Ryan Thalman<sup>f</sup> (7), Arthur Sedlacek (7), Aaron Funk (8), Courtney Schumacher (8), John E. Shilling (9), Johannes Schneider (10), Paulo Artaxo (4), Allen H. Goldstein (3), Rodrigo A.F. Souza (5), Jian Wang (7), Karena A. McKinney<sup>g</sup> (1), Henrique Barbosa (4), M. Lizabeth Alexander (11), Jose L. Jimenez (2), Scot T. Martin\* (1, 12)

- (1) School of Engineering and Applied Sciences, Harvard University, Cambridge, Massachusetts, USA
  - (2) Department of Chemistry and Cooperative Institute for Research in Environmental Sciences, University of Colorado, Boulder, Colorado, USA
  - (3) Department of Environmental Science, Policy, and Management, University of California, Berkeley, California, USA
  - (4) Institute of Physics, University of São Paulo, São Paulo, Brazil
  - (5) School of Technology, Amazonas State University, Manaus, Amazonas, Brazil
  - (6) National Institute for Amazonian Research, Manaus, Amazonas, Brazil
  - (7) Brookhaven National Laboratory, Upton, New York, USA
  - (8) Department of Atmospheric Sciences, Texas A&M University, College Station, Texas, USA
  - (9) Atmospheric Sciences and Global Change Division, Pacific Northwest National Laboratory, Richland, WA, USA
  - (10) Particle Chemistry Department, Max Planck Institute for Chemistry, Mainz, Germany
  - (11) Environmental Molecular Sciences Laboratory, Pacific Northwest National Laboratory, Richland, Washington, USA
  - (12) Department of Earth and Planetary Sciences, Harvard University, Cambridge, Massachusetts, USA
- <sup>a</sup> Now at Department of Civil and Environmental Engineering, Virginia Tech, Blacksburg, Virginia, USA  
<sup>b</sup> Now at Laboratory for Meteorological Physics (LaMP), University Blaise Pascal, Aubière, France  
<sup>c</sup> Now at Federal University of Uberlândia, Uberlândia, Minas Gerais, Brazil  
<sup>d</sup> Now at Department of Meteorology, Geosciences Institute, Federal University of Pará, Belém, Brazil  
<sup>e</sup> Now at University of California, Berkeley, California, USA  
<sup>f</sup> Now at Department of Chemistry, Snow College, Richfield, Utah, USA  
<sup>g</sup> Now at Colby College, Waterville, Maine, USA

Submitted: February 2018

*Atmospheric Chemistry and Physics*

\*To Whom Correspondence Should be Addressed

*E-mail: [scot\\_martin@harvard.edu](mailto:scot_martin@harvard.edu)*

*<https://martin.seas.harvard.edu/>*

## 1 S1. Positive-matrix factorization

### 2 S1.1 Diagnostics of the six-factor solution

3 Quantification of mass concentrations by the AMS was obtained from “V-mode” data,  
4 which corresponds to the shorter ion time-of-flight path and is therefore the more sensitive mode.  
5 The choice of ions to fit was aided by “W-mode” data, which correspond to the longer ion time-  
6 of-flight path and is therefore the mode with highest mass resolution. V-mode data were  
7 collected continuously, and W-mode data were collected for one of every five days. The time  
8 series of organic mass spectra measured by the AMS in V-mode was analyzed by positive-matrix  
9 factorization (PMF) using a standard analysis toolkit (Ulbrich et al., 2009). ~~High-resolution “V-~~  
10 ~~mode” data were used.~~ The PMF solution was based on minimization of the “Q-value” (i.e., the  
11 sum of the weighed squared residuals for a chosen number of factors) and the physical  
12 meaningfulness of factors, as evaluated by profile characteristics and correlations with gas and  
13 particle phase measurements by other instruments.

14 Technical diagnostics of the six-factor solution are presented in Figure S3 in complement  
15 to the diagnostics presented in de Sá et al. (2017). The analysis was run for a number of factors  
16 from 1 to 10, and the rotational ambiguity parameter  $f_{peak}$  was varied from -1 to 1 in intervals of  
17 0.2. Panel a shows the statistics of residuals for solutions with different number of factors. There  
18 was a large improvement in the solution when a sixth factor was introduced, as shown by a  
19 significant decrease in residuals, and only a marginal improvement when a seventh factor was  
20 added. Panel b shows, on the ordinate, the correlation between the time series of loadings for  
21 each pair of factors and, on the abscissa, the correlation between the profiles of each pair of  
22 factors. For the six-factor solution, the correlations among factor profiles are overall lower, also  
23 suggesting a better separation of factors and an improvement in the solution. Figure S4

24 corroborates this analysis by showing the factor profiles and loading time series of the 5- and 7-  
25 factor solutions. In the 5-factor solution, factors 4 and 5 seem to be a result of mixing of the three  
26 factors that are associated with secondary processing in the 6-factor solution (MO-OOA, LO-  
27 OOA, IEPOX-SOA). Conversely, in the 7-factor solution, some splitting seems to occur as factor  
28 7 is physically meaningless, and a few pairs of factors have higher correlations between their  
29 loading time series (cf. Figure S3). An  $f_{peak}$  of zero was chosen for the final 6-factor solution,  
30 since it yielded the minimum quality of fit parameter  $Q/Q_{expected}$  de Sá et al. (2017), and no  
31 significant improvements in the external validation of factors were observed by varying  $f_{peak}$ .

## 32 **S1.2 Discussion of the ADOA PMF factor**

33 ADOA is interpreted as a primary anthropogenic factor due to the correlation of its  
34 loadings with several tracers of anthropogenic activities (Figure 5), its spectral profile, and its  
35 diel behavior (Figure 4). Even though factors containing a characteristic  $m/z$  91 have been  
36 reported in the literature as a biogenic factor (Robinson et al., 2011; Budisulistiorini et al., 2015;  
37 Chen et al., 2015; Riva et al., 2016), the ADOA of this study showed similarity with primary  
38 organic material from cooking activities. Figure S5 shows the high similarity of ADOA of this  
39 study to a factor representing cooking emissions at an urban background site in Barcelona, Spain  
40 (Mohr et al., 2012), and to a factor representing a cooking source tied to restaurants in an urban  
41 background site in Zurich, Switzerland (Lanz et al., 2007). By contrast, a lower similarity is  
42 found with the “91fac” factor found in the Borneo forest, a predominantly biogenic site. This  
43 result emphasizes that a characteristic marker ion  $C_7H_7^+$  at  $m/z$  91 does not directly imply either  
44 biogenic or anthropogenic origin, and the interpretation of a PMF factor with such marker should  
45 also strongly rely on the atmospheric context of the measurements, including the correlations of  
46 the factor loadings with external measurements and the diel behavior.

## 47 **S2. Estimates of organic and inorganic nitrates based on AMS analysis**

48           The typical AMS analysis reports total nitrate, meaning that nitrate fragments originating  
49 from both organic and inorganic nitrates are reported indistinctively as nitrate. In the absence of  
50 external measurements of inorganic nitrate, an estimation method using the ratio of  $\text{NO}_2^+$  to  $\text{NO}^+$   
51 signal intensities measured by the AMS was employed (Figure S6; Fry et al., 2009; Farmer et al.,  
52 2010; Fry et al., 2013). Calculations were done on a 60-min time base to increase signal over  
53 noise. The obtained organic and inorganic nitrate time series were then interpolated into the  
54 original AMS timestamp for ambient measurements (i.e., one point every 8-min interval). The  
55 analysis excluded points that had total nitrate below the estimated detection limit,  $DL_{\text{Nitrate}}$ , which  
56 was estimated as three times the standard deviation for “closed AMS spectra”, i.e., when chopper  
57 was in closed position and particles did not reach the vaporizer. Mathematically,  
58  $DL_{\text{Nitrate}} = 3 \times \sqrt{E}$ , where  $E$  is the “closed” error calculated by the standard *PIKA* software  
59 (Ulbrich et al., 2009). The dark blue dashed line in Figure S6c that defines  $\text{NO}_2^+/\text{NO}^+$  for  
60 inorganic nitrate was determined by linear fit of ammonium nitrate calibrations performed  
61 regularly, as shown by the grey triangles. The small drift over time can be attributed to a gradual  
62 clean-up of the vaporizer. Worth noting, whether the linear fit or an average value was used for  
63 the calculations, the overall results did not change considerably, as all calibration ratios lied  
64 within  $\pm 20\%$  of the campaign-average ratio. The ratio  $\text{NO}_2^+/\text{NO}^+$  for organic nitrates was  
65 assumed to be a factor of 2.25 lower than that of inorganic nitrate based on previous field  
66 studies (Farmer et al., 2010; Fry et al., 2013). The resulting IOP1-average for the fraction of  
67 organic nitrate in total nitrate (Figure S6b) was 87%.

## 68 **S3. Fuzzy c-means clustering**



69 Fuzzy c-means (FCM) clustering was applied to the dataset consisting of concentrations  
70 of particle number, NO<sub>y</sub>, ozone, black carbon, and sulfate (Bezdek et al., 1984). The use of a  
71 fuzzy clustering method stems from the understanding that any point in time may be affected by  
72 a combination of different sources and processes and could therefore be anywhere on the scale  
73 between pristine background and extreme polluted conditions, as opposed to a simpler binary  
74 classification. Given the scope of the analysis as non-overcast afternoon times, data points were  
75 restricted to (i) local 12:00-16:00 h, (ii) local solar radiation over the past 4 h not less than 200 W  
76 m<sup>-2</sup> (i.e., excluding the lower 20 percentile), and (iii) insignificant precipitation (< 0.1 mm) over  
77 the previous 10 h along backward trajectory (a threshold was used as most rain radar grid cells  
78 had non-zero yet negligible values). The data were normalized prior to the FCM analysis using  
79 the z-score method, which transforms all variables into a common scale with an average of zero  
80 and standard deviation of one.

81 The FCM algorithm minimizes the objective function represented in Eq. S1, which is a  
82 weighted sum of squared errors where the error is the Euclidean distance between each data  
83 point and a cluster centroid.

$$84 \quad J(U,v)= \sum_{k=1}^N \sum_{i=1}^c u_{ik}^m \|y_k - v_i\|^2 \quad (\text{Eq. S1})$$

85 The input data is given by the matrix  $Y = [y_1, y_2, \dots, y_N]$ , where  $y_k$  is a vector of length  $X$  at the  $k$ -  
86 *th* time point.  $X$  is the number of variables (i.e., measurements) used as input in the analysis. The  
87 number of time points is represented by  $N$ , and the associated running index is  $k$ .  $N$  in this case  
88 was 313. The number of clusters is represented by  $c$ , and the corresponding running index is  $i$ .  
89 The coordinates of the centroid of each cluster  $i$  are represented by  $v_i$ , a vector of length  $X$ . The  
90 exponent of the Fuzzy partition matrix is represented by  $m$ . The algorithm returns (1) the Fuzzy  
91 partition matrix of  $Y$ , given by  $U = [u_{ik}]$  where  $u_{ik}$  is the degree of membership of time point  $k$  to

92 cluster  $i$ , (2) the vectors of coordinates of cluster centers, given by  $v = [v_i]$ , as well as (3) the  
93 value  $J$  of the objective function.

94 The analysis was performed in MATLAB® using the “fcm” function in the Fuzzy logic  
95 toolbox™. The stop criterion of the algorithm is that either the maximum number of iterations is  
96 reached or the improvement of the objective function between two consecutive iterations is less  
97 than the minimum amount of improvement specified. The default value of  $1 \times 10^{-5}$  was used for  
98 the minimum amount of improvement, and the maximum number of iterations was set to 1000 so  
99 that convergence always happened before this maximum was reached. A default value of 2 was  
100 used for the exponent  $m$  of the partition matrix. Fuzzy clustering algorithms are not sensitive to  
101 small fluctuations in  $m$  (Chatzis, 2011), and a value in the range of 1.5 to 3 is recommended  
102 (Bezdek et al., 1984; Hathaway and Bezdek, 2001).

103 The analysis was run for a number of clusters varying from two to eight, and the value of  
104 the objective function for each run is shown in Figure S7. The choice of number of clusters  
105 hinges on a balance between increased complexity and additional information provided by each  
106 extra cluster. The improvement in the objective function was larger in the range of two to four  
107 clusters, with marginal improvements above four clusters (Figure S7). The location of cluster  
108 centroids was also examined for evaluation of cluster overlap (Figure S8). The addition of a fifth  
109 cluster made two pairs of clusters very similar, as can be seen by the locations of cluster  
110 centroids in Figure S8. The solution of four clusters was therefore a reasonable choice to  
111 represent the studied system. The subsequent characterization of the PM chemical composition  
112 associated with each cluster further confirmed the meaningfulness of the solution. Although the  
113 three-cluster solution could also provide a reasonable representation of the system, the four-

114 cluster solution provided further insight by differentiating two background and two polluted  
115 conditions.

116 Subsequently, the PM composition associated with each of the clusters was determined  
117 by calculating the corresponding coordinates of the centroids for AMS species concentrations  
118 and PMF factor loadings, which were not input to the FCM analysis. The calculation followed  
119 the mathematical definition of the centroid (Eq. S2). The resulting characterization of clusters is  
120 shown in Figure 8 and Table 2.

121

$$v_i = \frac{\sum_{k=1}^N (u_{ik})^m y_k}{\sum_{k=1}^N (u_{ik})^m} \quad (\text{Eq. S2})$$

## References

- Bezdek, J. C., Ehrlich, R., and Full, W.: FCM: The fuzzy c-means clustering algorithm, *Computers & Geosciences*, 10, 191-203, 1984.
- Budisulistiorini, S. H., Li, X., Bairai, S. T., Renfro, J., Liu, Y., Liu, Y. J., McKinney, K. A., Martin, S. T., McNeill, V. F., Pye, H. O. T., Nenes, A., Neff, M. E., Stone, E. A., Mueller, S., Knote, C., Shaw, S. L., Zhang, Z., Gold, A., and Surratt, J. D.: Examining the effects of anthropogenic emissions on isoprene-derived secondary organic aerosol formation during the 2013 Southern Oxidant and Aerosol Study (SOAS) at the Look Rock, Tennessee ground site, *Atmos. Chem. Phys.*, 15, 8871-8888, 2015, 10.5194/acp-15-8871-2015.
- Chatzis, S. P.: A fuzzy c-means-type algorithm for clustering of data with mixed numeric and categorical attributes employing a probabilistic dissimilarity functional, *Expert Systems with Applications*, 38, 8684-8689, 2011, <https://doi.org/10.1016/j.eswa.2011.01.074>.
- Chen, Q., Farmer, D. K., Schneider, J., Zorn, S. R., Heald, C. L., Karl, T. G., Guenther, A., Allan, J. D., Robinson, N., Coe, H., Kimmel, J. R., Pauliquevis, T., Borrmann, S., Pöschl, U., Andreae, M. O., Artaxo, P., Jimenez, J. L., and Martin, S. T.: Mass spectral characterization of submicron biogenic organic particles in the Amazon Basin, *Geophys. Res. Lett.*, 36, L20806, 2009, 10.1029/2009GL039880.
- Chen, Q., Farmer, D. K., Rizzo, L. V., Pauliquevis, T., Kuwata, M., Karl, T. G., Guenther, A., Allan, J. D., Coe, H., Andreae, M. O., Pöschl, U., Jimenez, J. L., Artaxo, P., and Martin, S. T.: Submicron particle mass concentrations and sources in the Amazonian wet season (AMAZE-08), *Atmos. Chem. Phys.*, 15, 3687-3701, 2015, 10.5194/acp-15-3687-2015.
- de Sá, S. S., Palm, B. B., Campuzano-Jost, P., Day, D. A., Newburn, M. K., Hu, W., Isaacman-VanWertz, G., Yee, L. D., Thalman, R., Brito, J., Carbone, S., Artaxo, P., Goldstein, A. H., Manzi, A. O., Souza, R. A. F., Mei, F., Shilling, J. E., Springston, S. R., Wang, J., Surratt, J. D., Alexander, M. L., Jimenez, J. L., and Martin, S. T.: Influence of urban pollution on the production of organic particulate matter from isoprene epoxydiols in central Amazonia, *Atmos. Chem. Phys.*, 17, 6611-6629, 2017, 10.5194/acp-17-6611-2017.
- Farmer, D. K., Matsunaga, A., Docherty, K. S., Surratt, J. D., Seinfeld, J. H., Ziemann, P. J., and Jimenez, J. L.: Response of an aerosol mass spectrometer to organonitrates and organosulfates and implications for atmospheric chemistry, *Proc. Natl. Acad. Sci. USA*, 107, 6670-6675, 2010, 10.1073/pnas.0912340107.
- Fry, J. L., Kiendler-Scharr, A., Rollins, A. W., Wooldridge, P. J., Brown, S. S., Fuchs, H., Dubé, W., Mensah, A., dal Maso, M., Tillmann, R., Dorn, H. P., Brauers, T., and Cohen, R. C.: Organic nitrate and secondary organic aerosol yield from NO<sub>3</sub> oxidation of β-pinene evaluated using a gas-phase kinetics/aerosol partitioning model, *Atmos. Chem. Phys.*, 9, 1431-1449, 2009, 10.5194/acp-9-1431-2009.
- Fry, J. L., Draper, D. C., Zarzana, K. J., Campuzano-Jost, P., Day, D. A., Jimenez, J. L., Brown, S. S., Cohen, R. C., Kaser, L., Hansel, A., Cappellin, L., Karl, T., Hodzic Roux, A., Turnipseed, A., Cantrell, C., Lefer, B. L., and Grossberg, N.: Observations of gas- and aerosol-phase organic nitrates at BEACHON-RoMBAS 2011, *Atmos. Chem. Phys.*, 13, 8585-8605, 2013, 10.5194/acp-13-8585-2013.

- Hathaway, R. J. and Bezdek, J. C.: Fuzzy c-means clustering of incomplete data, IEEE Transactions on Systems, Man, and Cybernetics, Part B (Cybernetics), 31, 735-744, 2001, 10.1109/3477.956035.
- IBGE: Malhas digitais, Setor Censitário, 2010, <https://mapas.ibge.gov.br/bases-e-referenciais/bases-cartograficas/malhas-digitais.html>, last access: January 2018.
- Lanz, V. A., Alfara, M. R., Baltensperger, U., Buchmann, B., Hueglin, C., and Prévôt, A. S. H.: Source apportionment of submicron organic aerosols at an urban site by factor analytical modelling of aerosol mass spectra, Atmos. Chem. Phys., 7, 1503-1522, 2007, 10.5194/acp-7-1503-2007.
- Medeiros, A., Souza, R. A. F., and Martin, S. T., in preparation.
- Mohr, C., DeCarlo, P. F., Heringa, M. F., Chirico, R., Slowik, J. G., Richter, R., Reche, C., Alastuey, A., Querol, X., Seco, R., Peñuelas, J., Jiménez, J. L., Crippa, M., Zimmermann, R., Baltensperger, U., and Prévôt, A. S. H.: Identification and quantification of organic aerosol from cooking and other sources in Barcelona using aerosol mass spectrometer data, Atmos. Chem. Phys., 12, 1649-1665, 2012, 10.5194/acp-12-1649-2012.
- Riva, M., Budisulistiorini, S. H., Chen, Y., Zhang, Z., D'Ambro, E. L., Zhang, X., Gold, A., Turpin, B. J., Thornton, J. A., Canagaratna, M. R., and Surratt, J. D.: Chemical characterization of secondary organic aerosol from oxidation of isoprene hydroxyhydroperoxides, Environ. Sci. Technol., 2016, 10.1021/acs.est.6b02511.
- Robinson, N. H., Hamilton, J. F., Allan, J. D., Langford, B., Oram, D. E., Chen, Q., Docherty, K., Farmer, D. K., Jimenez, J. L., Ward, M. W., Hewitt, C. N., Barley, M. H., Jenkin, M. E., Rickard, A. R., Martin, S. T., McFiggans, G., and Coe, H.: Evidence for a significant proportion of Secondary Organic Aerosol from isoprene above a maritime tropical forest, Atmos. Chem. Phys., 11, 1039-1050, 2011, 10.5194/acp-11-1039-2011.
- Schneider, J., Freutel, F., Zorn, S., Chen, Q., Farmer, D., Jimenez, J., Martin, S., Artaxo, P., Wiedensohler, A., and Borrmann, S.: Mass-spectrometric identification of primary biological particle markers and application to pristine submicron aerosol measurements in Amazonia, Atmos Chem Phys, 11, 11415-11429, 2011, doi.org/10.5194/acp-11-11415-2011.
- Ulbrich, I., Canagaratna, M., Zhang, Q., Worsnop, D., and Jimenez, J.: Interpretation of organic components from positive matrix factorization of aerosol mass spectrometric data, Atmos. Chem. Phys., 9, 2891-2918, 2009, 10.5194/acp-9-2891-2009.

## List of Supplementary Figures

**Figure S1.** Location of the GoAmazon2014/5 sites relevant for this study. Image data: Google earth.

**Figure S2.** Scatter plot of the AMS signal fraction at  $m/z$  44 ( $f_{44}$ ) against that at  $m/z$  43 ( $f_{43}$ ).

Green and yellow markers correspond to measurements made by two different AMS instruments at T0t in the wet season of 2008 during the AMAZE-08 campaign (Chen et al., 2009; Schneider et al., 2011). Red markers correspond to measurements made at the T0a (ATTO) by an ACSM during the wet season of 2015. A correction factor of 0.75 was applied to the  $f_{44}$  values of the ACSM based on calibrations with standards. Solid squares represent median values, and whiskers represent 10 and 90 percentiles. The plot shows a significant variability between the observations of 2008 and 2015 for the two background sites. An explanation of the differences is not attempted herein and warrants further investigation through longer-term continuous measurements.

**Figure S3.** Diagnostics of the PMF analysis. (a) Statistics of the sum of for solutions with different number of factors. Box plots show the interquartile ranges, including the medians as a horizontal line. Red markers show the means. Whiskers show the 5 and 95 percentiles. (b) Correlations expressed as between each pair of factors within each PMF solution, with number of factors varying from 2 to 7. The Pearson  $R$  value between factor loadings is shown on the coordinate and between factor profiles is shown on the abscissa. Numbers in red indicate the identity of the pair of factors.

**Figure S4.** Results of the PMF analysis for 5 factors (a and b) and 7 factors (c and d). Panels on the left (a and c) show the time series of factor loadings and panels on the right (b and

d) show the profiles of factors. The signals shown in panels b and d were summed to unit mass resolution.

**Figure S5.** Comparison of the ADOA factor profile from the present study to factors found in three other field studies. “COA” are factors representative of cooking activities, and the “91fac” from Robinson et al. (2011) was tied to biogenic sources.

**Figure S6.** Summary of the analysis for estimating organic and inorganic nitrates from AMS bulk measurements. (a) Resulting time series of organic and inorganic nitrates are shown together with the original nitrate AMS times series. (b) Time series of the fraction of organic nitrate in total nitrate. (c) Time series of the measured  $\text{NO}_2^+/\text{NO}^+$  ratio is shown in red and values of  $\text{NO}_2^+/\text{NO}^+$  from ammonium nitrate calibrations are shown in gray triangles. A linear fit to those calibration ratios is shown by the dashed dark blue line and constitutes the reference ratio for inorganic nitrate over time. The dashed light blue line is the reference ratio for organic nitrates over time. Calculations were done for data binned to one hour (as plotted), and the resulting time series were interpolated to the native time stamp for evaluation of correlations in the PMF analysis.

**Figure S7.** Value of the objective function of the FCM analysis (Eq. 1) in the last iteration plotted against the number of clusters.

**Figure S8.** Locations of cluster centroids from the FCM analysis as visualized by a 2-D projection on the plane defined by each pair of input variables. Results for two to five clusters are shown in panels a to d. Red circles are observational data and black squares are cluster centroids.

**Figure S9.** Map of Manaus city depicting population density as well as main avenues and representative locations of industry, restaurants, and other businesses. Population density data are from the 2010 census by the Brazilian Institute of Geography and Statistics (IBGE, 2010).

**Figure S10.** Measurements showing the geographical heterogeneity of emissions from Manaus. On the top row, concentrations of sulfate (red) and particle number (white) measured onboard the G-1 aircraft on (a) March 19 and (b) Mar 21. Image data: Google earth. On the bottom row, rose plots of mean (c) sulfate mass concentrations and (d) particle number concentrations observed at T2 during IOP1. The angles represent wind direction, the radial scale (0 to 5 m s<sup>-1</sup>) represents wind speed, and the color scale represents the concentrations. The interactions of emissions from Manaus with the daily river breeze is complex, and the detailed interpretation of the data sets is not fully attempted herein. Of importance, the river breeze terminates well below 500 m based on the G-1 flights so that the complexities of the river breeze largely do not affect the measurements at T3 because most pollution is lofted above the river breeze before reaching T3 (Medeiros et al., in preparation). These surface-level plots, although complicated by the river breeze, demonstrate the heterogeneity of Manaus emissions.



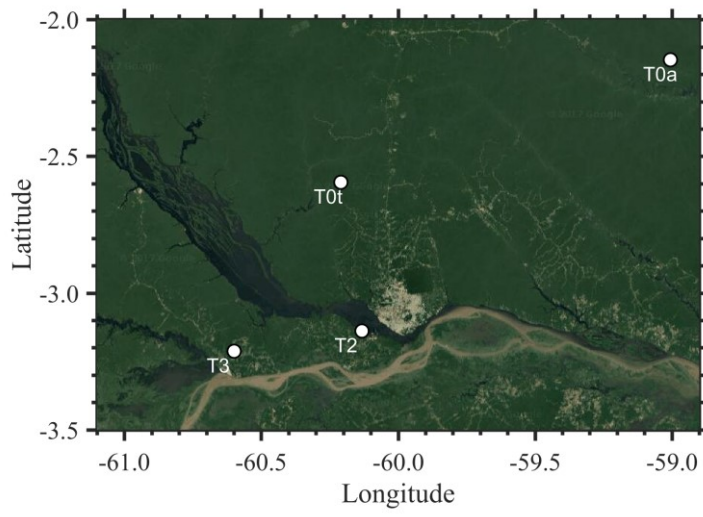


*Figure S1*

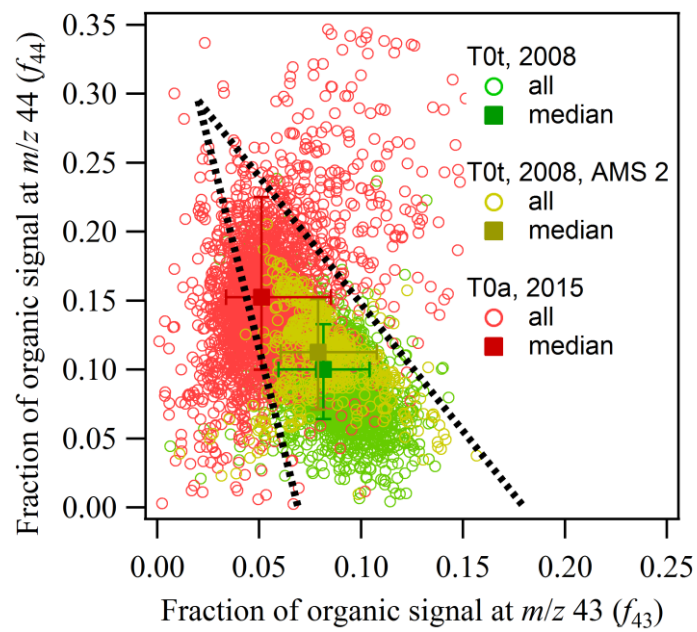


Figure S2

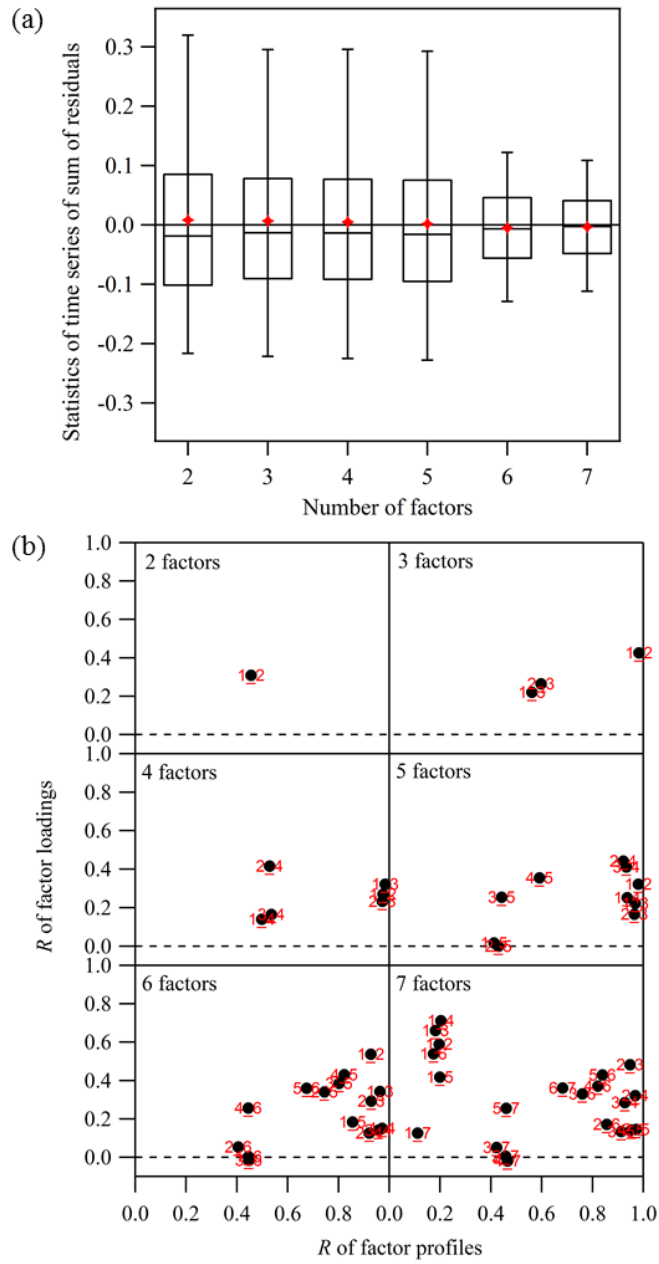


Figure S3

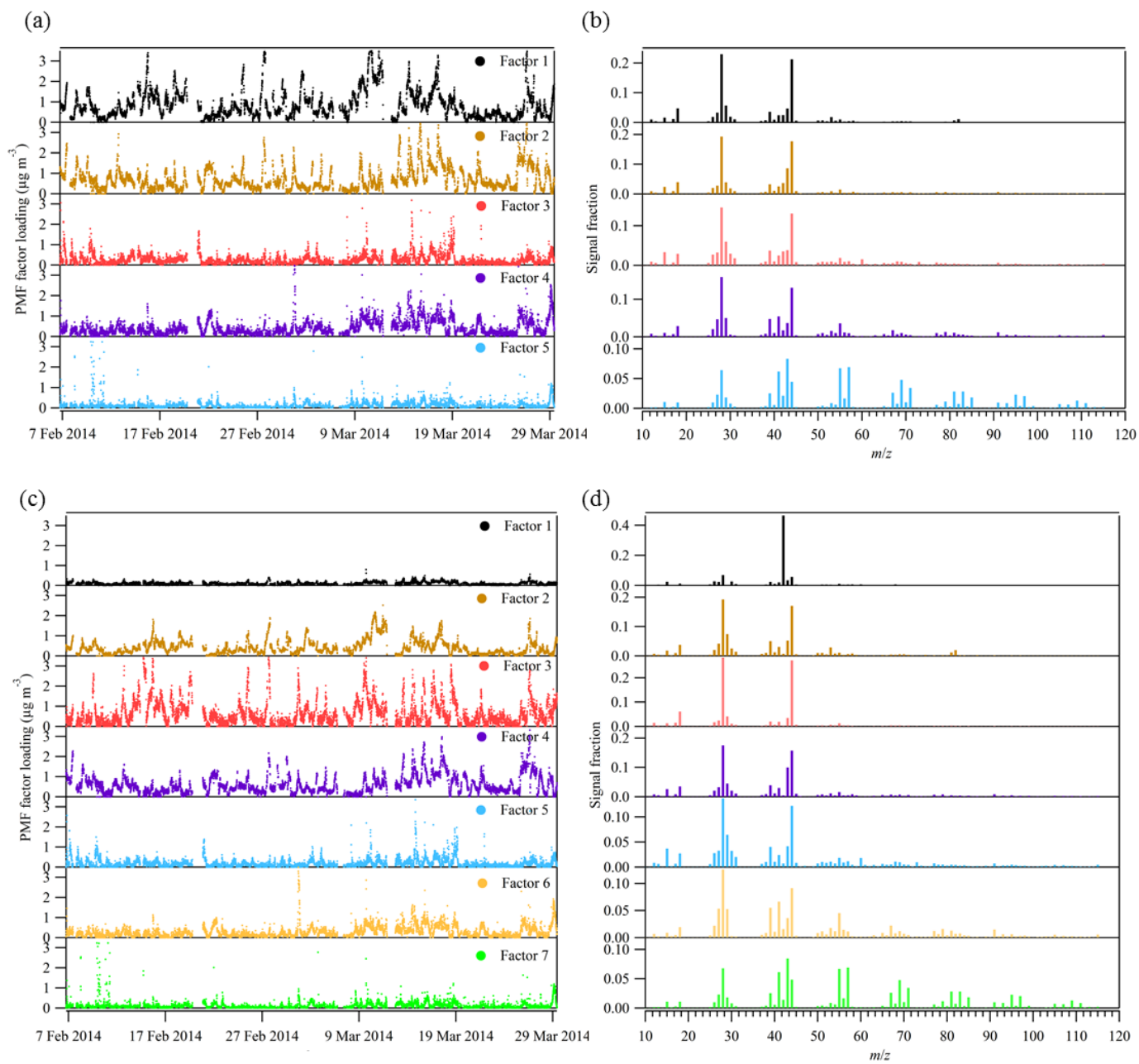


Figure S4

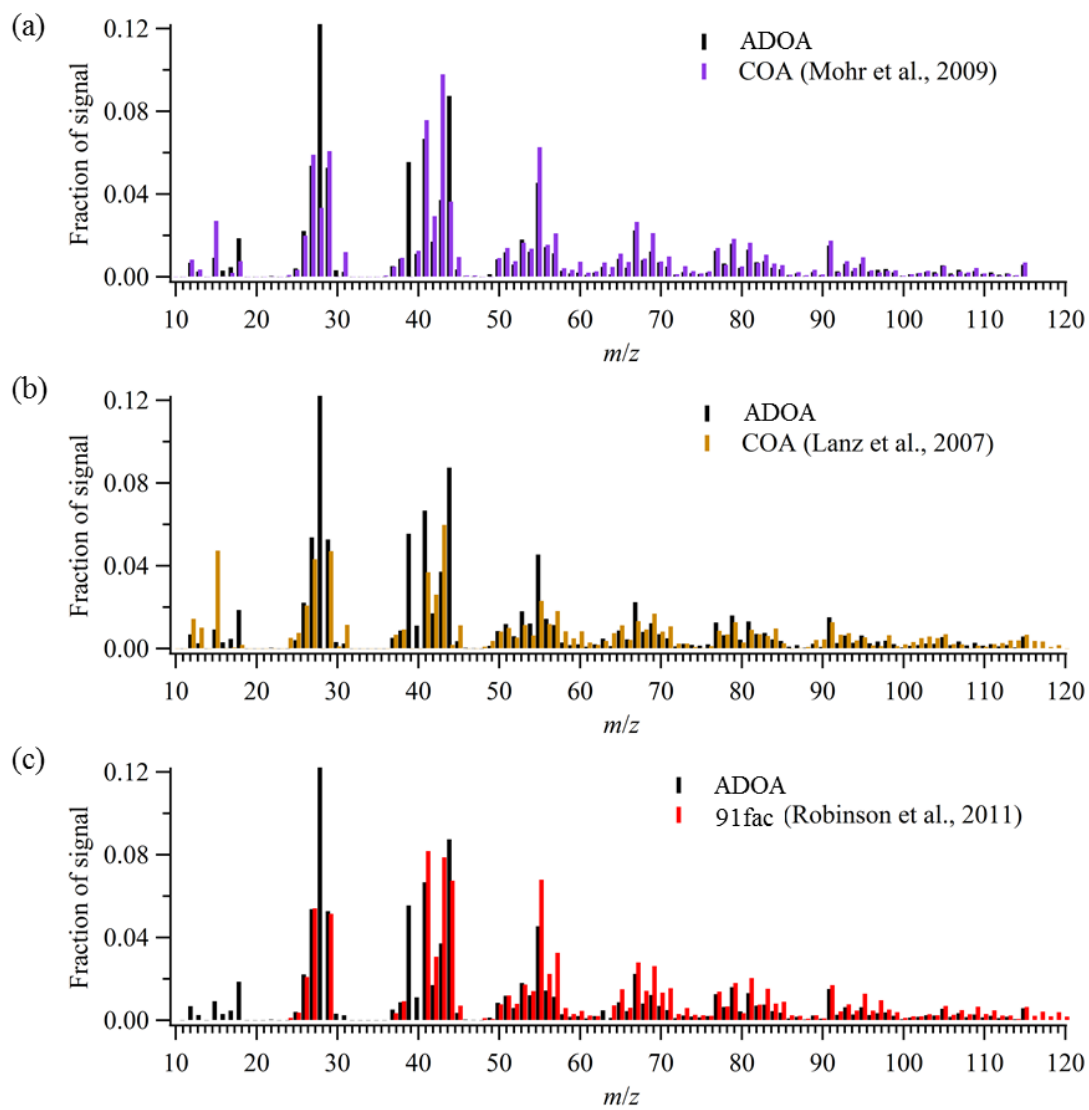


Figure S5

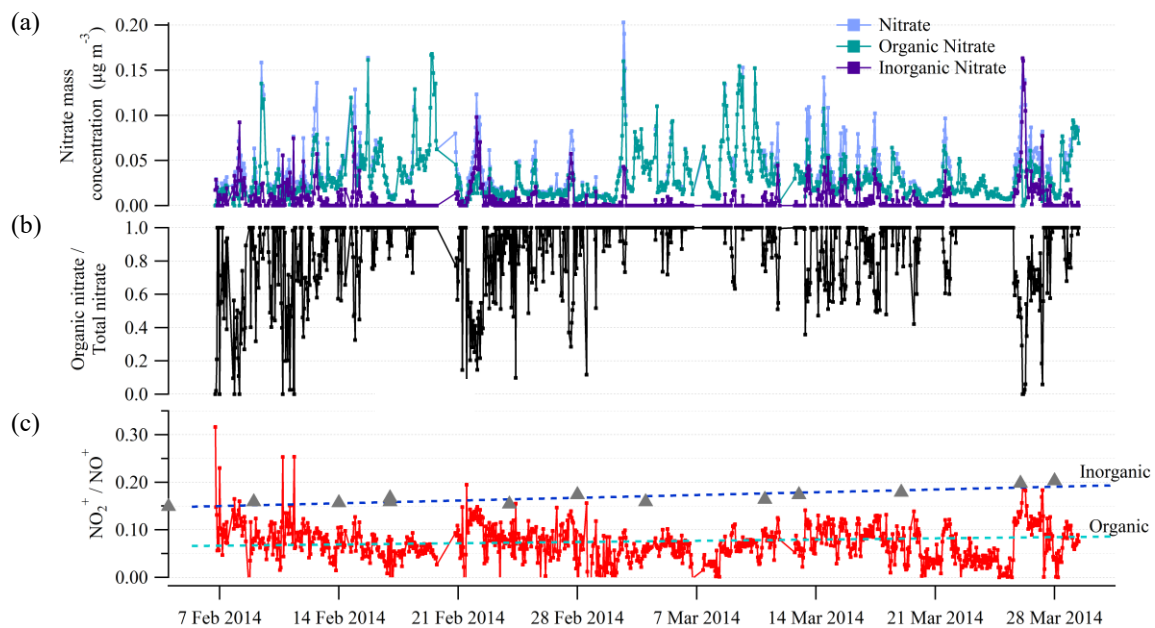


Figure S6

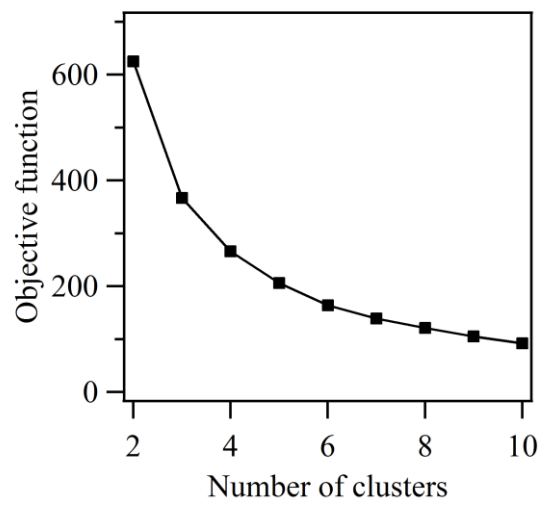


Figure S7

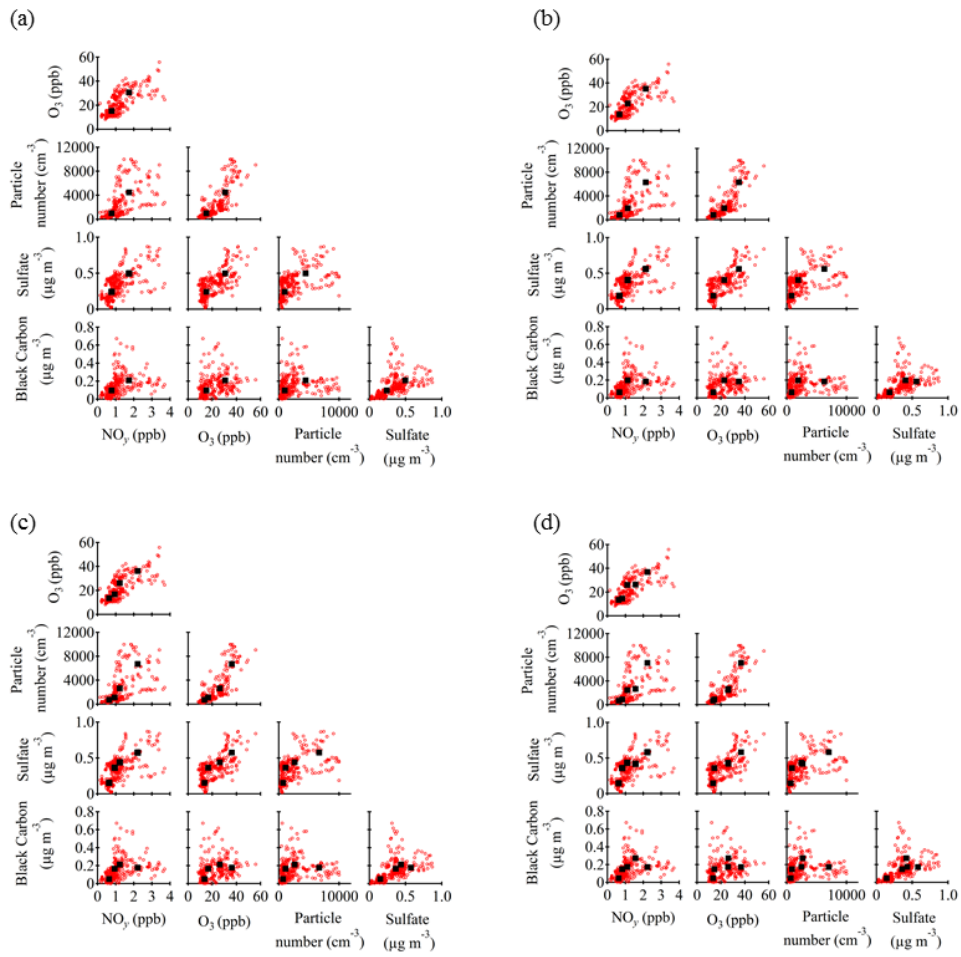


Figure S8



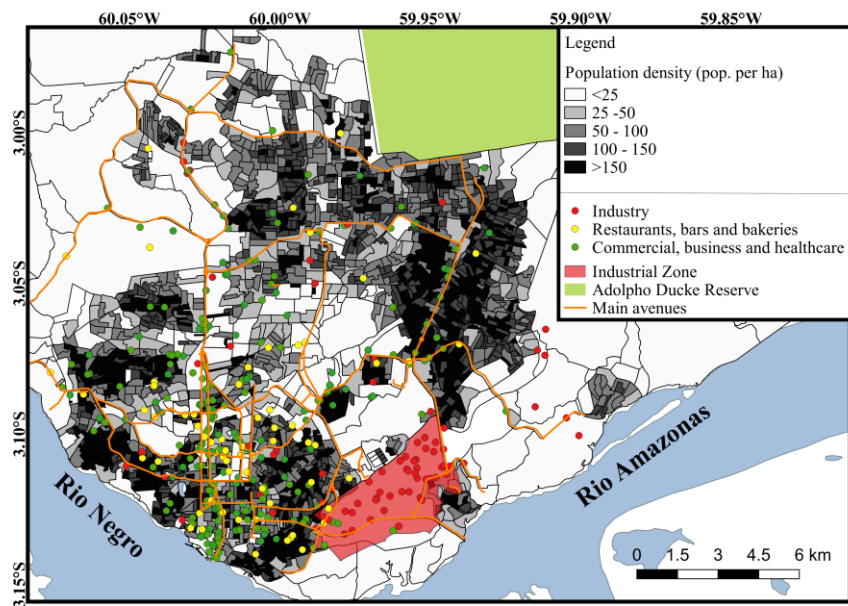
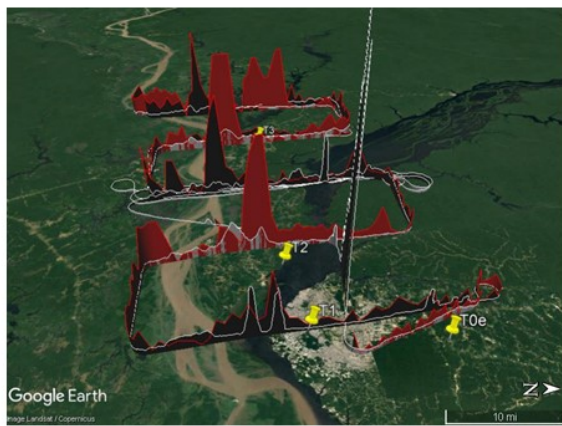
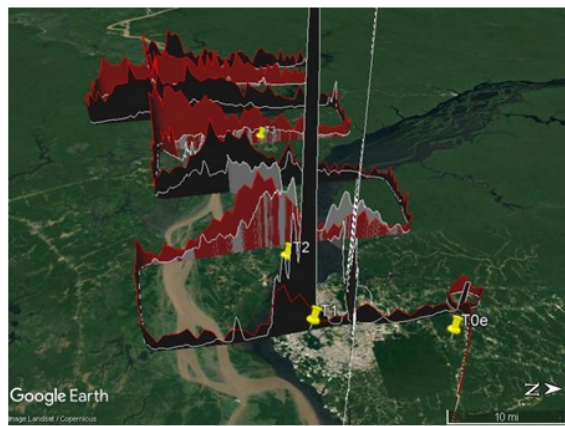


Figure S9

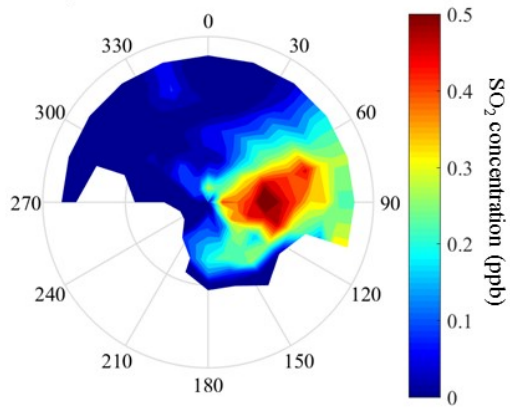
(a) 19 Mar 2014



(b) 21 Mar 2014



(c) IOP1, T2



(d) IOP1, T2

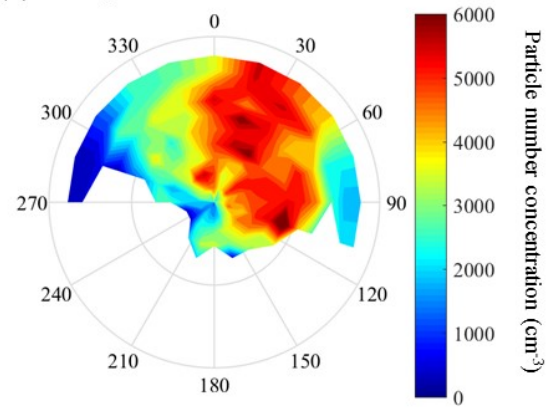


Figure S10